NASA CR-168317
NAUFP 202-2

EXPERIMENTAL STUDY OF UNCENTRALIZED SQUEEZE FILM DAMPERS

by

ROGER D. QUINN

December 1983

Departments of Mechanical and Civil Engineering
The University of Akron
Akron, Ohio 44325

Prepared for
Lewis Research Center
National Aeronautics and Space Administration
Cleveland, Ohio 44315

NASA Grants NSG 3283 and NAG 3-50

10 1 1 RN/NASA-CR-168317

DISPLAY 10/2/1

84N19927*# ISSUE 10 PAGE 1516 CATEGORY 39 RPT#: NASA-CR-168317 NAS 1.26:168317 NAUFP-202-2 CNT#: NSG-3283 NAG3-50 83/12/00 127 PAGES

UNCLASSIFIED DOCUMENT

UTTL: Experimental study of uncentralized squeeze film dampers

AUTH: A/QUINN, R. D.

CORP: Akron Univ., Ohio. CSS: (Dept. of Mechanical Engineering.) AVAIL.NTIS

SAP: HC A07/MF A01

MAJS: /*DAMPERS (VALVES)/*SQUEEZE FILMS/*VIBRATION EFFECTS

MINS: / CLEARANCES/ ECCENTRICITY/ FINITE ELEMENT METHOD/ FLUID PRESSURE/ INLET PRESSURE/ ROTORS/ VISCOSITY

1. Report No.	2. Government Accession No.	3. Recipient's Catalog No.
NASA CR-168317		

4. Title and Subtitle	5. Report Date
Experimental Study of Uncentralized Squeeze Film Dampers	December 1983
	6. Performing Organization Code

7. Author(s)	8. Performing Organization Report No.
Roger D. Quinn	
	10. Work Unit No.

9. Performing Organization Name and Address	11. Contract or Grant No.
The University of Akron Department of Mechanical Engineering Akron, OH 44325	NSG 3283, NAG 3-50
	13. Type of Report and Period Covered
12. Sponsoring Agency Name and Address	Topical
National Aeronautics and Space Administration Washington, DC 20546	14. Sponsoring Agency Code

15. Supplementary Notes

Technical Monitor: C. C. Chamis
NASA Lewis Research Center, MS 49-6
21000 Brookpark Road
Cleveland, OH 44135

16. Abstract

The vibration response of a rotor system supported by a squeeze film damper (SFD) was experimentally investigated in order to provide experimental data in support of the "Rotor/Stator Interactive Finite Element" theoretical development.

Part of the investigation required the designing and building of a rotor/SFD system that could operate with or without end seals in order to accommodate different SFD lengths. SFD variables investigated included clearance, eccentricity mass, fluid pressure, and viscosity and temperature. The results show inlet pressure, viscosity and clearance have significant influence on the damper performance and accompanying rotor response.

17. Key Words (Suggested by Author(s))	18. Distribution Statement
Dampers, squeeze film, orbits, clearance, pressures, temperatures, viscosity, masses, eccentricities, displacement, phase change, critical speeds, comparisons	Unclassified, Unlimited

19. Security Classif. (of this report)	20. Security Classif. (of this page)	21. No. of pages	22. Price*
Unclassified	Unclassified		

*For sale by the National Technical Information Service, Springfield, Virginia 22161

ABSTRACT

Until recently, there has been little literature available pertaining to the design of uncentralized squeeze film dampers (SFD). The purpose of this work was to design and build a rotor system supported by uncentralized SFD that could be operated with or without end seals and to conduct an experimental study of the system's vibrational response. Inlet pressure, viscosity and clearance were each found to have a great influence on damper performance. Comparisons were made with the results found in available literature and with a simplified computer analysis. Suggestions are included for design improvements and for future work.

ACKNOWLEDGEMENT

The author is especially grateful to Dr. M. L. Adams for his patience and guidance and to the machinists in the M.E. shop for their invaluable assistance. The author would also like to express his appreciation to Dr. D. G. Fertis for his assistance and support, and to all those responsible for the NASA LeRC grants through which this work was funded.

TABLE OF CONTENTS

LIST OF FIGURES

List of Symbols

c	Radial squeeze film clearance (R_h-R)
D	Journal diameter
e	Eccentricity of damper journal in bearing housing
e_B	Eccentricity of rotor disc mass
F_R, F_T	Radial and tangential components of dynamic squeeze film force
k	Supporting spring stiffness
K	Support stiffness/rotor-bearing stiffness
L	SFD land length
m	Rotor mass
m_B	Rotor mass acting at each bearing (symmetric rotor)
m_D	Rotor mass lumped at center of rotor (symmetric, flexible rotor)
M	m_B/m_D
P_c	Cavitation pressure, lowest possible film pressure
P_{in}	Inlet pressure to SFD
R	Journal radius
R_h	Damper housing radius
T	Transmissibility (actual force transmitted through bearings/force through bearings with rigid supports)
u	Unbalance moment of rotor disc ($e_D m_D$)
ε	Eccentricity ratio (e/c)
Ω	Design speed
ω	Rotor speed
ω_c	Critical speed
ω_s	Support resonance, k/m_B
μ	Oil viscosity

CHAPTER 1

INTRODUCTION

As the earth's material resources become more scarce and therefore more expensive, the development of greater sophistication in technologies which conserve materials becomes more economical. In the power and aerospace industries, more "power per pound" generally means lighter, higher speed, more flexible rotating equipment. Since all rotors have some amount of unbalance which increases with use, higher rotating speed can mean unacceptable vibrations and instability problems. The need for a damping device to control vibration and instability is apparent.

Beginning with experimental use in the early 1960's, hydrodynamic squeeze film dampers (SFD) have found increasing use over the past twenty years in the gas turbine industry. Today most modern gas turbine engines use SFD coupled with rolling contact bearings. Since rolling contact bearings have little inherent damping, the extra damping is necessary for safe flexible rotor operation, operation at speeds near or in excess of the pinned-pinned critical speed of the rotor.

A SFD is a fluid (usually oil) filled annulus surrounding the bearing (or bearing housing) with a radial clearance on the order of 10 mils. The damper bearing is "dogged" to prevent rotation but is free to "whirl" or precess about the center of rotation of the rotor, while squeezing a pressure film ahead of it. The driving mechanism which causes the motion of the damper journal through the fluid film thereby creating the desired damping effect is the translational vibration of the rotor.

A properly designed squeeze film damper can (1):

a) reduce the level of forces transmitted through the bearings.
b) reduce the vibrational amplitude of the rotor.
c) smooth operation through the critical speeds.
d) protect the rotor from sudden unbalance.
e) protect the rotor from self-excited instability.

Since rolling contact bearing life is related to the applied forces, (a) above can mean greatly increased bearing life (a transmissibility of 0.20 can mean an extension of bearing life by 125 times (3)). In compressors and turbines, blade tip clearance is critical suggesting that (b) above is a clear advantage. The advantage of (c) is the capability of safe, flexible rotor operation. Catastrophic failure from blade loss during operation can

be avoided because of (d). Non-synchronous, self-excited whirl instability can limit the rotational speed of rotors mounted on fluid film bearings. This instability can also be caused by internal friction or variable aerodynamic loading with rolling contact bearings (10). In view of (e), SFD could be a solution to this instability problem.

As suggested by Cookson and Kossa, SFD can be divided into two main categories based on basic design philosophy (14). The design generally used in the U.S. is a SFD in parallel with a flexible rotor support which preloads the rotor centrally in the damper bearing. The flexible preloading is usually accomplished with a set of cantilever rods referred to as a "squirrel cage". See Figure 1.1. On the other hand, the British design is the more basic uncentralized SFD with the rotor free to find its own position within the damper bearing.

In the early analysis of SFD the rotor center was assumed to follow a circular synchronous orbit around the center of the damper bearing clearance circle. This applies for centrally preloaded or vertical rotors. Though uncentralized SFD are simpler and less expensive, analysis of this design is non-linear and much more difficult. Proper design is important, however, since a poor design can amplify rather than attenuate transmitted bearing forces. (14)

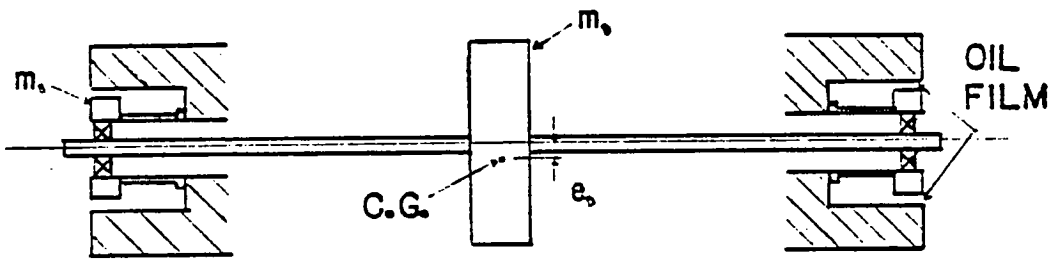

Figure 1.1 Symmetric, Lumped Mass Rotor with Damped, Flexible Supports

A flexible support in parallel with a SFD effectively reduces the natural frequencies of the system so that the rigid rotor critical speeds can be traversed well before the operating speed. The flexible element is also useful for carrying the static load for a heavily loaded rotor. A SFD used alone does not have such a marked effect on the system's natural frequencies. Since most gas turbines now run well above the rigid rotor modes, the flexible element is often unnecessary (12).

A secondary classification of SFD which applies to both of the above mentioned types of design involves the use or non-use of end seals. Non-use of damper end seals and low inlet pressure allows damper fluid to flow freely longitudinally in the damper annulus yielding a parabolic longitudinal pressure distribution for a short bearing. A damper with no end seals and a "short" bearing ($L/D < .3$) can be analytically approximated with the "short bearing solution" of the Reynolds equation. The fluid feed for a damper with no end seals is usually accomplished with use of a circumferential groove in the center of the outer race of the damper bearing, which divides the damper into two parallel bearings. See Figure 1.2.

A damper with end seals will have no longitudinal flow and therefore, a constant longitudinal pressure distribution. This type of damper can be analytically

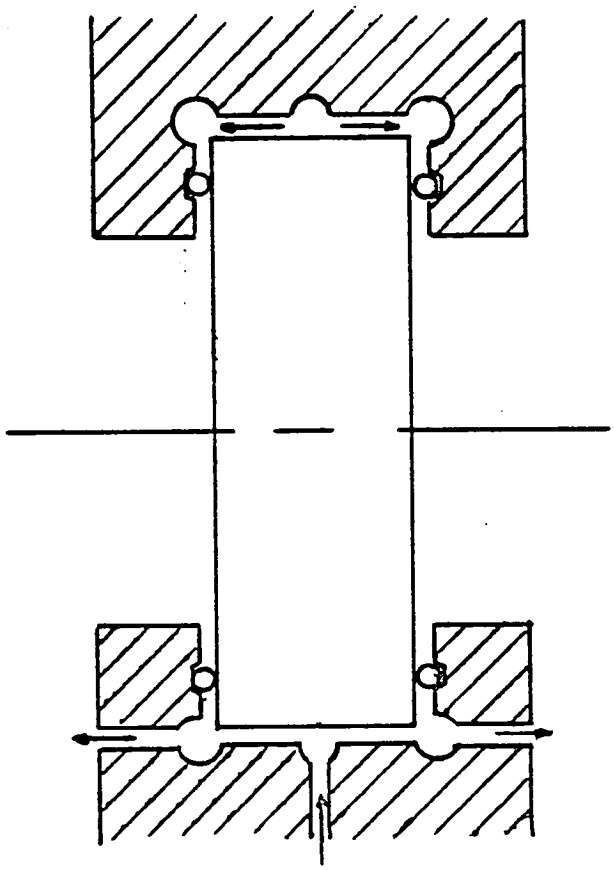

Figure 1.2 Circumferential Groove Inlet/Outlet With No End Seals

approximated with the "long-bearing solution" of the Reynolds equation. Oil flow through this type of damper, which is required for heat dissipation, is usually maintained with the use of inlet and outlet ports located centrally in the damper annulus 180° apart on the bottom and top, respectively. See Figure 1.3.

Most designs include sealing devices, but the seals may be used to channel flow through the desired outlet at ambient pressure rather than to form pressurizing end seals. See Figure 1.2. The actual sealing arrangement can take many forms, but the sealing devices are usually O-rings, used in shear or compression, or piston rings. See Figures 1.3 and 1.4. The particular application typically constrains the flow rate and, therefore, the sealing arrangement.

The proper design of a SFD depends on the type of vibration that is to be suppressed, the one type being the synchronous, forced, unbalance response and the other being nonsynchronous whirl instabilities. It is difficult to design a SFD for all conditions in a wide operating range. It is possible for a SFD to suppress the responses to small normal unbalances but provide worse than rigid support response for large unbalances such as from a blade loss (10).

When a rotor is said to be "rigid", the operating speed of the rotor can include the rigid rotor critical

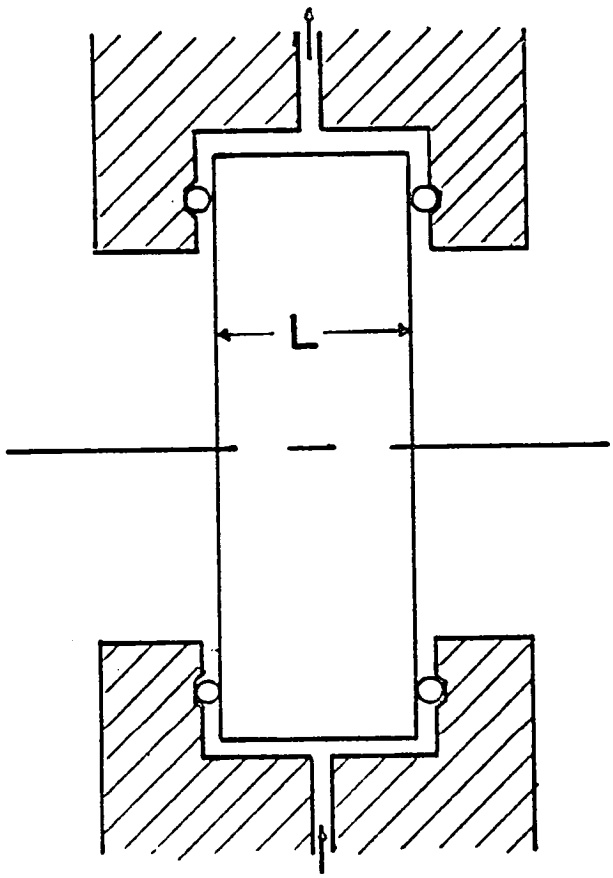

Figure 1.3 Port Inlet/Outlet With O-Ring End Seals Used in Shear

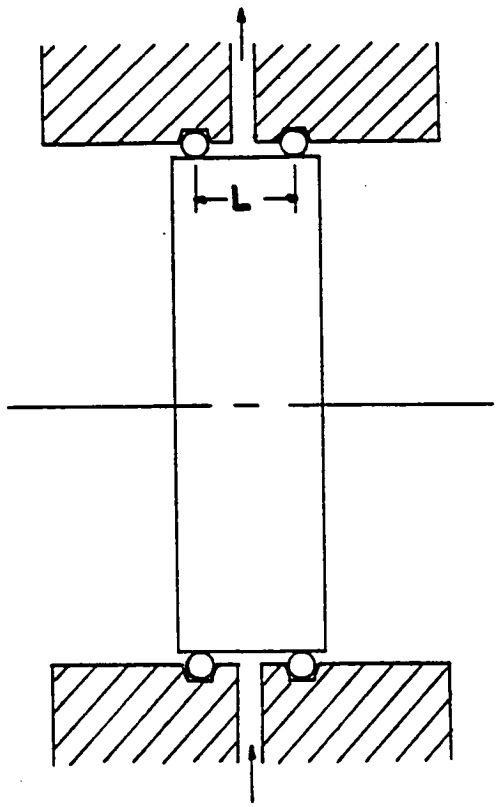

Figure 1.4 Port Inlet/Outlet With O-Ring End Seals Used in Tension/Compression

speeds (cylindrical and conical "bounce" modes) but is kept well below the first bending critical speed (1). Whereas a rotor operating near or above its first bending critical speed is termed "flexible".

In a linear analysis the SFD is modeled as a spring and damper system where the stiffness and damping coefficients are constant for a certain speed. In a non-linear analysis the damping and stiffness are functions of the displacement and velocity of the damper journal. For circular, centered, constant speed orbits the non-linear analysis simplifies to one of amplitude dependent coefficients (4).

CHAPTER 2

A REVIEW OF SOME RECENT STUDIES CONCERNING SFD

In 1970, Gunter published an investigation concerning the determination of the desirable values of rolling element bearing support stiffness and damping for rigid rotors (1). The mathematical model simulated a general four degree-of-freedom unbalanced rotor mounted on two damped, linearly flexible supports. The stiffness and damping coefficients could be constant or speed dependent.

The four simultaneous differential equations of motion for the rotor system were developed and then solved with a computer for synchronous precession over a wide range of rotor speeds and with various support conditions. To simplify the analysis, isotropic stiffness and damping were used, yielding circular, steady-state rotor orbits.

For optimization of support coefficients, a computer program was written that calculated the rotor amplitudes and forces at each speed increment and iterated the speed until the maximum forces and amplitudes of rotor motion were obtained. For a certain stiffness, an optimum value of damping could be found. Gunter noted that the optimum value of damping was a compromise between the

forces transmitted through the bearing supports at the rigid rotor critical speeds and at the maximum rotor speed. Additional damping attenuated forces at the critical speeds, but raised the force level at higher speeds.

A "stiff" bearing support that placed the second rigid body critical speed above the design speed, led to excessive transmitted forces with unbalance. Gunter also noted that any amount of damping was ineffective for attenuating force transmission when placed in parallel with stiff supports.

Large amounts of damping were also found to be undesirable since excessive damping values caused force transmission to increase rapidly with speed. A study was made of the displacement phase angles of both bearings with respect to the radial unbalance vector. With light damping the phase changes at the critical speeds were abrupt. With moderate damping, the phase changes were smooth. As the rotor speed was increased, the rotor inverted to rotate about its principal inertial axis. Excessive damping suppressed the inversion of the rotor, thus causing high bearing forces to be generated.

With certain support conditions there was no observable critical speed response. Undamped, "soft" supports could minimize rotor force transmission over the entire speed range considering only synchronous,

small-unbalance response. However, Gunter recommended some damping to control instability problems (nonsynchronous whirl) and in case of shock loading, such as from the loss of a turbine blade. A combination of low stiffness and moderate damping was also found to be effective in minimizing transmitted forces resulting from unbalance. With these support conditions the rotor could be safely operated at a critical speed.

Gunter states that the behavior of a SFD is highly non-linear so that in certain conditions a SFD can cause amplification of force rather than attenuation.

In 1973, Giberson, ~~of Turbo~~ Research Inc., published a paper acclaiming the ability of SFD to stabilize otherwise unstable rotors supported with journal bearings (2). When rotor speed surpasses the threshold of instability for the journal bearings, "whirl" amplitude theoretically grows without bound, possibly destroying the machine. Pivoted pad journal bearings can stabilize a system by themselves, but "pivoted pad bearings supported by SFD is the arrangement with the greatest ability to stabilize a rotor bearing system that uses hydrodynamic bearings."

To demonstrate the stabilizing effect of SFD, Giberson used a computer simulation of an analytical model that contained non-linear force-displacement (stiffness) and force-velocity (damping) relationships.

The equations of motion for the rotor masses were integrated through time, yielding time transient trajectories for the rotor discs, journal center, and damper journal center.

The modeled system was a multimass rotor mounted on fixed pad journal bearings supported by SFD. O-rings used in compression/tension acted as flexible support elements as well as end seals. Oil entered through an inlet port centered axially in the damper housing. Damper length, damper film cavitation pressure, oil supply pressure, and rotor speed were kept fixed for all presented simulation runs. The objective was to "tune" the system by varying three support parameters; the radial damper clearance, O-ring stiffness, and oil viscosity. Decreasing the clearance, raising the viscosity, or stiffening the O-rings tended to increase support rigidity.

The results showed that the system was unstable with rigid supports and was stable for only one out of nine choices of parameters. As Giberson points out, SFD are capable of solving whirl problems, but they must be "tuned" (tested to determine the correct combination of design parameters for the particular system) to be effective. In fact, an improper design can lower rather than increase the threshold of instability.

In 1974 Mohan and Hahn published a paper on the "Design of SFD Supports for Rigid Rotors" (3). The publication includes a general design guide for centrally preloaded SFD, supporting a rigid rotor, mounted on rolling contact bearings. The authors also investigated the transient solutions of the fully non-linear equations of motion to discover the effect of central preloading.

The rotor that was modeled was a rigid, symmetric rotor mounted on ball bearings, supported by retainers springs and SFD with no end seals. The fluid film forces necessary for solving the equations of motion for the system were obtained with the use of the short bearing approximation of the Reynolds lubrication equation for constant fluid properties. The assumptions used in solving for the film forces required that;

1) an incompressible lubricant and an average fluid viscosity in the squeeze film be used. (constant properties)
2) fluid inertia and turbulence effects be negligible. (necessary to derive Reynolds equation)
3) the length to diameter ratio (L/D) be less than 1/4. (short bearing)
4) the end pressures be ambient. (no end seals, low feed pressure)

5) the tensile forces in the film be negligible despite below ambient pressures.

6) the extent of the positive film pressure region be the same for a full film and a cavitated film.

The Reynolds equation was integrated over the length of the bearing to yield an expression for film pressures in terms of damper journal position and velocity. The expression for the pressure was then integrated over the positive pressure region of the damper, yielding the desired tangential and radial film force components. The equations of motion for the rotor system could then be solved for each time step, yielding the journal position and velocity and the fluid film forces.

The solutions were dependent on the following non-dimensional parameters:

1) $B = \frac{\mu R L^3}{2 m_B \Omega C^3}$ (bearing parameter)

2) $U = \frac{u}{m_B C}$ (unbalance eccentricity)

3) $\frac{\omega}{R}$ (ratio of operating speed to design speed)

4) $W_S = \frac{\omega_S}{R}$ (spring parameter)

5) $\frac{g}{C\Omega^2}$ (gravity parameter)

6) spring preload parameters

Consideration of the transient, non-linear equations of motion yielded one, two, or three stable modes of operation (at design speed above rigid critical speed) depending on the operating conditions.

1) A circular synchronous journal orbit called the "inverted mode" (the rotor rotates about its principal inertial axis, the journal displacement and unbalance force are out of phase by 180°). This is a desirable mode in that it is characterized by a small journal orbit and low transmissibility (T).
2) The "whirl mode" characterized by a circular, synchronous orbit but with an uninverted rotor (the journal displacement and unbalance force are out of phase by 110° or less). This mode is undesirable in that it has a large journal orbit (high eccentricity) and a $T > 1$.
3) An extremely undesirable mode with a nonsynchronous, noncircular orbit including violent excursions, high eccentricity (ε) and high transmissibility.

The third mode was only observed for low values of the bearing coefficient ($B < 10^{-2}$) with certain boundary conditions. Operation in either the first or second mode depended on the values of the damping and unbalance parameters (B,U). Note the agreement with Gunter's 1970 analysis concerning the inverted and uninverted modes.

While central preloading eased the steady state solution by reducing the number of parameters involved, it did not adversely affect the transmissibility or operation modes. The design data found in this paper is restricted to steady state conditions for centrally preloaded SFD. Linear theory was found to apply adequately for low unbalance ($U < .2$) for obtaining the frequency response from knowledge of the resonant speed and transmissibility. For $U > .2$ the system had to be treated as non-linear.

When U was plotted against steady state T for a certain bearing it was found that for increasing U there was a critical unbalance (U_c) at which T suddenly increased (jumped). The "jump phenomenon" occurred as the system changed from operation in the inverted mode to operation in the uninverted mode. For high unbalances, the rotor did not invert at all.

It was found that lowering the spring rate had the desirable effects of raising U_c and lowering T at both the design speed and resonant speed. This suggests,

as Gunter did in 1970, the use of as low a spring rate as possible for maintaining central preloading.

It was also discovered and shown graphically that a large B is desirable at resonant speed but a small value of B is desirable at design speed (above critical) from the standpoint of producing a low T. This suggests (as Gunter's analysis did in 1970) a compromise value of B that allows for safe acceleration through resonance but low T at design speed. The authors suggest that for an uncertain unbalance condition, it is best to choose a value of B that maximizes the critical unbalance. Plots are provided for designing SFD with flexible supports for centrally preloaded rigid rotors.

In 1975 Cunningham, Fleming, and Gunter published an analytical investigation on the design of a centrally preloaded SFD for a multimass flexible rotor mounted on rolling contact bearings (4). The paper demonstrates a technique for the use of single mass, symmetric, flexible rotor analysis to optimize the stiffness and damping for a symmetric five mass rotor. The single mass analysis was taken from a 1972 NASA Report by Kirk and Gunter.

To aid in the analysis of the single, lumped mass flexible rotor system, the following dimensionless parameters were considered:

$$M = \frac{\text{bearing housing mass}}{\text{rotor mass}} \quad \text{(mass ratio)}$$

$$K = \frac{\text{support stiffness}}{\text{rotor-bearing stiffness}} \quad \text{(stiffness ratio)}$$

$$C = \frac{\text{total support damping}}{\text{rotor-bearing damping}} \quad \text{(damping ratio)}$$

The flexible supports effectively reduce the first critical speed to some fraction of the pinned-pinned rigid support, bending critical speed. Increased support damping was found to decrease the rotor amplitude at the critical speed but increase the amplitude at the rigid support critical speed. In other words, increased damping tended to "lock up" the rotor support. The "optimum" value of damping provided about equal rotor amplitude at the critical and rigid support critical speeds. (Note the increased complication due to the flexible rotor). It was demonstrated that for high rotor speed (above rigid support critical), T increased with increasing damping while rotor orbit amplitude was unaffected, as noted for rigid rotors in the previous paper. In choosing the damping, the forces and amplitudes of motion throughout the operating range must be taken into consideration.

For a given mass ratio (M), rotor amplitude of motion is minimized for a tuned system (K = M). The smallest possible value of M is desirable for lowering rotor amplitudes of motion. However, too small of a

value of K leaves the system susceptible to shock and self-excited whirl problems (in the absence of proper damping).

For a multimass flexible rotor, if the maximum rotor speed is below the second critical speed, single mass theory is shown to be adequate in some cases. The rotor that was simulated was a five mass symmetric rotor mounted on ball bearings with damped, flexible supports that were to be designed for optimum performance. Oil feed to the SFD was through a central circumferential groove. Piston rings and metered orifices controlled oil flow. The rigid support critical speeds were first calculated with computer simulation. For support design calculations, the five masses were replaced by a single, centered mass that resulted in the same first critical speed. The optimum support damping was found for this single mass rotor configuration. See Figure 1.1.

The assumption of a centralized circular orbit of the damper journal was used in designing a SFD that would provide the desired damping. Dimensionless stiffness and damping coefficients were obtained from the short-bearing approximation of the Reynolds equation assuming full 180° cavitation, no tensile stress and constant properties.

$$K_d = \frac{K_d C^3}{\mu \omega R L^3} = \frac{2\varepsilon}{(1-\varepsilon^2)^2}$$

$$B_d = \frac{B_d C^3}{\mu R L^3} = \frac{\pi}{2(1-\varepsilon)^{1.5}}$$

Note the non-linearity in terms of orbit size (eccentricity). Damping can be seen to be a function of damper clearance, radius, length, oil viscosity, and damper journal orbit.

A maximum eccentricity of $\varepsilon = .4$ at the critical speed was chosen for the design, somewhat arbitrarily. The maximum support amplitude of motion should be about equal to the mass eccentricity (rotor mass C.G. offset from axis of rotation) for optimum damper performance according to the authors. Thus, from knowledge of the maximum expected unbalance, the damper clearance could be calculated. Considering the radius and viscosity to be given, the desired damping then determined the damper length.

An unbalance response computer program was used to discover the effectiveness of the designed supports for the five mass rotor. The dampers successfully attenuated rotor orbit amplitudes of motion and bearing forces at the first critical speed by factors of 16 and 36, respectively, from the rigid support case. The vibration and forces were also reduced at higher critical speeds. However, for unbalances much greater than the design unbalance, the SFD supports provided worse performance than

rigid supports.

In 1979 Tonneson, of the Technical University of Denmark, published a study on experimental squeeze film bearing orbits (5). The purpose of the investigation was to compare experimentally measured damping coefficients with those obtained from simple linearized theory. Comparisons were made for both eccentric (offset) and concentric (centralized) damper journal orbits. (See Figure 2.1).

Two typical experimental apparatus are described. The first was a ball bearing supported rigid rotor mounted on SFD. The oil feed was accomplished with a circumferential groove in the damper land. End flow seals were provided. The length to diameter ratio was 0.34. The second test rig used was a similar SFD but the bearing housing was excited by an electrodynamic shaker.

The first apparatus used a flexible support, with a differential adjustment for centering the damper journal, in parallel with the SFD. Both rigs were instrumented for measurement of forces, displacements, phase angles, frequencies, and extent of cavitation.

The theory used for comparison with experiments was the short-bearing approximation of the Reynolds equation for small, circular, centered orbits ($\varepsilon < .3$ and constant). The damping coefficients for this linear (independent of position, ε, and velocity) approximation are

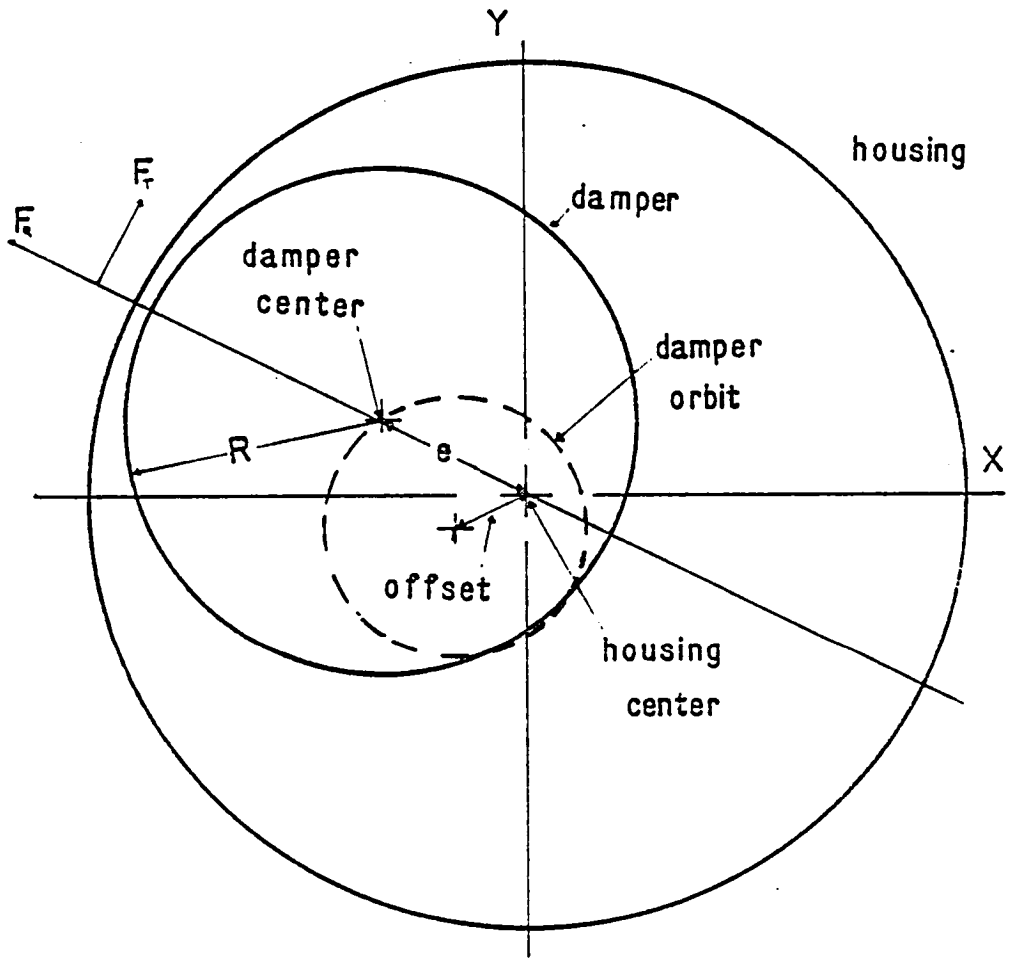

Figure 2.1 Offset Circular Damper Orbit

$$B_d = B_x = B_y = \frac{\pi}{2} \mu R \left(\frac{L}{3}\right)^3$$

for a 180° positive pressure film (expression should be doubled for a 360°, uncavitated film).

The results for the concentric orbit case show that the measured damping coefficients were between the theorized damping coefficients for 180° and 360° film. For the first test rig, for a constant viscosity and clearance, the damping coefficients were shown to be independent of frequency until the orbit amplitude exceeded a certain value. The shaker driven test rig yielded data showing that varying the viscosity, radial clearance, or orbit size yielded a linear relationship of B_d with the frequency for small amplitudes.

The experiments also revealed that the end seals added stiffness and damping which could be significant for low values of B_d for the SFD. The theory assumed atmospheric end conditions (short bearing), but the test rigs used end seals which change the end conditions to that of the inlet pressure so that the long bearing approximation may have been more valid. The supply pressure was found to affect the film extent and therefore the damping.

The author suggests that the eccentric case (damper orbits about a position off-center of the damper

housing) is more typical of SFD operation since exact central preloading is difficult due to built in tolerances. Reasonable agreement with theory was again found for small offsets and small orbit amplitudes. For large offsets the damper characteristics were pronouncedly nonlinear, for instance, lowering the viscosity at a large offset drastically increased the orbit amplitude.

For design applications, Tonneson suggests that a small L/D (about .1 to .2) is desirable and C/R should be no less than .002. A soft spring support is again recommended for effective SFD performance. For linear theory to apply, the flexible support must be stiff enough to accomplish approximate central preloading.

In 1977 Bansal and Hibner of Pratt and Whitney published an "Experimental and Analytical Investigation of (dynamic) SFD Forces Induced by Offset Circular Whirl Orbits." (6) In agreement with Tonneson, the authors suggest that offset orbits are more realistic for flexible damped supports. The offset is the distance between the steady state orbit center and the damper housing center, not to be mistaken with the eccentricity, e, which is the instantaneous distance between the journal center and housing center (see Figure 2.1). Offset circular orbits were induced mechanically on a single SFD supporting a rolling contact bearing. The experimentally measured pressure distribution was used to calculate the dynamic

forces. The purpose of the investigation was to study the effect of varying the inlet pressure, viscosity, journal speed and damper eccentricity on damper forces.

A motor driven eccentric cam produced the required offset circular orbits (actually, the dynamic orbits were elliptical because of the dynamic forces of the damper and the tolerances in the roller bearing). The damper oil inlet was a pressure fed circumferential groove at one end of the damper annulus, which provided uniform flow into the damper, and the oil exit was a single port on the other end of the annulus. O-ring end seals were used. Eight pressure transducers, axially centered and distributed circumferentially about the damper housing, sensed the film pressure and proximotor probes sensed the orbit shape and size.

The analytical solution for the pressure profiles was produced with the use of the long bearing approximation of the Reynolds equation assuming constant properties. The experimentally measured values of orbit position and shape were used in the analytical solution and experimental data reduction. The dynamic pressure at any circumferential angle, θ, $P(\theta)$, within the damper annulus was determined by superimposing the effect of the inlet pressure , P_{in}, on the hydrodynamic pressure $P_H(\theta)$; $P(\theta) = P_H(\theta) + P_{in}$. If $P(\theta)$ for θ from θ_1 to θ_2, was

less than the cavitation pressure, P_c of the oil, then the film had cavitated. Note that P_{in} could be increased so that $P(\theta) > P_c$ for all θ yielding an uncavitated film. The cavitated portion could range from 180° (P_{in} = ambient pressure) to 0° (full film). When cavitation was present, the damper film stiffness and damping were very sensitive to a change in the inlet pressure. For circular centralized orbits, an increase in inlet pressure increased the damping forces and decreased the stiffness.

For a centered circular orbit, the eccentricity is constant and the circumferential pressure distribution measured at any point of the annulus is identical, so, dynamic pressure measurement requires only one transducer. For an offset orbit, the dynamic pressured induced by the orbit is a function of the instantaneous position of the damper center and many pressure sensors are necessary. The pressure measured by each transducer would be dependent upon damper position and the location of the transducer on the rig.

The data reduction yielded an instantaneous experimental pressure profile for every 30° position of the damper center. Each profile was integrated to find the radial and tangential force for each damper position. The predicted pressure distributions, including inlet pressure effects and measured orbit parameters, were within 12% of the measured pressure distributions. The

comparisons of forces showed much poorer correlations. The authors suggested that small errors in measuring orbit parameters could cause significant errors in the analytical results due to the complex data reduction.

As noted previously the effect of inlet pressure is important with a cavitated film. The general trend was noted to be a decrease in radial force and an increase in tangential force for an increase in inlet pressure which the authors note is the same trend as for centralized orbits (increase in P_{in} means an increase in damping and a decrease in the stiffness of the film).

In 1977 Hibner, Bansal and Buono of Pratt and Whitney published a paper on the control of instability for intershaft SFD (7). An earlier analytical and experimental investigation had shown the existence of an intershaft viscous damper instability. The intershaft location in question was between the low and high speed shafts of a gas turbine engineer, at a roller bearing location. The outer race of the roller bearing was fixed to the outer, higher speed shaft, and the inner race was fixed to rotate with the inner, lower speed, fan shaft. The damper annulus was located between the inner race housing and the low speed rotor, so, the SFD journal and housing rotated with the low speed rotor. It was found that the "intershaft SFD would excite an instability at

low rotor speed as the cantilever natural frequency of the high speed rotor was approached."

The authors demonstrated that a flexible element in parallel with the SFD could add the necessary radial stiffness needed to raise the instability threshold above the operating speed.

In 1979 Hahn published an analytical investigation on the "Unbalance Behaviour of Squeeze Film Supported Rigid Rotors." (9) Equilibrium load capacity and transmissibility data for a wide range of operating conditions are presented for centrally preloaded and unloaded vertical rigid rotors mounted on rolling element bearings.

Hahn noted that the performance of a SFD is strongly influenced by:

1) the damper design parameters
2) the degree of rotor unbalance
3) the damping inherent in the system
4) the operating speed
5) the degree of oil supply pressurization.

The theoretical model of the damper came from the short bearing approximation of the constant property Reynolds equation. The analysis was restricted to steady state, centralized, circular, synchronous orbits. The solution for the orbit eccentricity was presented

as plots of two speed dependent dimensionless parameters Δ vs. B/U.

$$\Delta = (1 - 1/\delta^2)/U$$

$$B = \frac{2\mu RL^3}{mC^3\omega} \quad \text{(Load Number)}$$

$$\delta = \frac{\omega}{\omega_c}$$

U = Unbalance Parameter

Two plots are given, for an unpressurized and a fully pressurized film. Given a rotor system (ω_c,m,U), the SFD design parameters (μ,R,C,L), and the operating speed it is possible to locate predicted values of eccentricity and the system's operating line on the plots. The operating line would indicate the speed at which the maximum vibration amplitude would occur.

On the orbit eccentricity plots for unpressurized bearings there is a region where a point on the plot can suggest three possible equilibrium orbits (note the agreement with the earlier papers of Hahn and Gunter). The intermediate orbit has been shown to always be unstable, leading the author to label this region the bistable region. During operation in the bistable region it is possible for the system to jump from one to the other stable orbit. The possibility of jump depends on the conditions at entry into or exit from the region. To

avoid a jump to a higher orbit (higher eccentricity is associated with higher transmissibility), it is best to maintain operating conditions that keep the system out of the bistable region.

Unpressurized Dampers

Hahn recommends $\delta > 2$ for maintaining $T < 1$ and operation generally above the bistable region on the design plots. There is significant vibration attentuation possible for $U < .43$. For unloaded vertical rotors, there is no advantage in using external flexible supports in parallel with the SFD.

Fully Pressurized Dampers

There is no bistable region, but external radial support stiffness in parallel with the SFD is required for the stability of the solution. In this case, vertical rotors must have retainer springs. For $\delta > 2$, T will always be less than unity despite the value of unbalance, but as U gets large, T approaches one.

Note that vibration isolation can only be achieved at the expense of increasing rigid rotor vibration, so rotor motion constraints (tip clearances) must be considered.

In 1979 Vance of Gas Turbine Laboratories published a review of rotor dynamics which included the current role of SFD as a solution to dynamical problems (10).

The author stated that it was still not clear that SFD could be designed purely analytically for safe reliable performance for all cases.

Vance pointed out that the then current analytical techniques used the constant property Reynolds equation which does not apply for certain practical cases. The questionable assumptions generally used are;

1) negligible fluid mass inertia effects
2) single phase fluid film (no gas bubbles in the pressure region),
3) constant viscosity throughout the film.

The author also pointed out that the Reynolds equation is highly nonlinear (despite the typical use of a linear analysis) and that designers must be aware of instability problems, the neglect of which has been a costly error in the past.

U.S. army turboshaft helicopters now run at "supercritical" speeds (above the third critical flexural speed) using SFD to attenuate vibration and suppress whirl instability. Journal bearings are not used in aircraft engines because of potential catastrophic failure if oil flow is blocked. Vance argued that SFD should not be used to suppress instabilities in aircraft engines for the same reason.

In 1979 Hibner and Bansal published an experimental and theoretical investigation into "The Effects of

Fluid Compressibility on Viscous Dampers." (11) The investigation was begun because of the questionable validity of the Reynolds equation when cavitation exists in the squeeze film. The effects of cavitation could explain why correlations between theory and experiment for SFD have been excellent in some cases and poor in others.

The experimental test rig consisted of a controlled orbit, end sealed SFD. Circular, centered damper journal orbits were produced with an offset cam. A single pressure transducer measured the circumferential pressure distribution and probes measured the orbit eccentricity.

The theoretical analysis made use of the conventional long-bearing approximation of the constant property Reynolds equation. The experimentally measured dynamic values of eccentricity were used in the theoretical calculations.

The results showed better theoretical/experimental correlation for a decreasing extent of cavitation. For a cavitated film, theory overpredicted the pressure distribution. Raising the supply pressure or lowering the speed decreased the extent of cavitation and improved the correlation. With a cavitated damper, the supply pressure could not be superimposed on the hydrodynamic pressure, since an increase in supply pressure yielded an increase in hydrodynamic pressure.

It was hypothesized that the "deviation from theory is due to fluid compressibility caused by sub-atmospheric cavitation pressures liberating dissolved gas and creating a two phase fluid." The liberated bubbles "persist within the pressure region thereby reducing the hydrodynamic pressure." An increase in the supply pressure yielded less cavitation, less bubbles, and higher, closer to predicted hydrodynamic pressures.

The effect of compressibility when ignored in a design can yield improvement or degradation in the desired vibrational response of a SFD. The authors suggest designing SFD in the range where the incompressible Reynolds equation works well or do experimental testing of the design because the influence of a two-phase fluid on a viscous damper is complex.

In 1979 Holmes of the University of Sussex, U.K., published a study on the control of rotor vibration using SFD with and without a parallel flexible element (12). The experimental and analytical investigation includes a general design philosophy.

SFD with a Flexible Support

A SFD as used in a typical application provides light, non-linear damping which makes it susceptible to two classical disadvantages of such a damper, jump phenomenon and subharmonic resonance instability. Holmes

notes that, as earlier shown by Hahn, jump can only occur when cavitation is present, but cavitation is not necessary for subharmonic resonance to occur.

The experimental test rigs had rotors (one rigid, one flexible) mounted on journal bearings supported with SFD and centrally located with adjustable springs.

The results from the rigid rotor test rig showed good agreement with conventional Reynolds theory for a fully pressurized, uncavitated damper. Note the agreement with Hibner and Bansal on this point. When cavitation is present, the author suggests that the uncertainty of the extent of the cavitation makes theoretical predictions difficut. Holmes recommends that the supply pressure should be as high as possible for the particular design to reduce the extent of cavitation.

For the flexible shaft test rig the optimum squeeze film damping for reducing the maximum shaft amplitude at the first and second critical speeds was found to be about the same for both theory and experiment. For light squeeze film damping (below the optimum) the system was stable and well damped in the entire operating speed range, but for large amounts of damping instability thresholds were observed. For moderate damping (near the optimum value) steady sub-synchronous whirling would appear at a certain speed, grow and die out as speed was

increased. The whirl was indicative of the non-linearity of the damper and journal bearing oil films.

Linear analysis can be used for SFD with parallel flexible supports for damper amplitudes less than one third of the radial clearance. Above this, Holmes suggests a quasi-linear analysis using amplitude dependent stiffness and damping coefficients.

SFD Used Alone as Vibration Isolators

The lift for this type of damper emanates from the non-linear effects of the oil film. Jump phenomenon and subharmonic resonance are also possible for this type of support. Generally, theoretical predictions must be performed with non-linear analysis. For regions near the critical speeds where the dynamic load is much greater than the static load, circular, concentric orbits can be assumed and quasi-linear analysis performed. The extent of cavitation greatly affects the static and dynamic load carrying capacity. In fact, the assumption of an uncavitated film leads to an elimination of the load carrying capacity. This appears to be in agreement with Hahn's statement that flexible supports in parallel with the SFD are necessary for stability for pressurized dampers.

The experimental test rig consisted of a rigid rotor mounted on rolling contact bearings supported by SFD with no end seals. A negative pressure region (about -40 psi) was measured suggesting that tension forces may

exist. The measured pressure peaks and dynamic forces were less than predicted by a conventional short-bearing solution of the Reynolds equation. Holmes, in agreement with Bansal and Hibner's previous paper, suggests that cavitation bubbles trapped in the oil film are responsible for the lower pressure peaks. Since the journal of a SFD does not rotate, there is no inducement for the bubbles to leave except the supply pressure. The author showed that by varying the cavitation extent, the theoretical model for the pressure distribution could be adjusted to agree with experimentally measured pressures.

In 1980 and 1981, Cookson and Kossa published the results of their experimental and analytical investigations into the effectiveness of SFD, without parallel flexible supports, used for supporting flexible rotors (13,14).

The short-bearing approximation of the Reynolds equation was used with a 180° film model, thus assuming atmospheric inlet and outlet oil flow conditions (no end seals, low inlet pressure). In developing the equations of motion, the rotor was assumed to be symmetric, with its mass lumped at the bearing stations and at the middle of the rotor. The theoretical analysis required constant speed and that the rolling contact bearings introduced no exciting forces (no source for generation of whirl instability).

Four simultaneous non-linear differential equations were developed as the equations of motion for the system with the damper journal and rotor disc displacements and velocities as the independent variables. The solutions of the equations were found to be dependent on six independent dimensionless parameters three for the damper and three for the flexible rotor system. The equations were integrated forward in time for certain values of the system parameters yielding steady state solutions.

The experimental test rig consisted of a disc centrally located on a rotor mounted in rolling contact bearings supported by SFD. Interchangeable damper parts produced a wide range of bearing and gravity parameters;

$$B = \frac{\mu R h^3}{m_B \omega_c C^3}$$

$$W = \frac{g}{C\omega_c{}^2}$$

A circumferential groove in the damper housing provided the oil inlet. Oil supply pressure was kept low (about 2 psi) and no end seals were used. Noncontacting transducers measured the disc and journal orbits.

The predicted orbits and the measured orbits were found to be similar. Disc amplitude vs. frequency plots showed a smooth transition through the critical

speed, not a "peaky" response. The maximum amplitude still occurred approximately at the pinned-pinned critical speed. The authors suggest that the dampers operate by allowing for bearing movement instead of disc movement (for a flexible rotor). Remember that, as Hahn noted, for a rigid rotor the price of vibration isolation is shaft movement.

The theory was reasonably accurate in predicting the experimental results for the response curves and for the orbits for various parameter combinations. The authors suggest that a better film model would have improved the correlation.

A vertical rotor could be analyzed by setting the gravity parameter equal to zero. For this case, the rotor orbits become circular and concentric as noted by Holmes for rotors with light static loading.

The orbit amplitudes were found to vary little for a wide range of values of the bearing parameter, suggesting that the land length is not an important parameter. In general, for greatest damper efficiency, Cookson and Kossa recommend that:

1) The mass ratio, M. should be kept small. This allows for freer movement of the damper journals. Note the agreement with the 1975 paper by Cunningham, Fleming, and Gunter for

a SFD with flexible supports supporting a flexible rotor.

2) the bearing parameter should be approximately equal to .1.

3) the gravity parameter should be less then .1 (light static/dynamic load ratio). This also allows for freer movement of the damper journals.

The authors recommend a transient analysis for shock loading situations.

CHAPTER 3

EXPERIMENTAL SET-UP

The rotor system was designed for use on a Bently-Nevada rotor dynamics test rig. The rotor was powered by a 1/10 horsepower infinitely controllable drive motor capable of driving the test rotor at speeds in excess of 10,000 RPM. The system included a shaft supported by two sets of preloaded duplex ball bearings, with each duplex set mounted in an uncentralized SFD. A quill shaft was used to couple the motor and rotor. Rotor discs of various weights could be located at any position between the bearing stations. See Figure 3.1

The preloaded duplex ball bearings provided for stiff bearing-rotor coupling, so that the bearings could be assumed to be rigid in comparison with the rotor and damper film. The preload on the bearings also increased the rolling friction which decreased the maximum attainable rotor speed and increased heat generation.

The ball bearing housings which preloaded the duplex bearings acted as the damper journals. The damper journal diameters were 3.3125 inches; the journal land lengths were .475 inches. So, the length to diameter

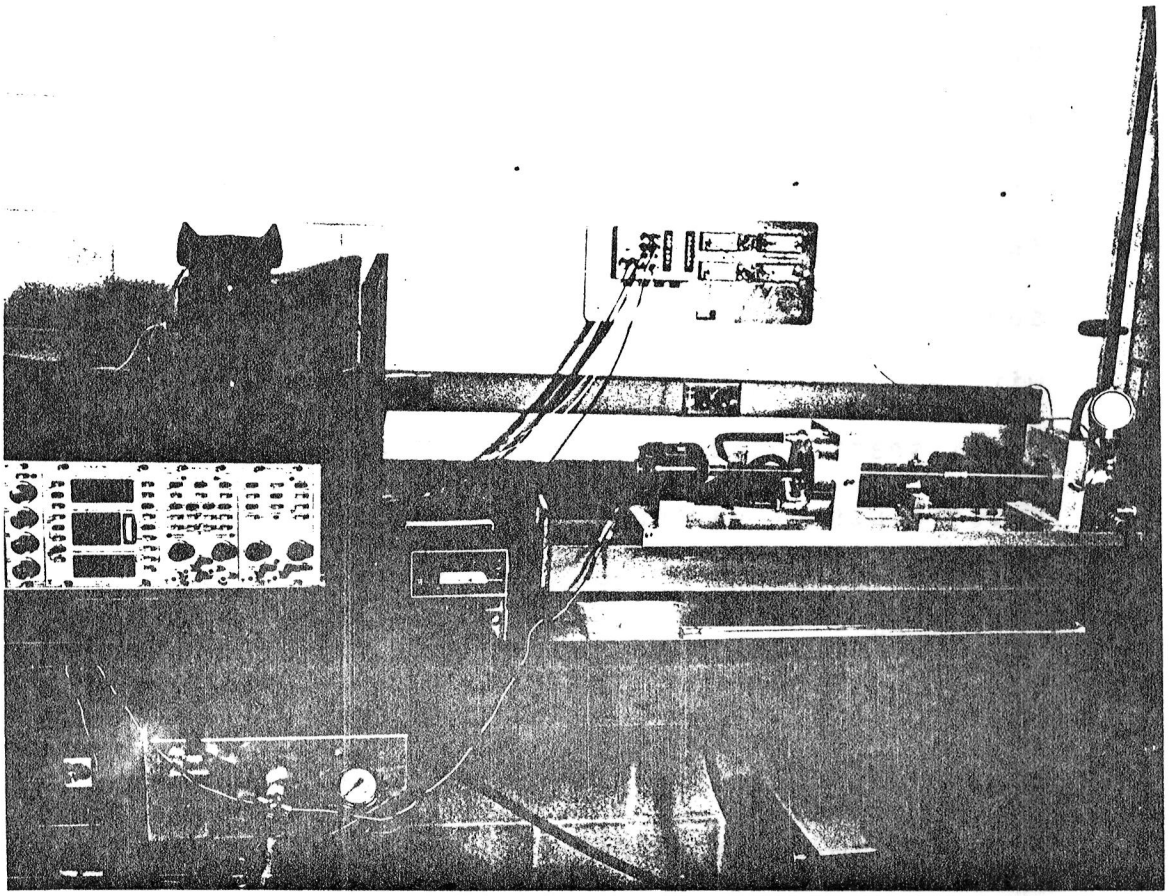

Figure 3.1 Experimental Test Facility Rotor

ratio was .143, suitably short for a short bearing approximation of the Reynolds equation to apply.

The damper housings had interchangeable inserts allowing the radial clearance for the fluid annulus between the damper bearing and journal to be varied from .004 to .020 inches. Sealing between the journal and damper bearing was accomplished with O-rings in shear. The lateral clearance between the damper journal and housing was dimensioned to yield .007 inches of "squeeze" on each O-ring. This amount of O-ring squeeze was determined with a trial and error approach to be near the optimum, sealing adequately under the required oil pressure yet contributing minimal impedance to journal motion. Circumferential grooves with outlet ports were located in the sides of the damper housings at the edges of the fluid film annulus. Ports were also provided to check the static oil pressure in the grooves at the end of the annulus with a pressure gauge. Also, inlet and outlet ports were located centrally in the damper inserts and housings at the top and bottom of the dampers. Flow metering valves at the outlet ports allowed for the end seal or no end seal conditions (or any amount of end leakage or end pressure desired). On/off valves at the inlet ports allowed for circumferential groove or port oil feed into the damper annulus. With the appropriate ports closed or open the damper configuration could be

modeled validly by either the short or long bearing approximation of the Reynolds equation. An antirotation pin was threaded through the outside of the damper housing, through the inserts and into an oversized hole in the journal, allowing journal translation but not rotation. See Figure 3.2. Also see Appendix B for drawings of damper parts.

The steel rotor shaft was 13/16 inches in diameter and 12 inches long between bearings. The quill shaft used as the flexible coupling between the motor and the rotor was 6 inches long and an 1/8 inch in diameter. See Appendix A for rotor and quill sizing calculations. The flexible coupling eliminated the need for exact alignment of the motor and the two rotor bearings. Two rotor discs could be located at any position between the bearings with set screws. Each rotor disc had threaded holes through its thickness located symmetrically about its outside circumference for the positioning of balancing weights. The discs were modeled after those that were furnished with the Bently-Nevada test rig. With both discs axially centered on the shaft, the first flexible mode could be excited.

A gear pump was used to pump the oil from a heated bath through the SFD. A metered bypass line provided a wide range of damper inlet pressure and flow rate. Heating the SAE 10W oil provided a wide range of damper

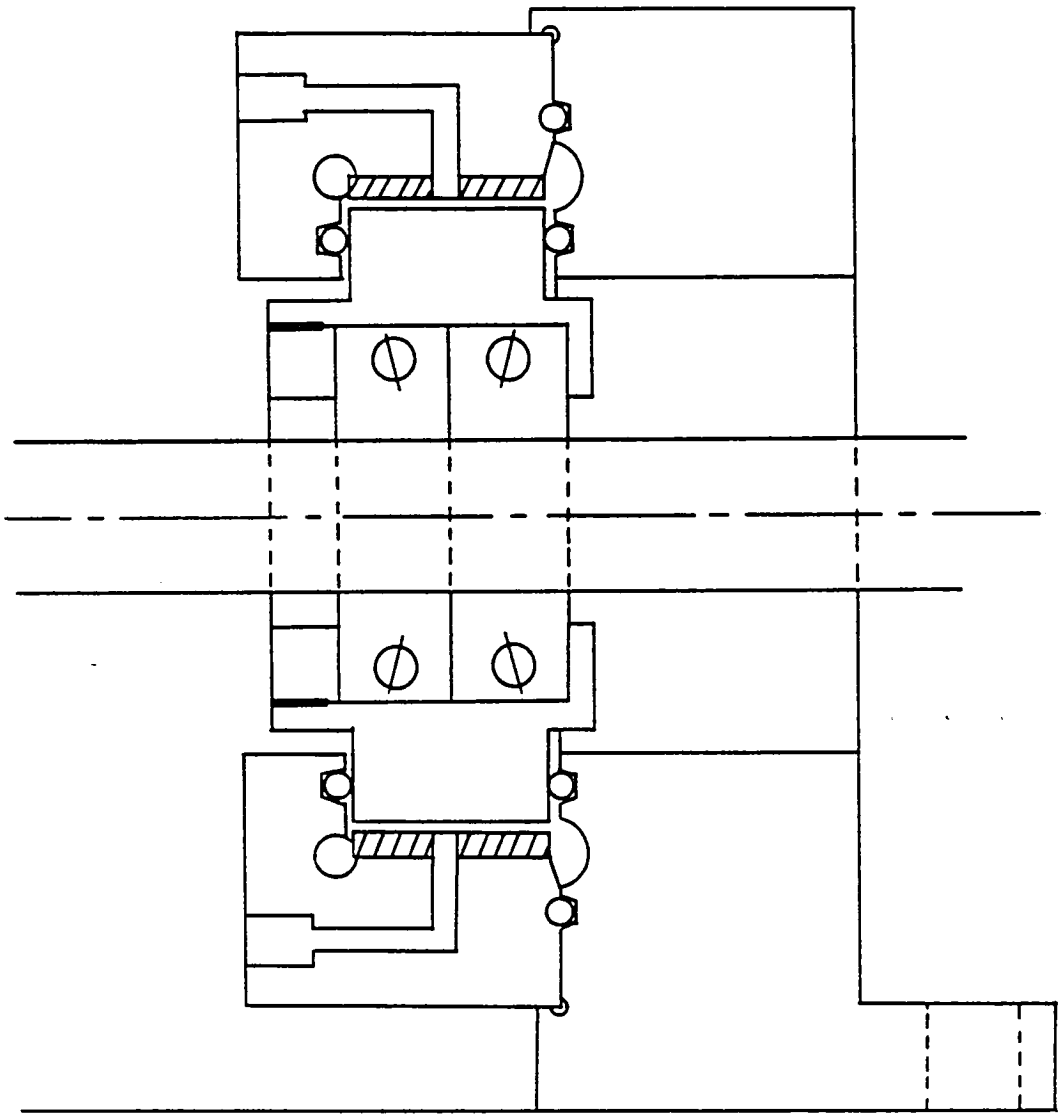

Figure 3.2 Schematic Side View of Experimental Damper Bearing Configuration

fluid viscosity. Copper-Constantan thermocouples were used to monitor the oil inlet and outlet temperatures from the dampers. A thermalwell was used for monitoring the pressurized inlet temperature.

Vibration detection was accomplished with Bently-Nevada non-contacting proximity displacement transducers. The output of the proximitors was wired into a digital vector filter (DVF2) also manufactured by Bently-Nevada. The DVF2 provided a digital readout of peak to peak displacement, RPM, and phase angle for location of the rotor's "high spot" for balancing. Two Tektronix oscilloscopes, an X-Y-Y plotter, and an HP spectrum analyzer were also useful aids in studying and recording vibrational response. The spectrum analyzer was especially useful for investigating nonsynchronous responses. A five thermocouple input, digital readout potentiometer was used to monitor oil temperature into and out of the SFD. See Appendix B for the wiring diagram.

CHAPTER 4

EXPERIMENTAL METHOD AND PURPOSE

The initial purpose of the experimentation was to verify that the test apparatus could work properly as designed and that operational data could be taken as desired. Once the system was debugged the next step was to conduct a brief parametric study.

The parameters that could be varied for both the "short" and "long" bearing configurations of the damper were as follows:

1) rotor speed
2) unbalance
3) clearance
4) oil temperature
5) oil inlet pressure

The second purpose was then to discover the effect on the rotor system's performance of varying each parameter while holding the others constant. Comparisons could then be made with other authors results and with a simplified analysis and conclusions made.

The third and final purpose was to recommend possible improvements to the test equipment and to suggest further work.

Bode plots of peak to peak amplitude and phase vs. rotor speed could be made at both damper locations and at any point along the shaft for both x and y positions. Also, damper and shaft orbits could be obtained and photographed for a particular rotor speed. The orbits (oscilloscope tracings) have a gap in them made by a reference mark useful for phase studies. The phase mentioned here is the angle between the high spot of the rotor and a reference mark on the shaft. The meaningful information is the change in this angle with speed (denoting changes of angles between the high spot and the unbalance position).

The first task was to balance the rotor after the system was assembled with the null-clearance inserts in the dampers providing "rigid" bearing supports. The DVF2 aided in this endeavor. Figure 4.1 shows the midspan vibrational response of the balanced rotor. Note that all Bode plots were made from a location two inches from the midspan location. Comparing with the other plot on the same figure for a small unbalance, it can be seen that the residual unbalance is small. The sharp critical speed response on Figure 4.1 and the abrupt phase change shown on Figure 4.2 for a small unbalance demonstrates the high stiffness and lack of damping of the ball bearings. The first critical speed of the rotor can be seen to be about 9200 RPM.

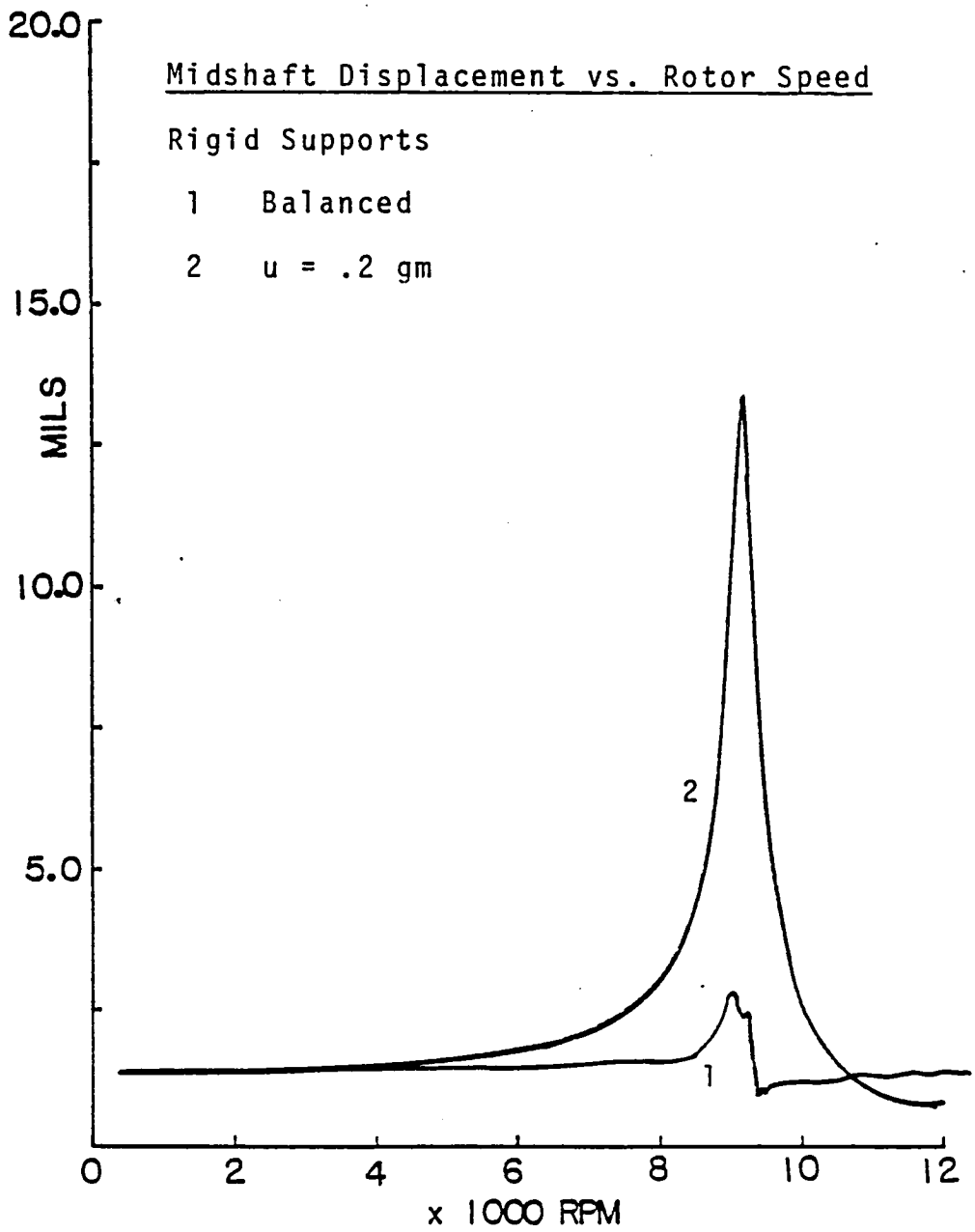
Midshaft Displacement vs. Rotor Speed
Rigid Supports
1 Balanced
2 u = .2 gm
20.0
15.0
10.0
5.0
MILS
0
2
4
6
8
10
12
x 1000 RPM
1
2

Figure 4.1

Midshaft Phase vs. Rotor Speed

Rigid Supports

u = .2 gm

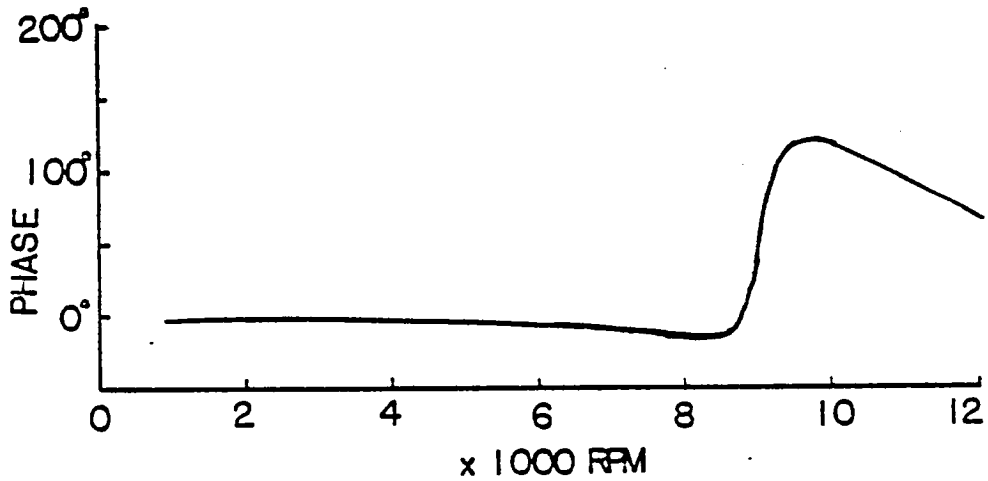

Figure 4.2

In practice, the four damper mounting screws on each SFD were used to adjust the O-ring squeeze to seal adequately, yet contribute minimal impedence to journal motion. Shims were then required to restrain the damper bearings from vibrating relative to their respective housings.

When damper orbit studies were made the GAP button on the DVF2 was used to obtain the approximate orbit center coordinates within the clearance circle. The GAP button provides a measure of the distance between the proximotor probes and the rotor. This method was also used to measure the radius of each clearance circle.

Figure 4.3a and b are examples of typical photographs of the damper and shaft orbits, respectively, taken from oscilliscope tracings. The rotation of the shaft is clockwise with respect to all orbits presented in this paper. Copies of each orbit photograph of interest were reduced to their proper scale, and placed in the correct position and orientation on drawings of their particular clearance circle. This was done because knowledge of the location (offset from center) of the orbit within the clearance circle was found to be useful.

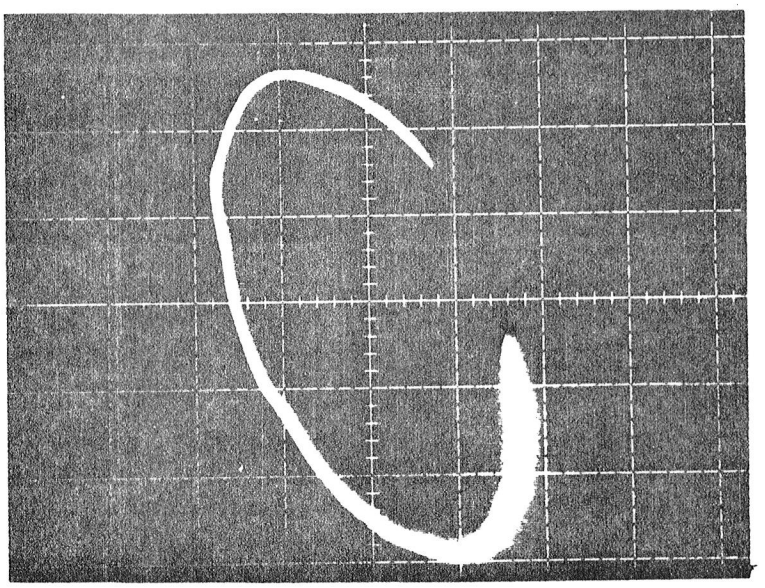

a. Damber Orbit, Groove Inlet, c = .01", 80°F, 9000 RPM, 10 psi, 3.0 gm unbalance, 1 MIL/DIV.

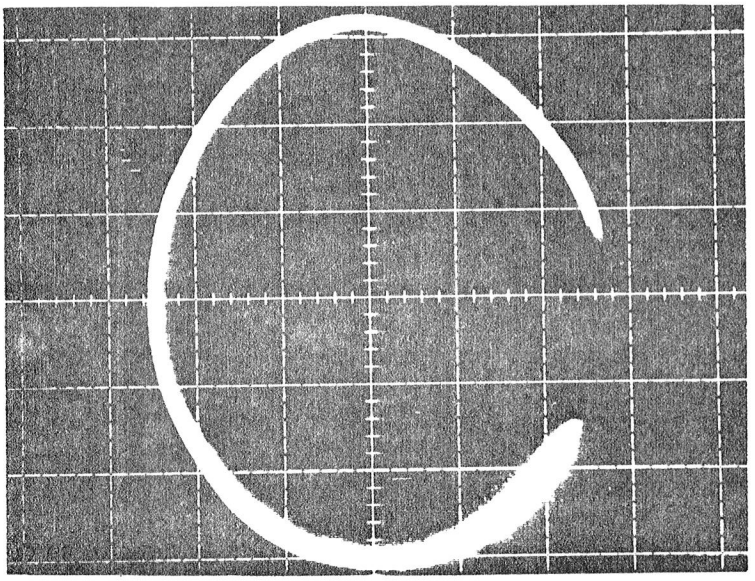

b. Shaft Orbit, same as above except 2 psi, 2.5 MIL/DIV.

Figure 4-3. Photographs of Oscilliscope Tracings of Damper and Shaft Orbits

CHAPTER 5

RESULTS

The experimental results are presented here for the rotor system supported by SFD without end seals (annular oil inlet/outlet) and with end seals (port inlet/outlet).

SFD Without End Seals

Figure 5.1, a superpositioning of four separate damper orbits, shows the effects of changing the unbalance while holding the other parameters constant. Increasing the unbalance increased the vibration of the rotor which resulted in a further "lifting off" of the dampers from the bottom of the clearance circle as well as larger elliptical orbits.

Figures 5.2 through 5.6 show amplitude plots of the rotor's x-axis for different values of unbalance. Note that the trends are consistent despite the clearance size. All cases show that at least as a small amount of effective damping was present, yielding a response superior to the "rigid" response of Figure 4.1. This is apparent from the lower amplitudes and the less abrupt phase shifting with additional dissipation. As more unbalance

Damper Orbits Relative to Clearance Circle

Groove Feed, 80°F, P_{in} = 2 psi, 9000 RPM

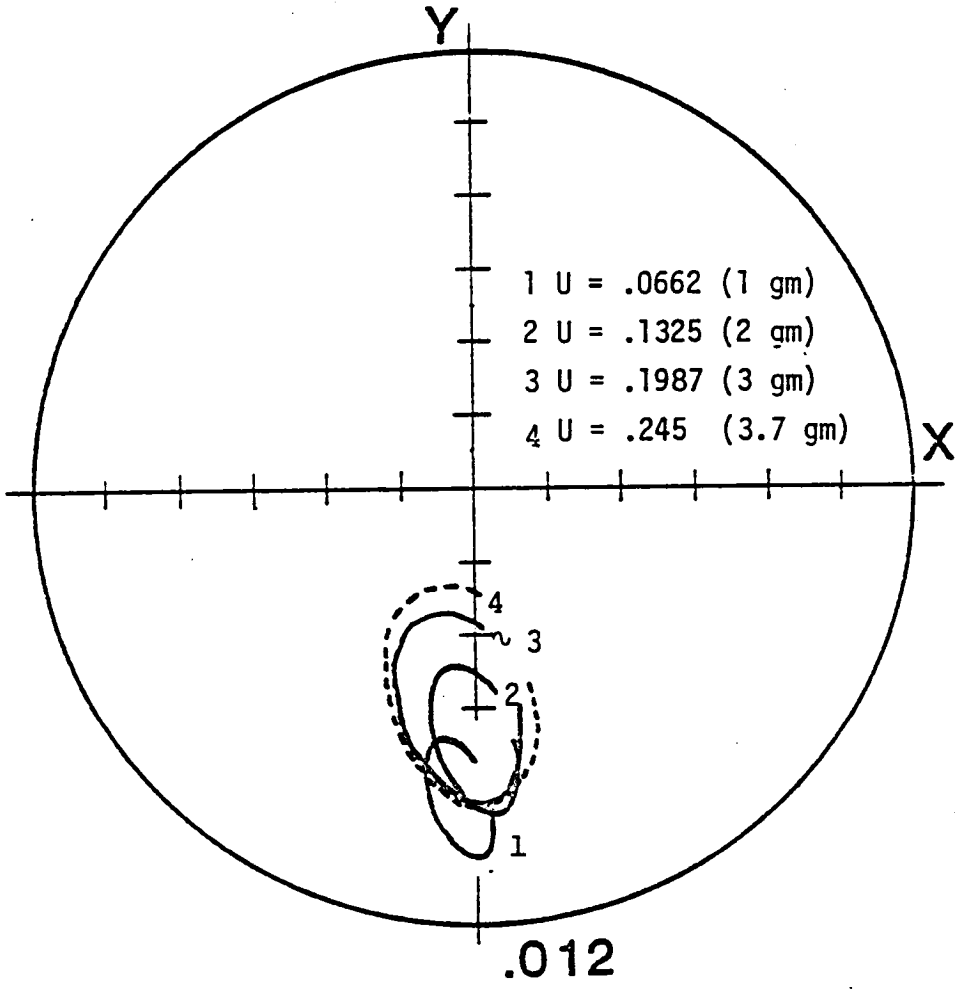

Figure 5.1

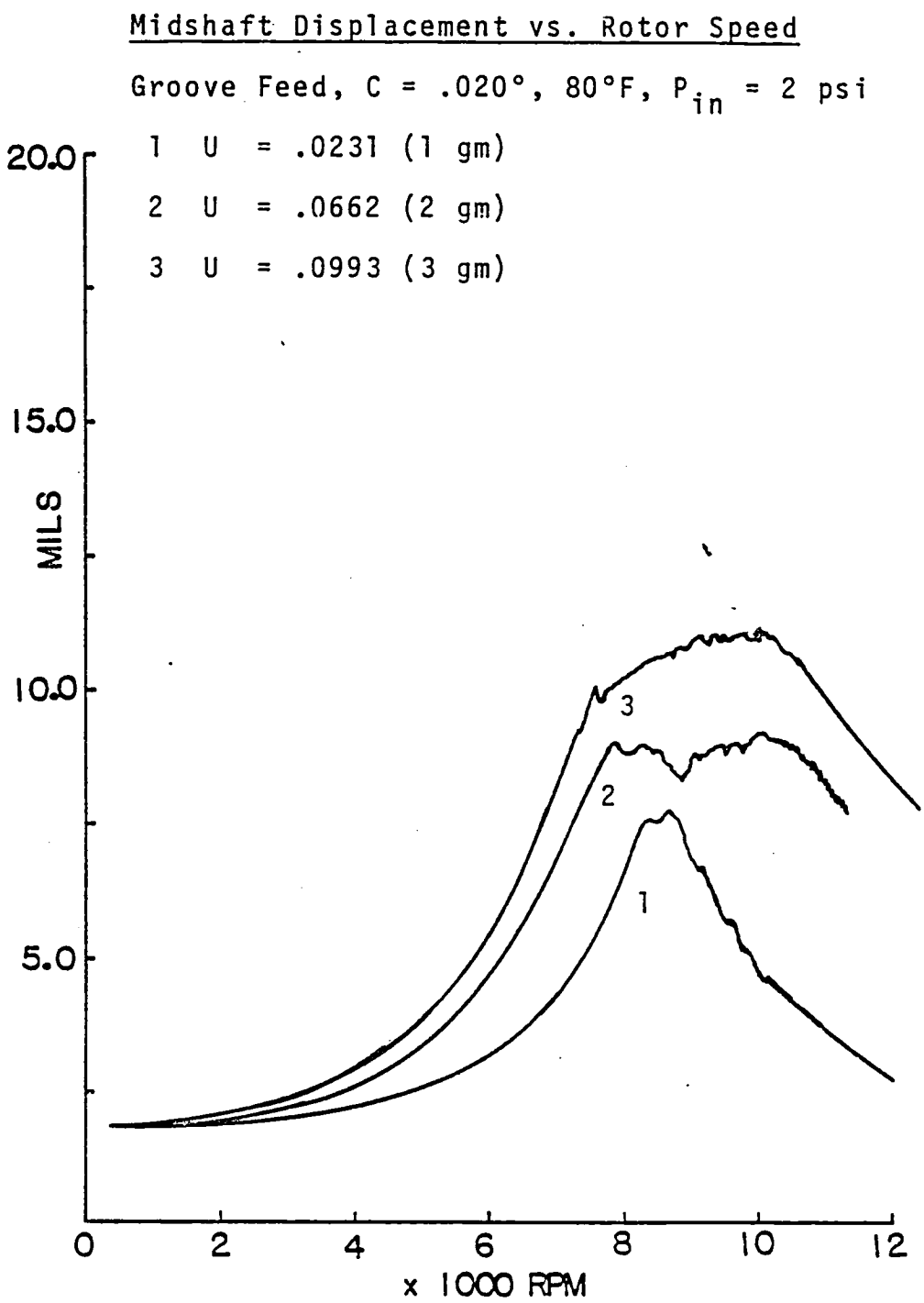
Midshaft Displacement vs. Rotor Speed
Groove Feed, C = .020°, 80°F, P_{in} = 2 psi
1 U = .0231 (1 gm)
2 U = .0662 (2 gm)
3 U = .0993 (3 gm)
20.0
15.0
10.0
5.0
MILS
0
2
4
6
8
10
12
x 1000 RPM
1
2
3

Figure 5.2

Midshaft Phase vs. Rotor Speed

Groove Feed, 80°F, C = .010", P_{in} = 2 psi

1 U = .0662 (1 gm)

2 U = .1987 (3 gm)

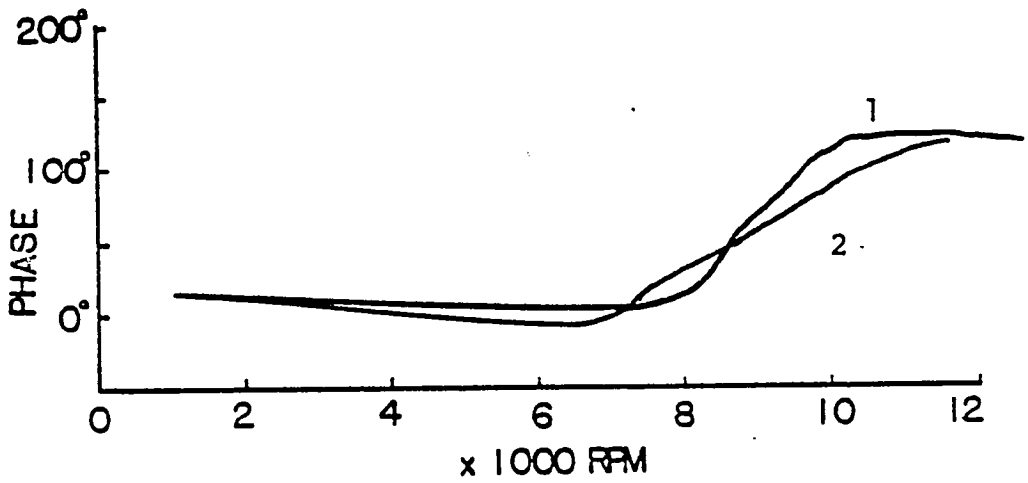

Figure 5.3

Midshaft Displacement vs. Rotor Speed

Groove Feed, C = .010", 80°F, P_{in} = 2 psi

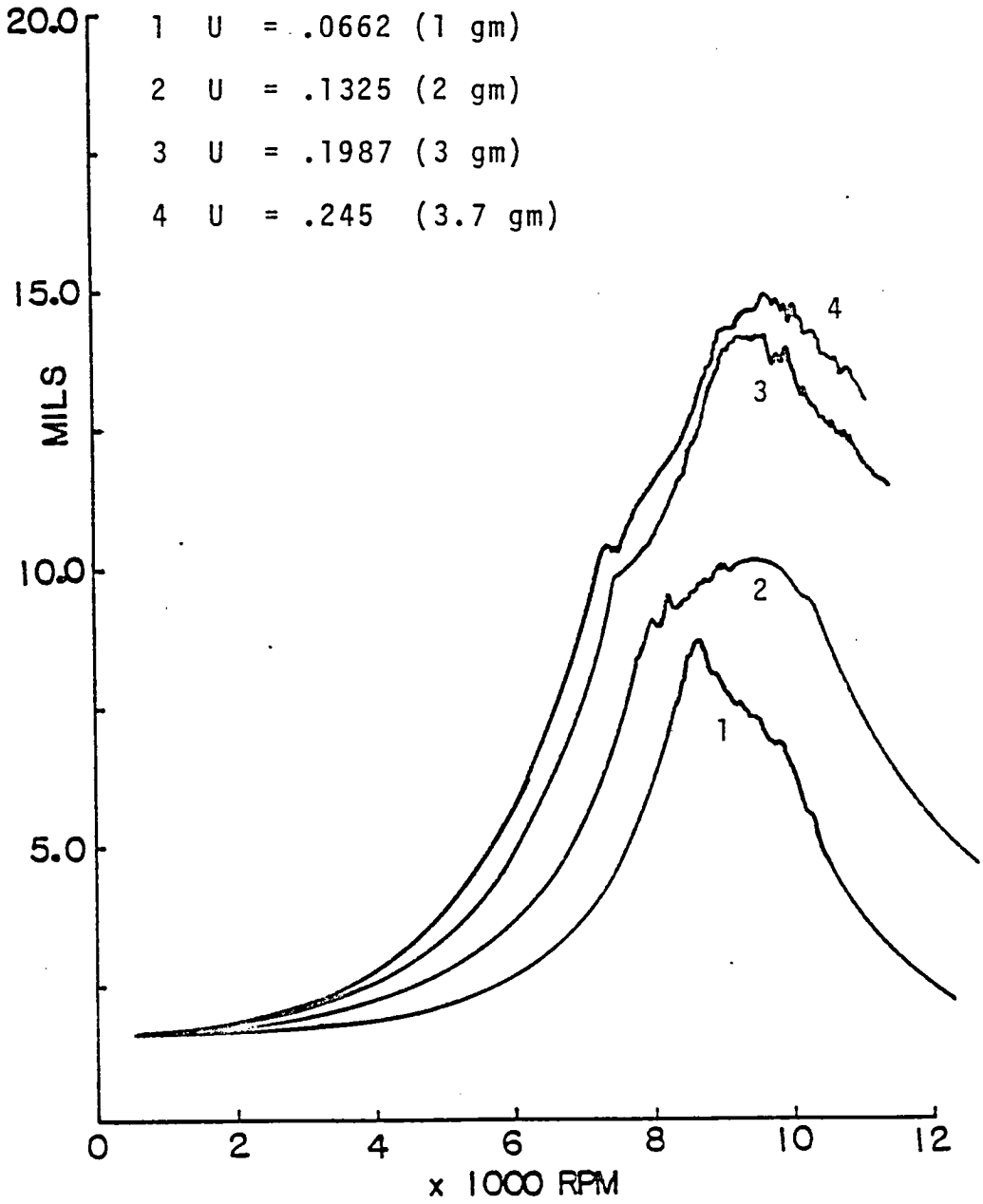

Figure 5.4

Midshaft Phase vs Rotor Speed

Groove Feed, 80°F, C = .006", P_{in} = 2 psi

1 u = 1 gm

2 u = 2 gm

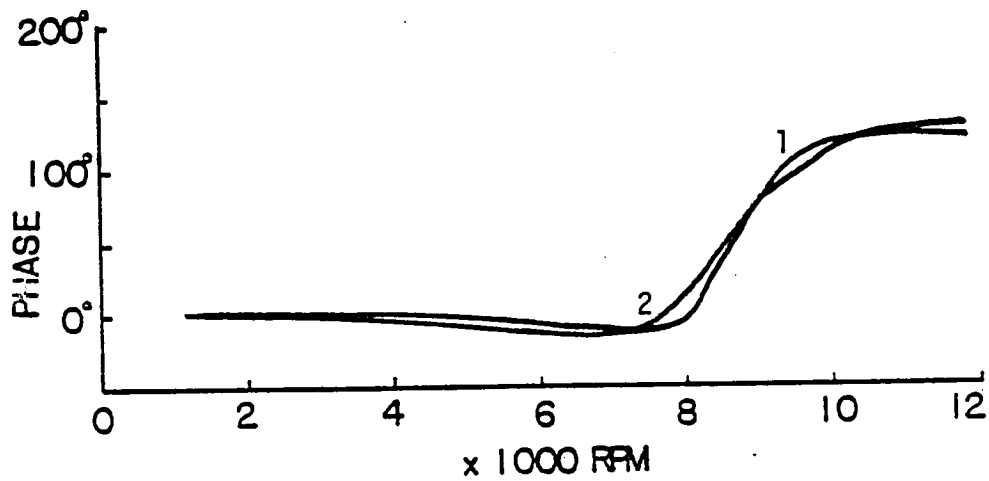

Figure 5.5

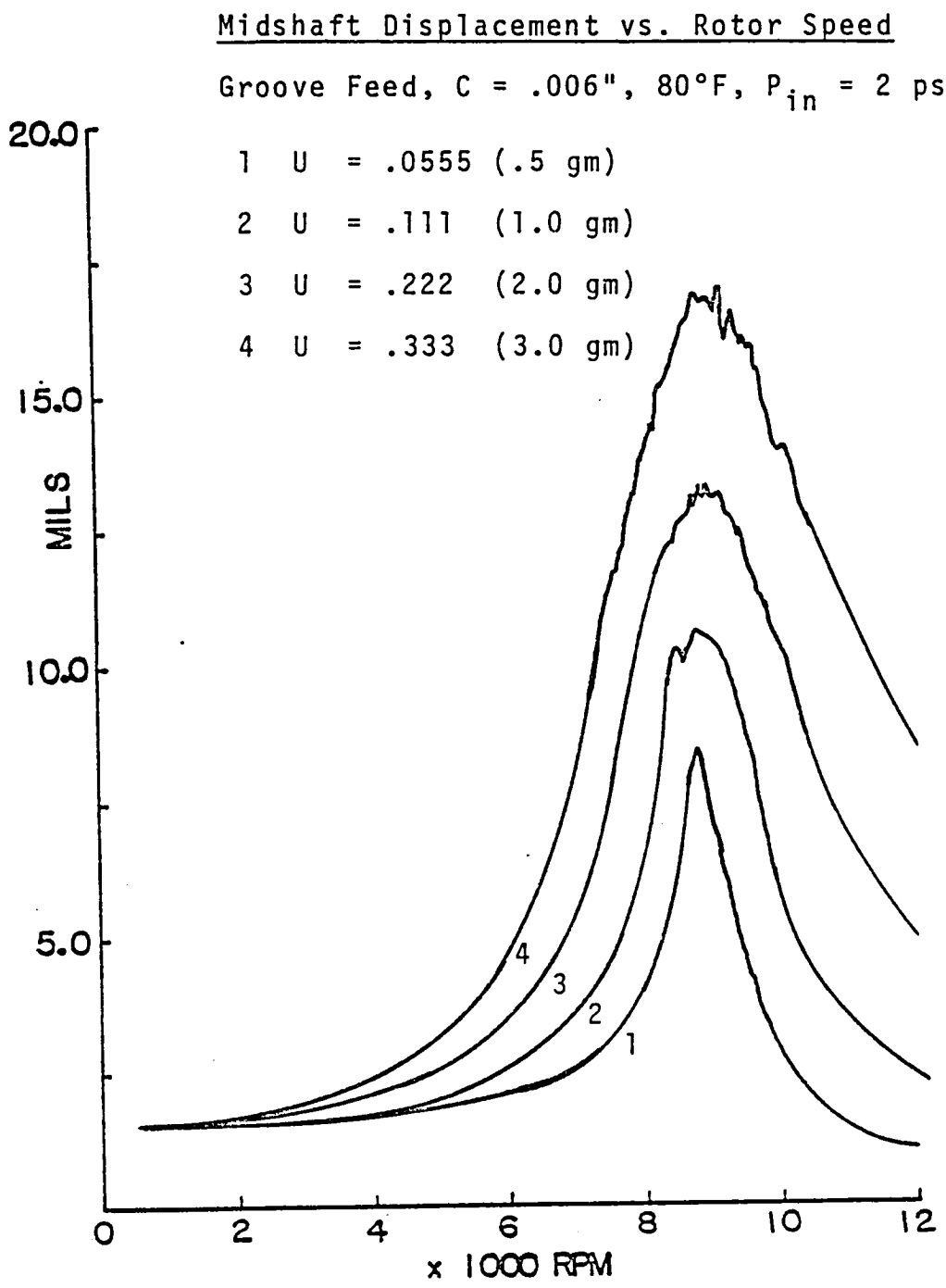
Midshaft Displacement vs. Rotor Speed
Groove Feed, C = .006", 80°F, P_{in} = 2 psi
1 U = .0555 (.5 gm)
2 U = .111 (1.0 gm)
3 U = .222 (2.0 gm)
4 U = .333 (3.0 gm)
20.0
15.0
10.0
5.0
MILS
0
2
4
6
8
10
12
x 1000 RPM
1
2
3
4

Figure 5.6

was applied, larger orbits were observed and the effective damping increased, displaying the amplitude dependent damping characteristics of the SFD. As noted by Cookson and Kossa for this type of dampers, the critical speed did not change appreciably. As will be described later, damping tended to decrease the critical speed slightly. This shows that SFD act only as energy dissipators not as springs in series with the rotor. Note that the resonance peaks are not well defined, appearing as eroded versions of what they might have been with "rigid" supports. The onset of a noise which was taken to be that of cavitation was noted at the peaks where the "erosion" begins. Comparing the plots for the various clearances, it can be seen that larger clearances yielded freer motion of the damper journals and thus "softer" dampers.

Larger clearances yielded more favorable rotor responses (for this system) as seen in Figures 5.7 and 5.8. Considering Figures 5.9,5.10, 5.11, the damper orbits tended to "lift off" and centralize with decreasing clearance. In view of this series of figures, larger more centralized orbits with respect to the clearance circle provided stiffer damping and less dissipation to the system than did offset orbits.

Increasing the inlet pressure delayed and lessened in intensity the cavitation noise noted earlier and,

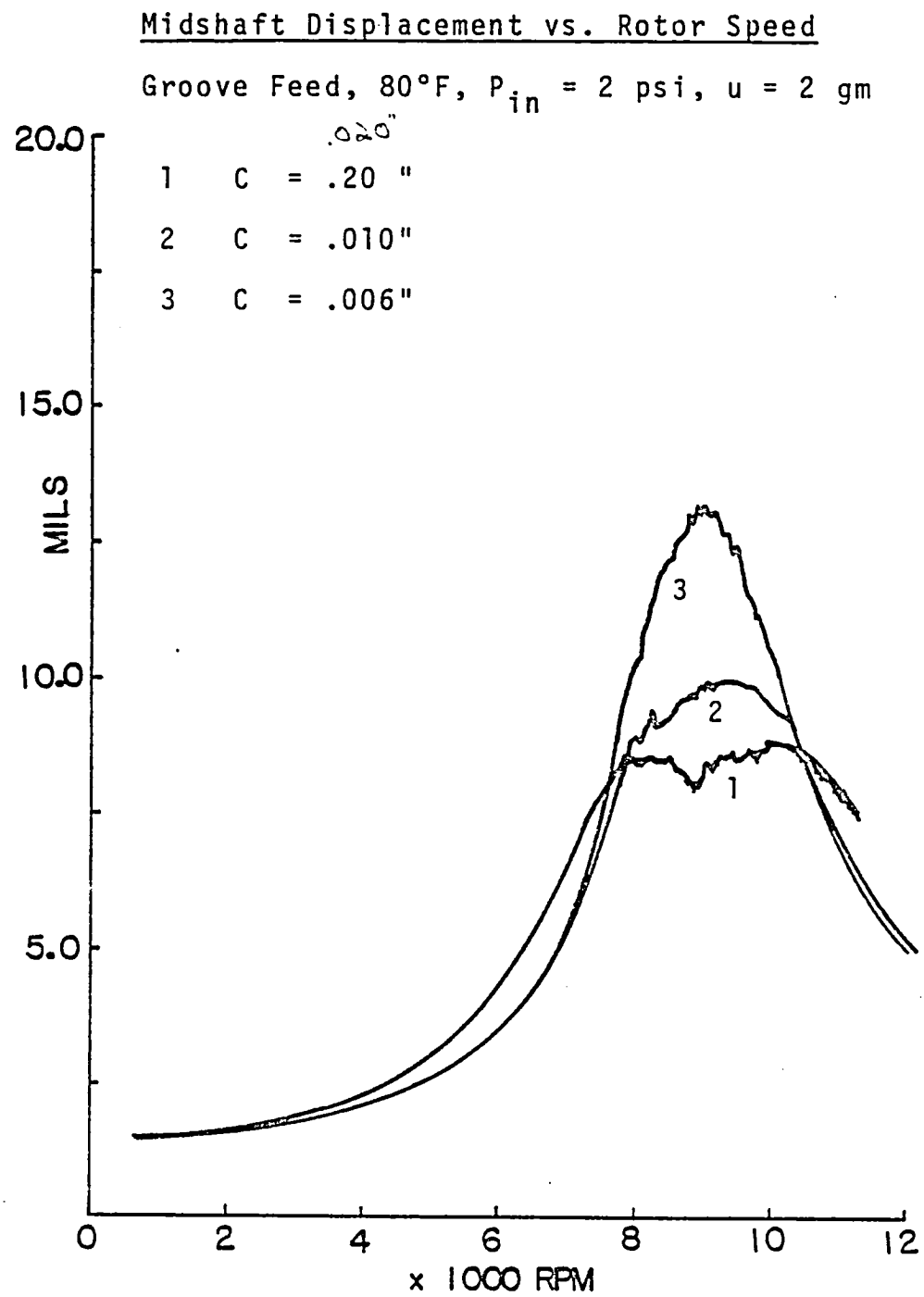
Midshaft Displacement vs. Rotor Speed
Groove Feed, 80°F, P_{in} = 2 psi, u = 2 gm
1 C = .20 "
2 C = .010"
3 C = .006"
20.0
15.0
10.0
5.0
MILS
0
2
4
6
8
10
12
x 1000 RPM
1
2
3

Figure 5.7

Midshaft Phase vs. Rotor Speed

Groove Feed, 80°F, P_{in} = 2 psi, u = 2 gm

1 C = .020"

2 C = .010"

3 C = .006"

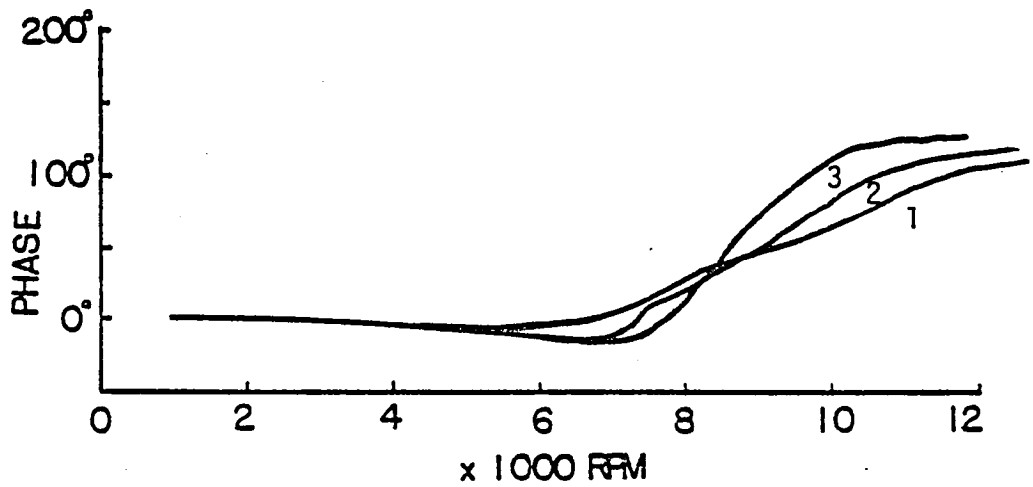

Figure 5.8

Damper Orbit Relative to Clearance Circle

Groove Feed, 80°F, P_{in} = 2 psi, u = 3 gm, 9000 RPM

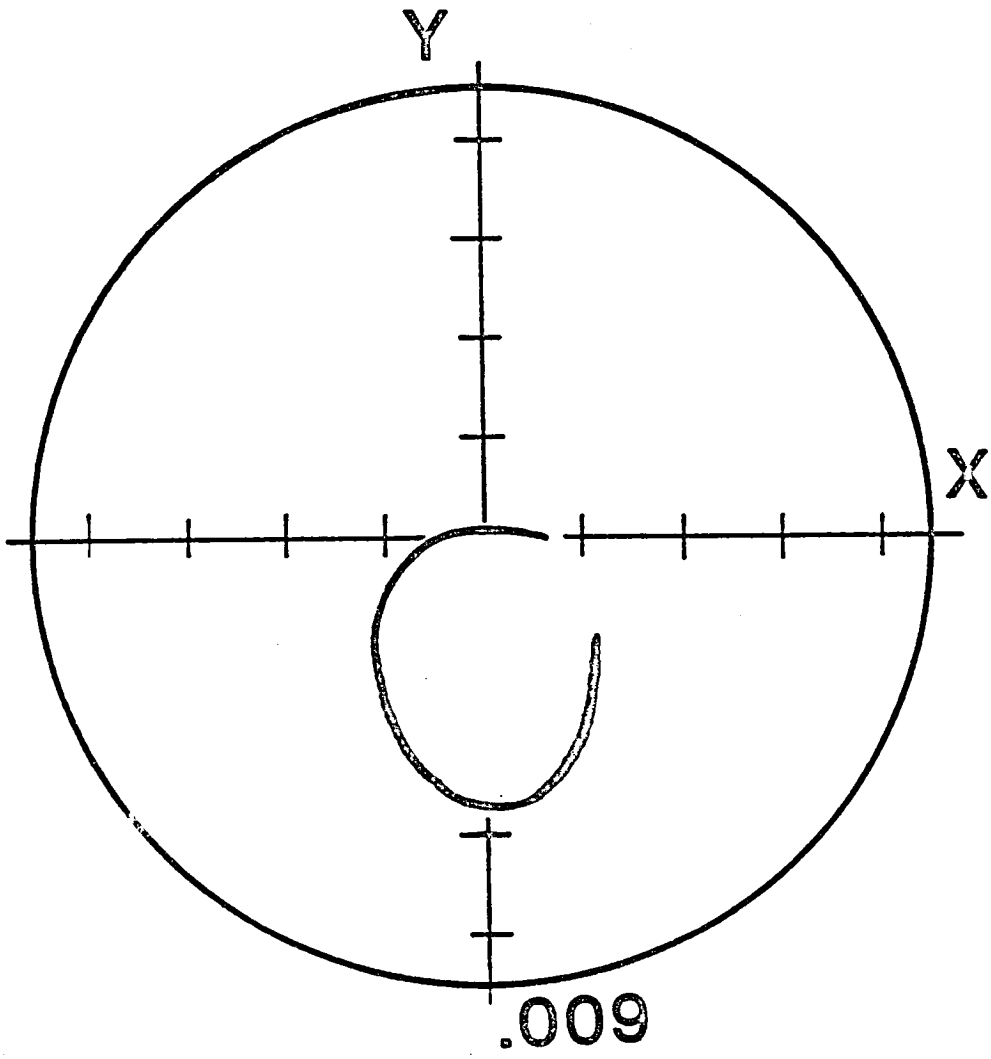

Figure 5.9

Damper Orbit Relative to Clearance Circle

Groove Feed, 80°F, P_{in} = 2 psi, u = 3 gm, 9000 RPM

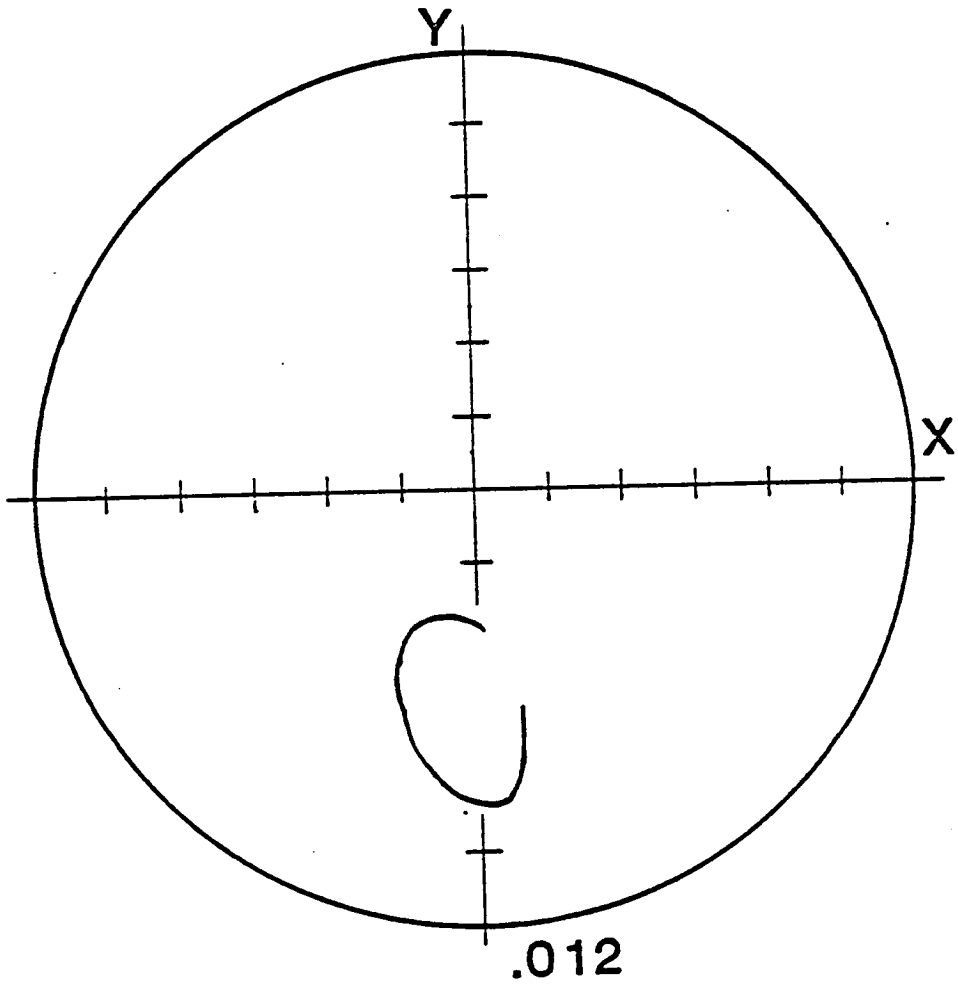

Figure 5.10

Damper Orbit Relative to Clearance Circle

Groove Feed, 80°F, P_{in} = 2 psi, u = 3 gm, 9000 RPM

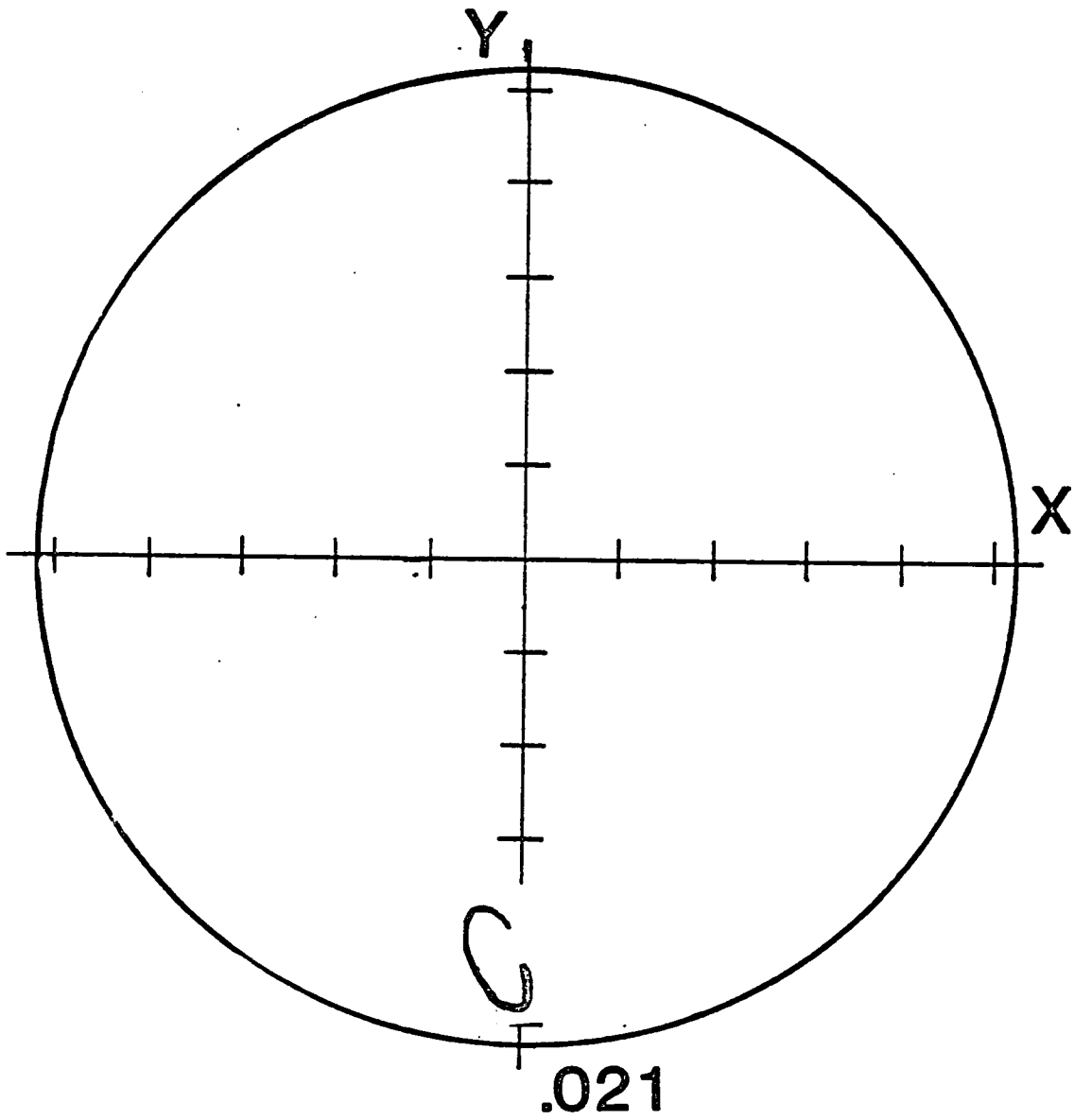

Figure 5.11

considering Figures 5.12 through 5.16, also decreased the dissipation. Again, examining Figure 5.12, cavitation tends to "erode" the resonance peak. In view of Figures 5.17 through 5.20 with increasing pressure the damper orbits tended to increase in size and slightly in offset until a pressure was reached that centralized the journals due to the circumferential inlet effect (see Figure 5.20 for 30 psi). Holmes suggested that less cavitation leads to less load carrying capacity (pg 38) which implies larger orbit offsets in agreement with these results. So, increasing inlet pressure softens the damper but decreases cavitation and energy dissipation. This suggests that cavitation is a powerful dissipating device since less cavitation yielded less dissipation despite the resulting larger orbits and offsets (which tended to increase dissipation).

Figures 5.21 through 5.24 clearly show that raising the oil temperature improved the vibrational response of the system by increasing dissipation. Increasing the temperature lowers the viscosity which allows for freer motion (softening) of the dampers. Figures 5.25, 5.26, show that with higher oil temperatures the elliptical damper orbits are elongated and the offset is increased coinciding as before with increased dissipation.

Figure 5.27 shows damper orbits at three different speeds. As the speed was increased through the

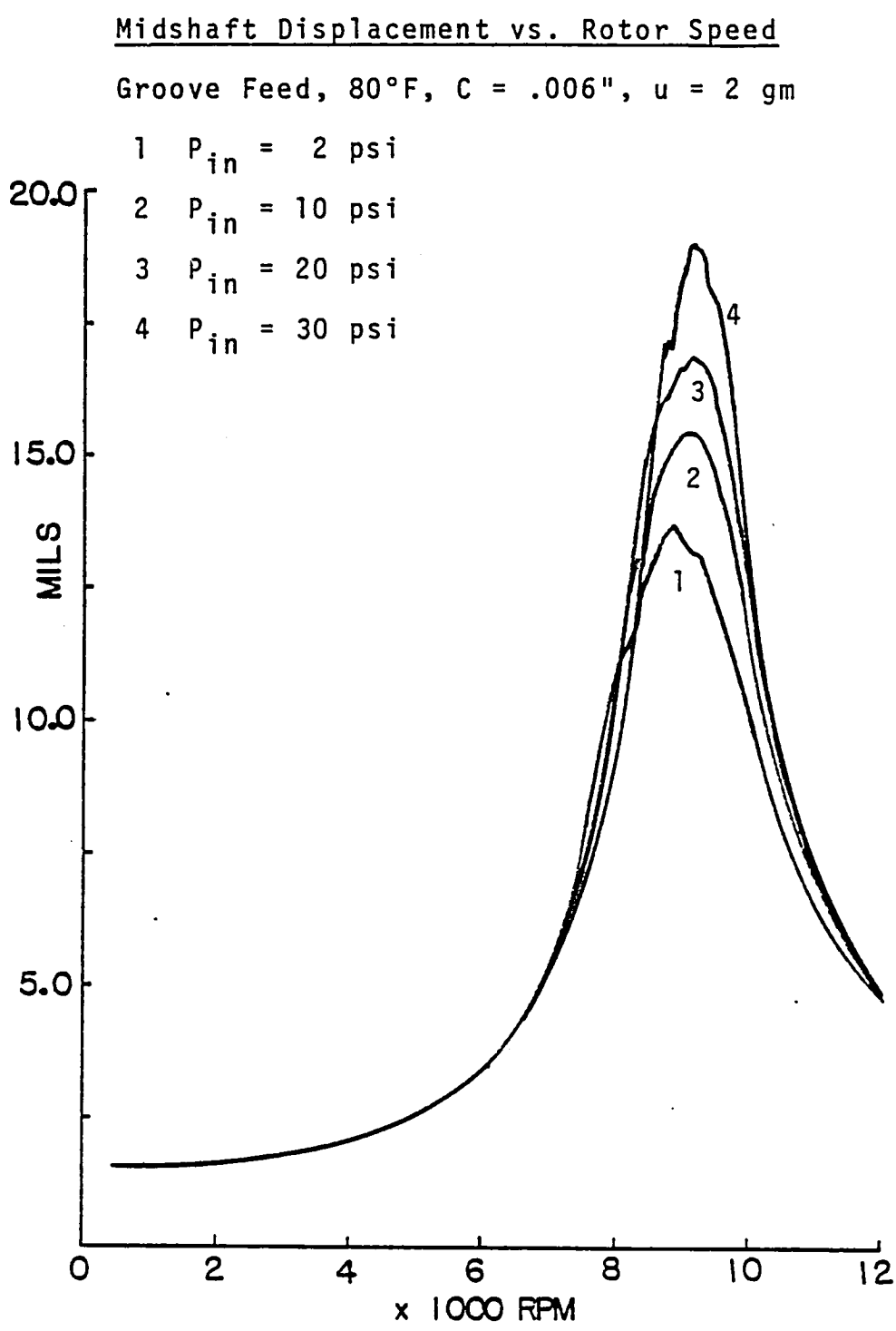
Midshaft Displacement vs. Rotor Speed
Groove Feed, 80°F, C = .006", u = 2 gm
1 P_{in} = 2 psi
2 P_{in} = 10 psi
3 P_{in} = 20 psi
4 P_{in} = 30 psi
20.0
15.0
10.0
5.0
MILS
0
2
4
6
8
10
12
x 1000 RPM
1
2
3
4

Figure 5.12

Midshaft Phase vs. Rotor Speed

Groove Feed, C = .006", 80°F, u = 2 gm

1 P_{in} = 2 psi

2 P_{in} = 30 psi

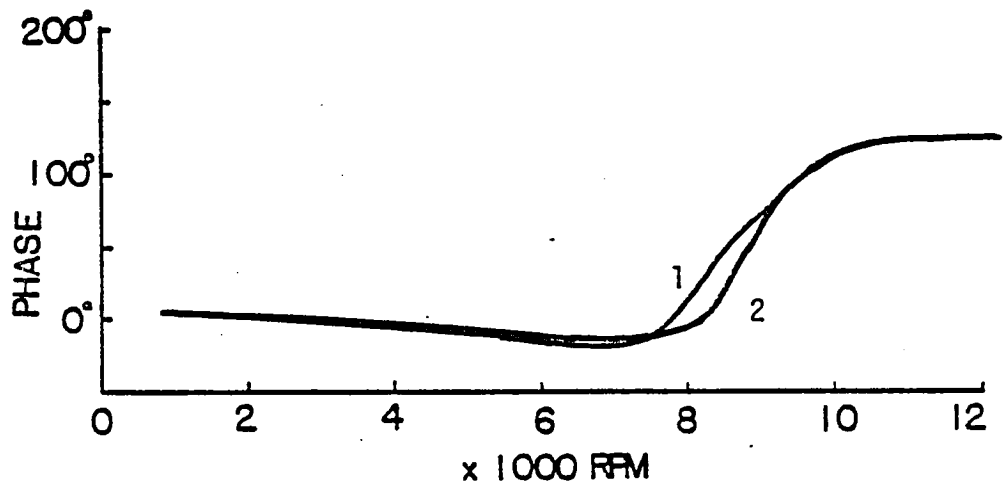

Figure 5.13

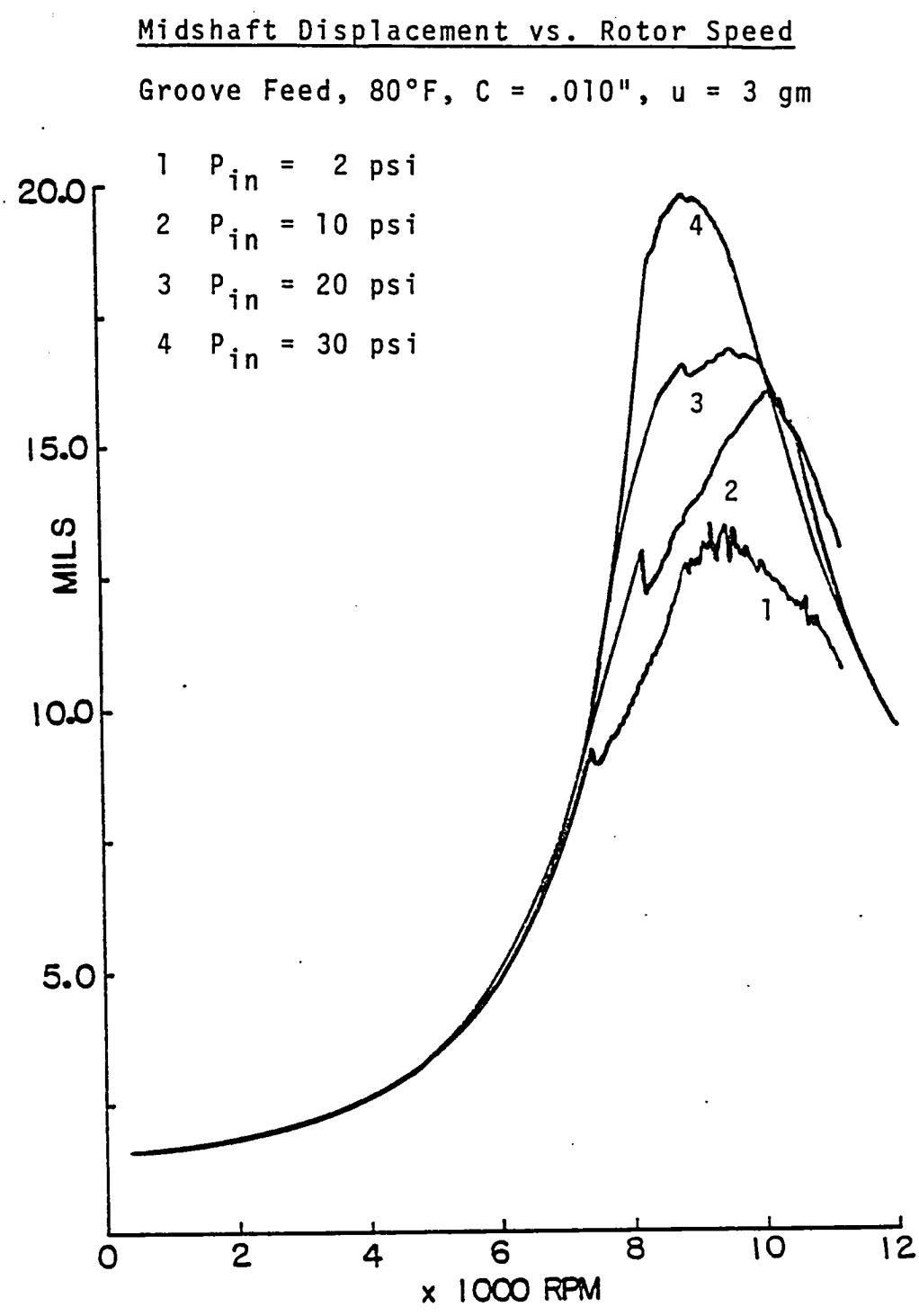
Midshaft Displacement vs. Rotor Speed
Groove Feed, 80°F, C = .010", u = 3 gm
1 P_{in} = 2 psi
2 P_{in} = 10 psi
3 P_{in} = 20 psi
4 P_{in} = 30 psi
20.0
15.0
10.0
5.0
MILS
0
2
4
6
8
10
12
x 1000 RPM

Figure 5.14

Midshaft Displacement vs. Rotor Speed

Groove Feed, C = .020°, 80°F, u = 1 gm

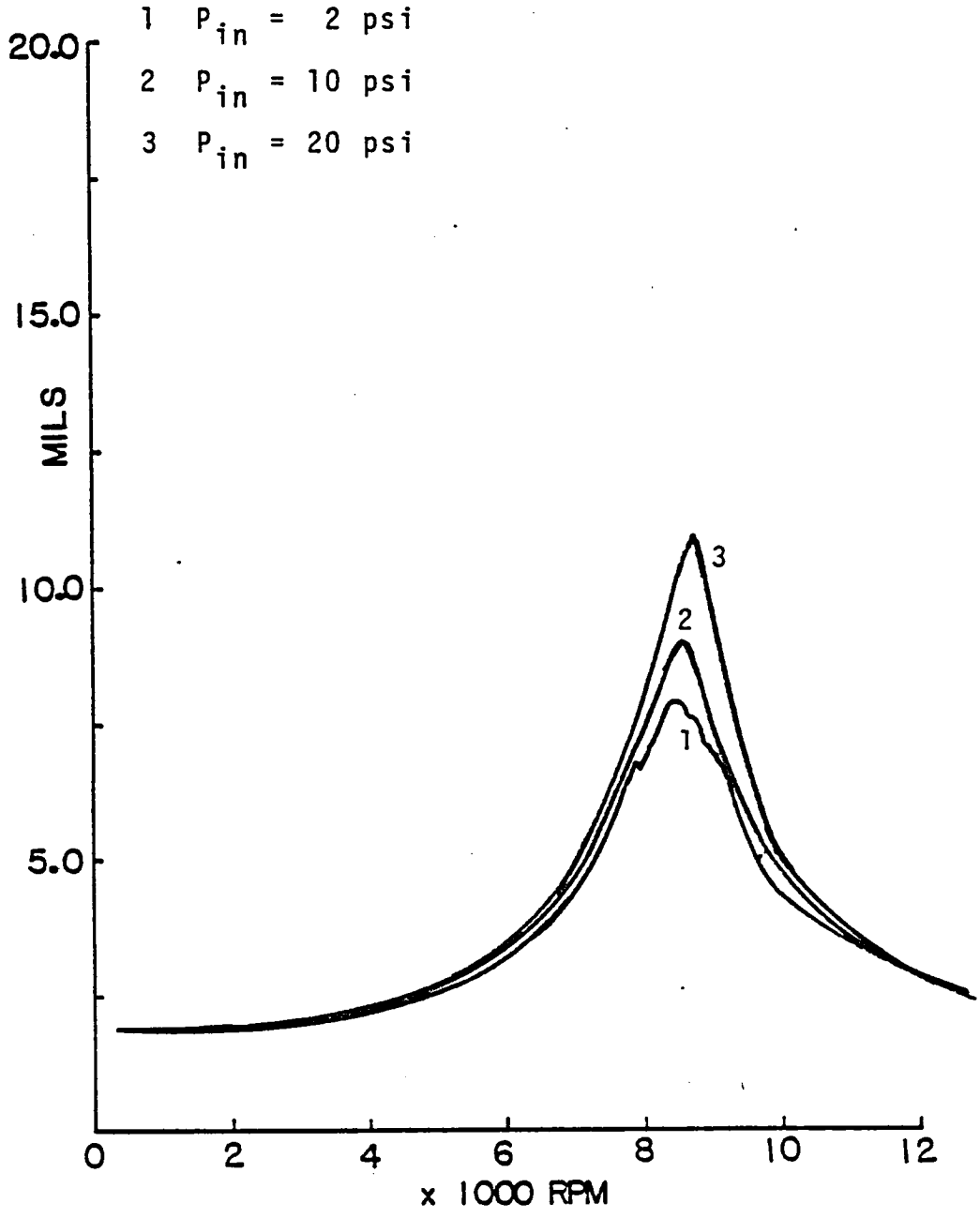

Figure 5.15

Midshaft Phase vs. Rotor Speed

Groove Feed, C = .020", 80°F, u = 1.0 gm

1 P_{in} = 2 psi

2 P_{in} = 20 psi

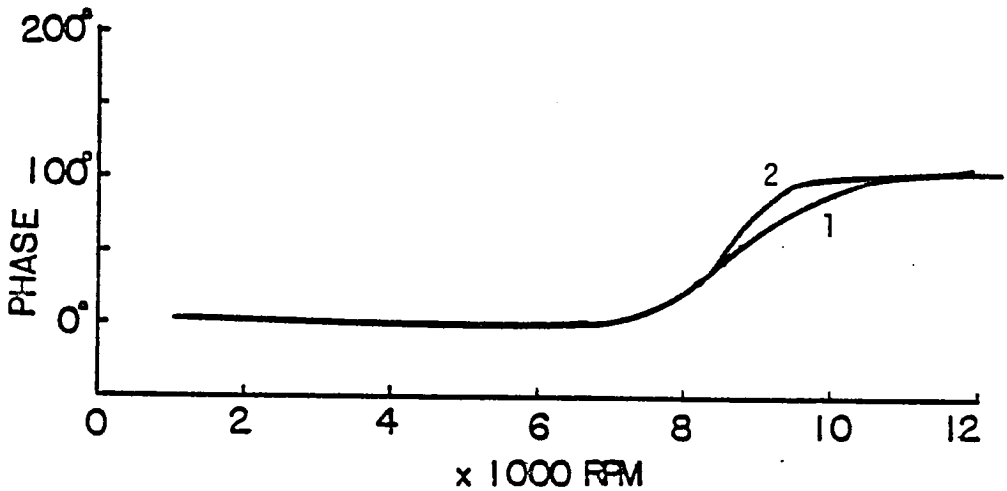

Figure 5.16

Damper Orbits Relative to Clearance Circle

Groove Feed, 120°F, u = 3.0 gm, 9000 RPM

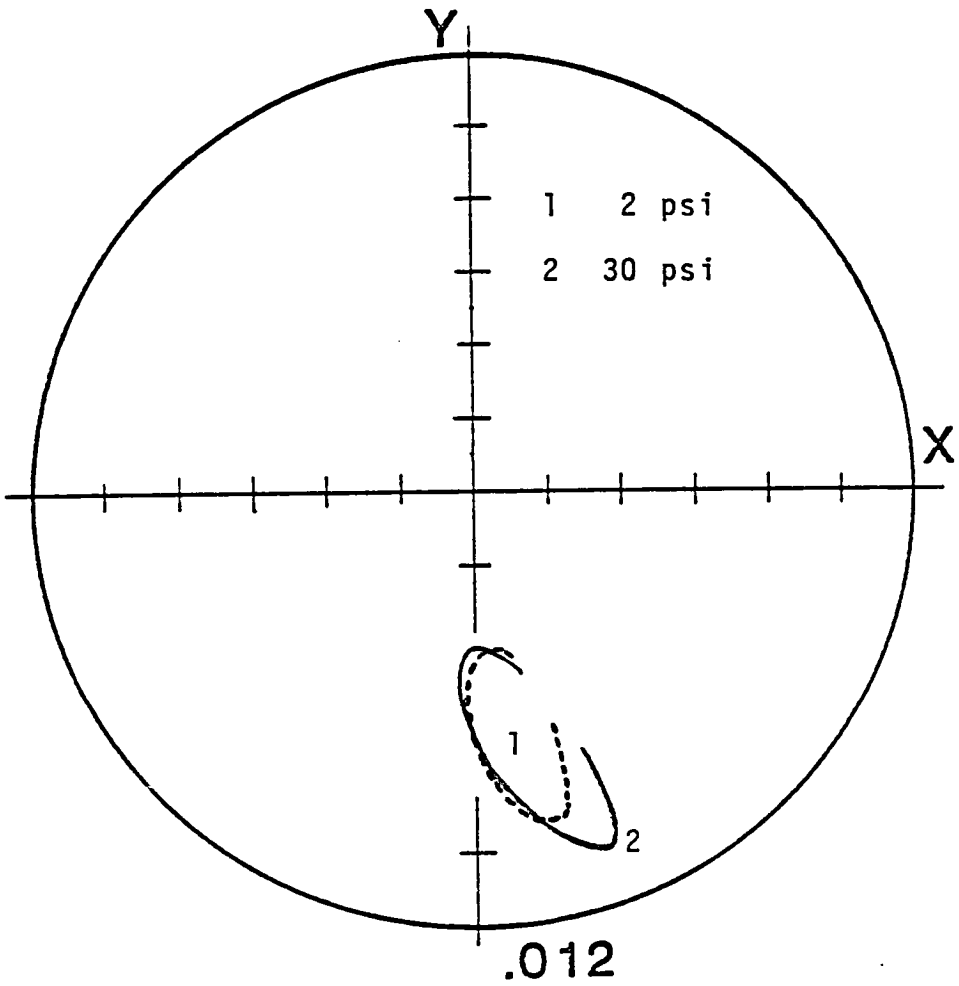

Figure 5.17

Damper Orbits Relative to Clearance Circle

Groove Feed, 80°F, u = 3.0 gm, 9000 RPM

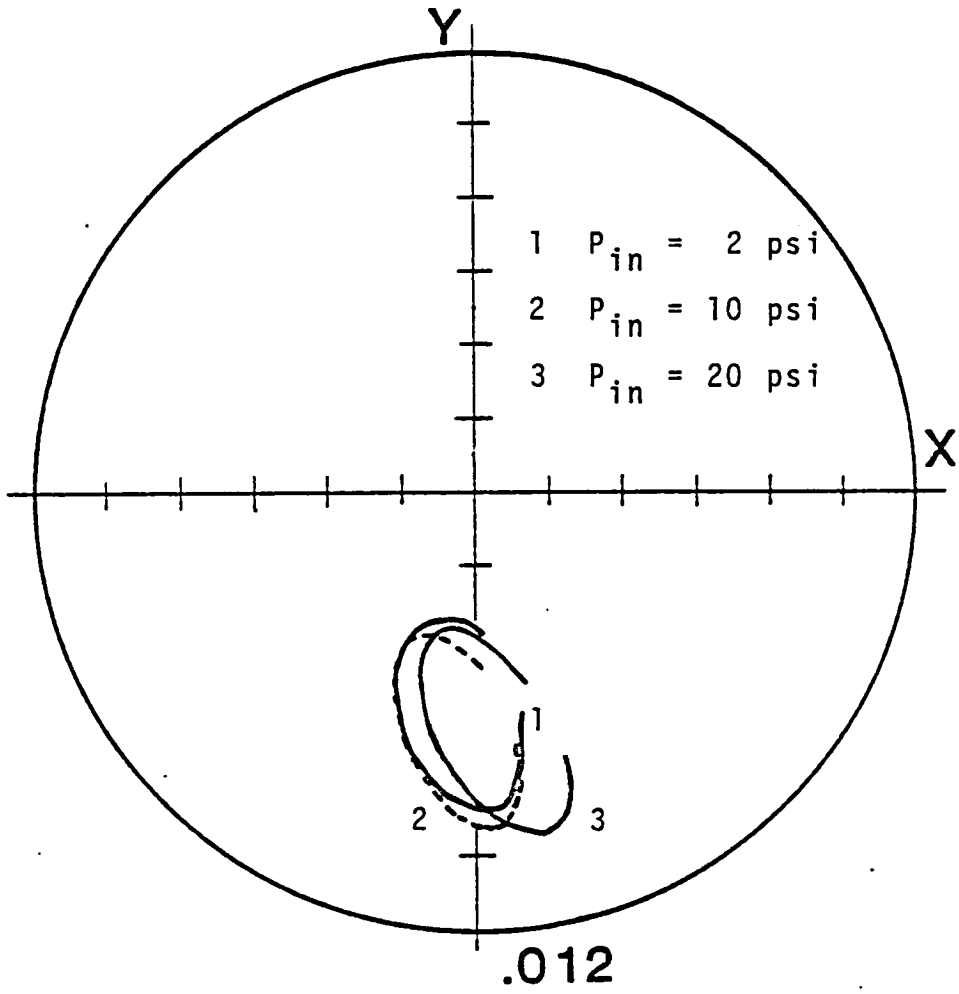

Figure 5.18

Damper Orbits Relative to Clearance Circle

Groove Feed, 80°F, u = 2 gm, 9000 RPM

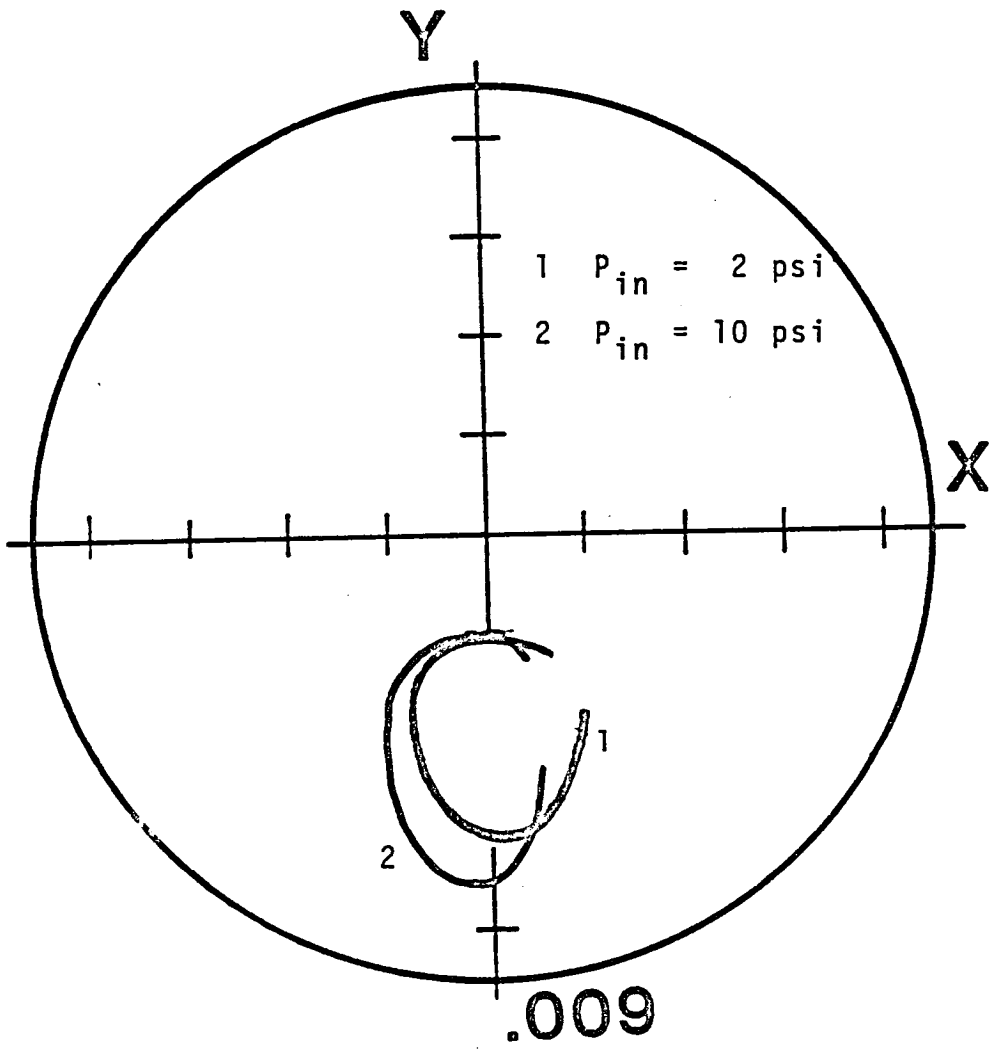

Figure 5.19

Damper Orbits Relative to Clearance Circle

Groove Feed, 80°F, u = 2.0 gm. 9000 RPM

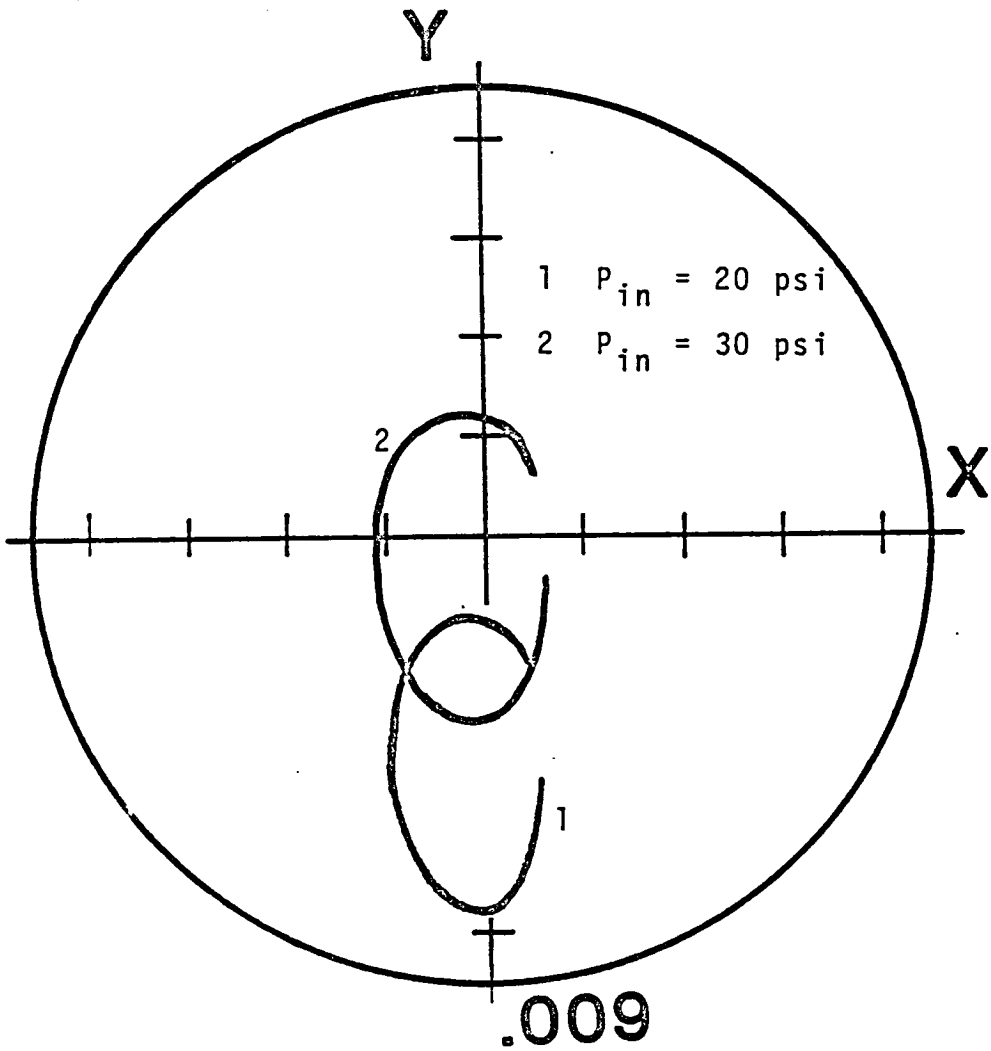

Figure 5.20

Midshaft Phase vs. Rotor Speed

Groove Feed, C = .020", P_{in} = 2psi , u = 1.62 gm

1 96°F

2 120°F

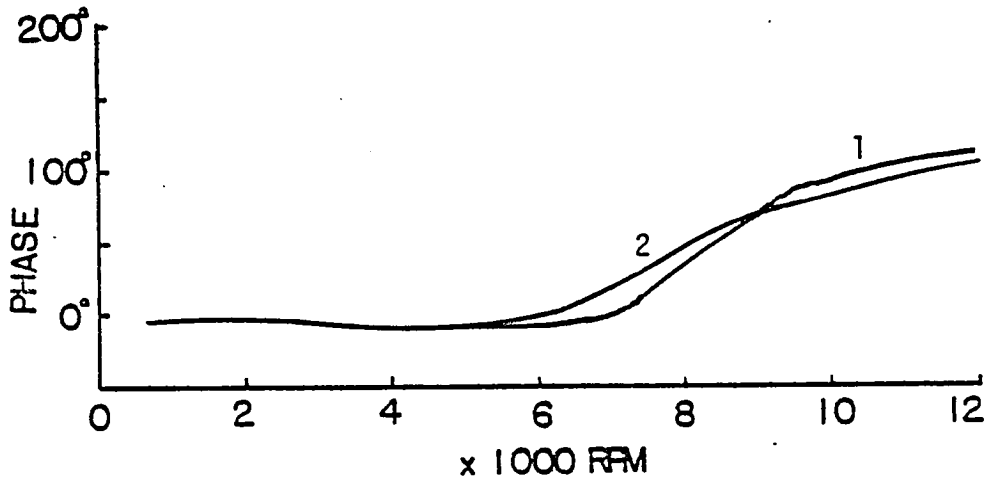

Figure 5.21

Midshaft Displacement vs. Rotor Speed

Groove Feed, C = .020", P_{in} = 2 psi, u = 1.62 gm

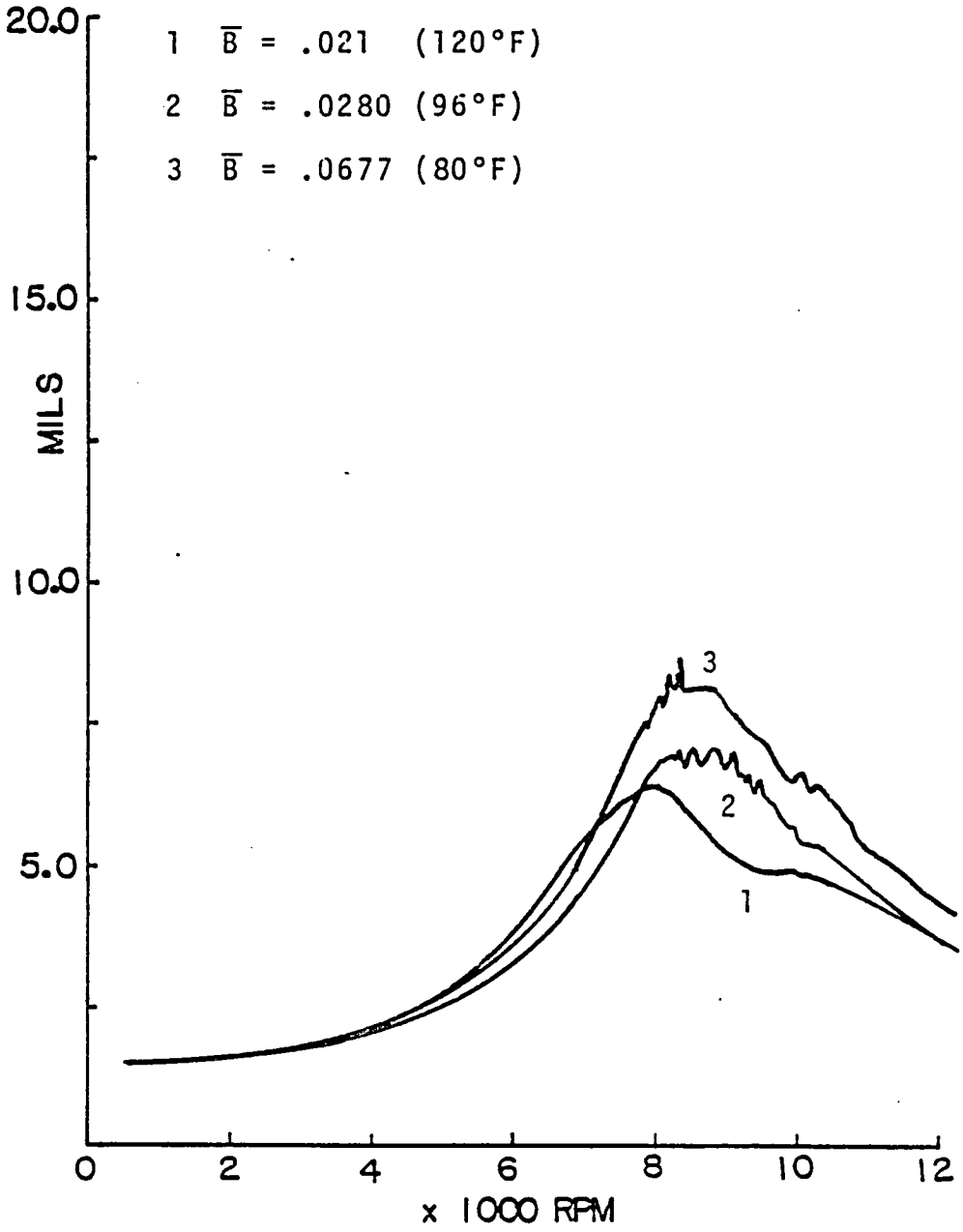

Figure 5.22

Midshaft Displacement vs. Rotor Speed

Groove Feed, C = .010", P_{in} = 2 psi, u = 3 gm

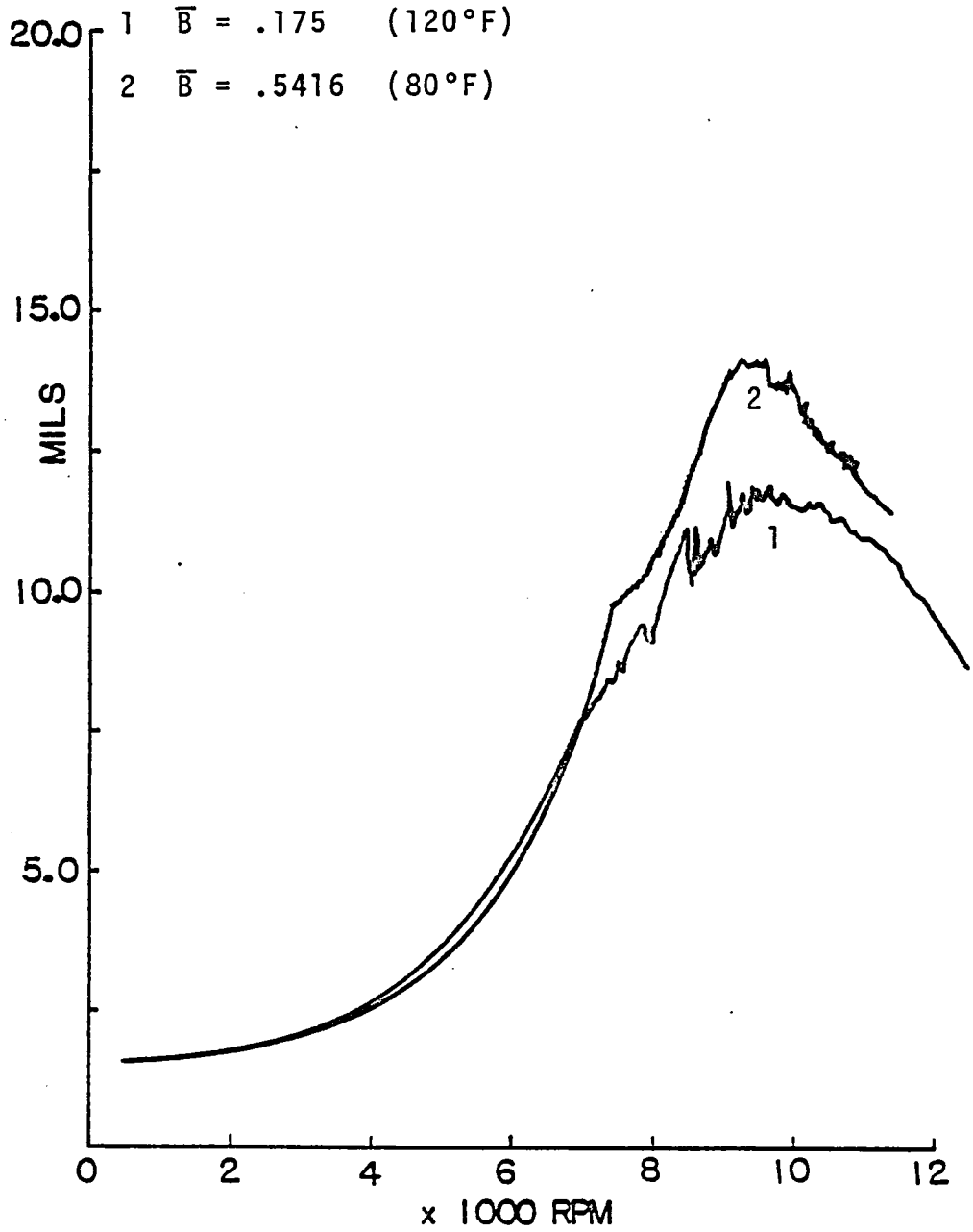

Figure 5.23

Midshaft Phase vs. Rotor Speed

Groove Feed, C = .010", P_{in} = 2 psi, u = 3 gm

1 120°F

2 80°F

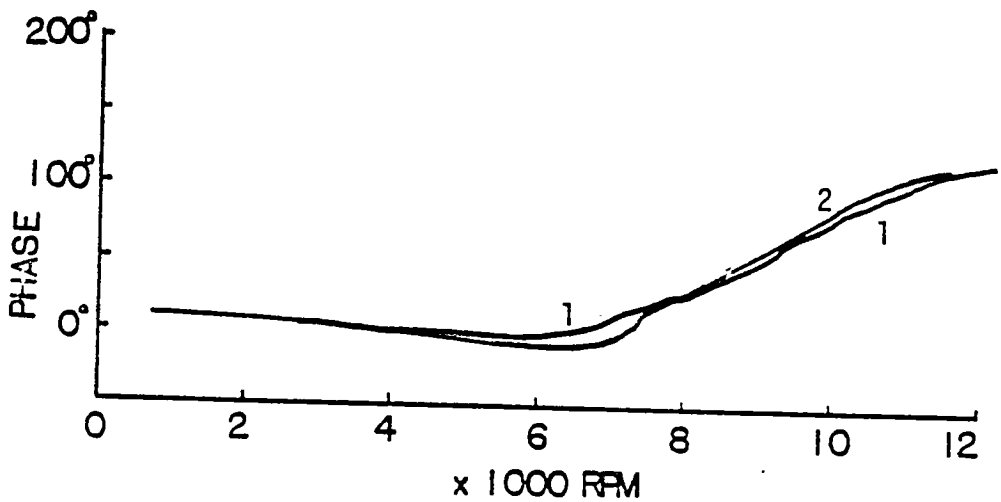

Figure 5.24

Damper Orbits Relative to Clearance Circle

Groove Feed, P_{in} = 2 psi, u = 3 gm, 9000 RPM

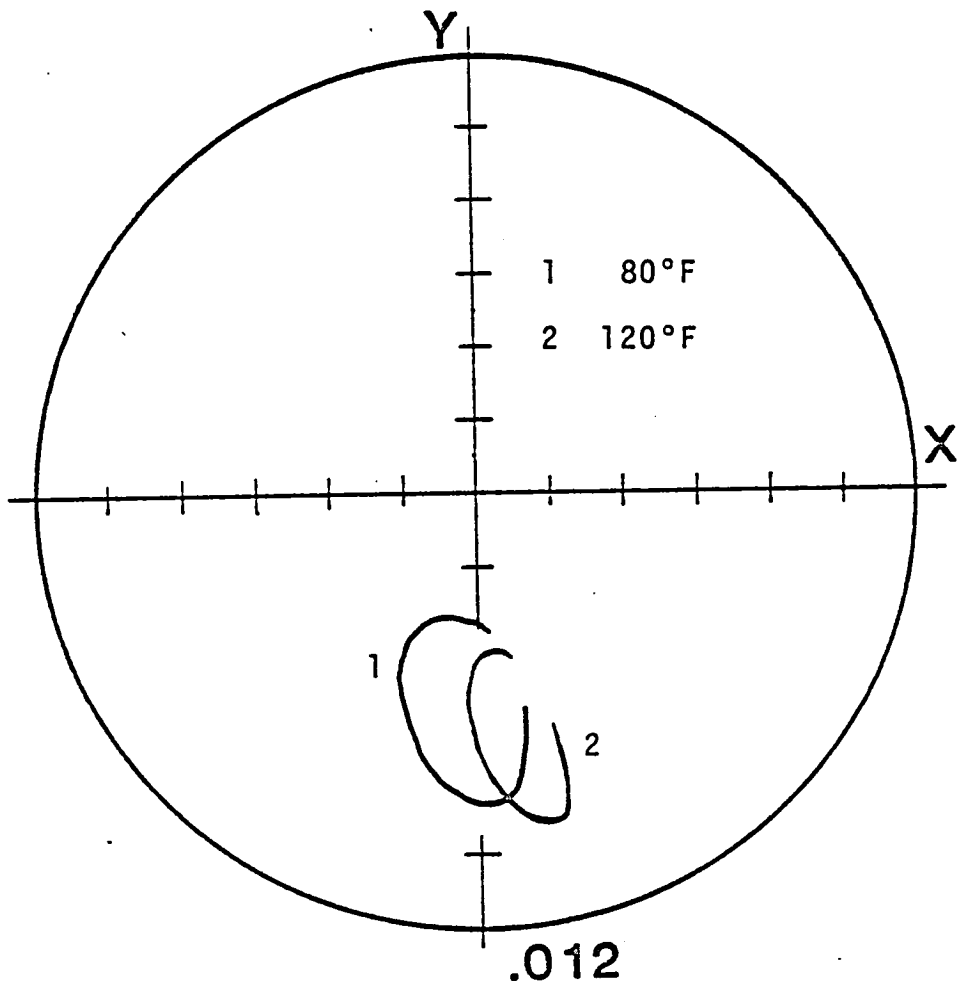

Figure 5.25

Damper Orbits Relative to Clearance Circle

Groove Feed, P_{in} = 20 psi, u = 3 gm, 9000 RPM

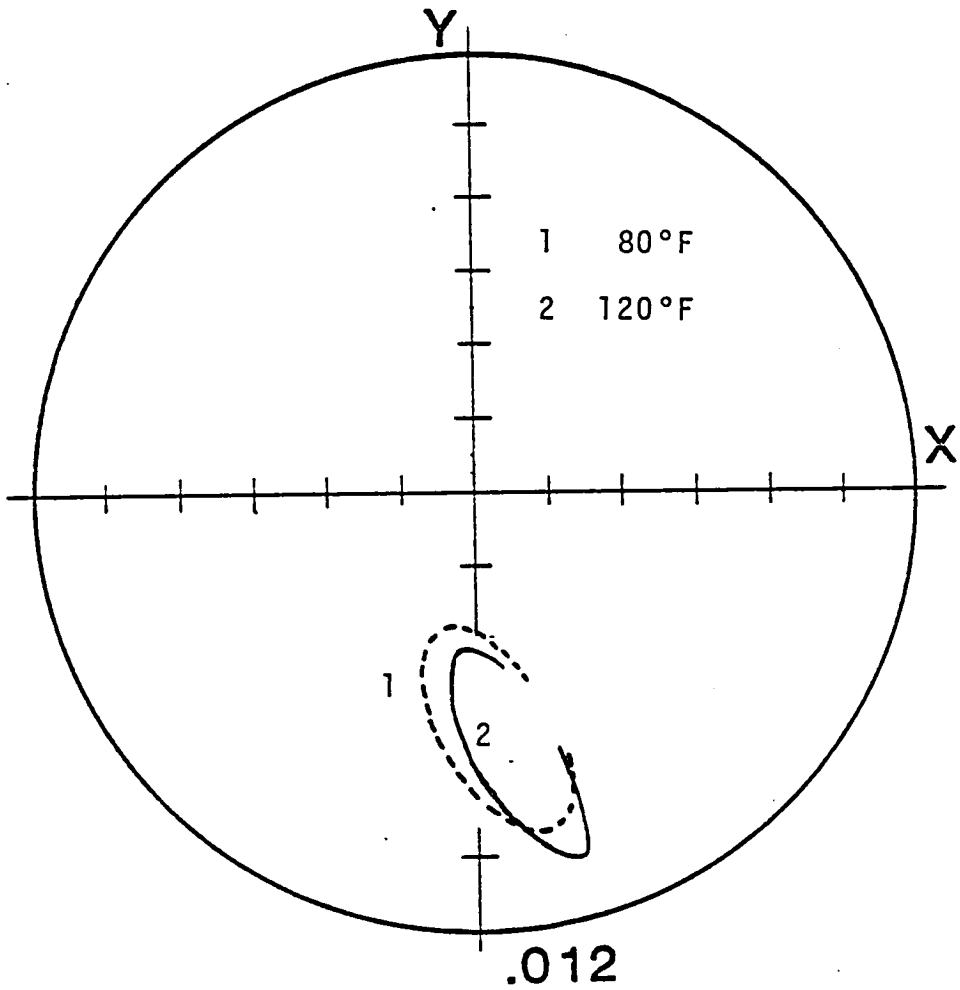

Figure 5.26

Damper Orbits Relative to Clearance Circle

Groove Feed, 80°F, P_{in} = 10 psi, u = 3 gm

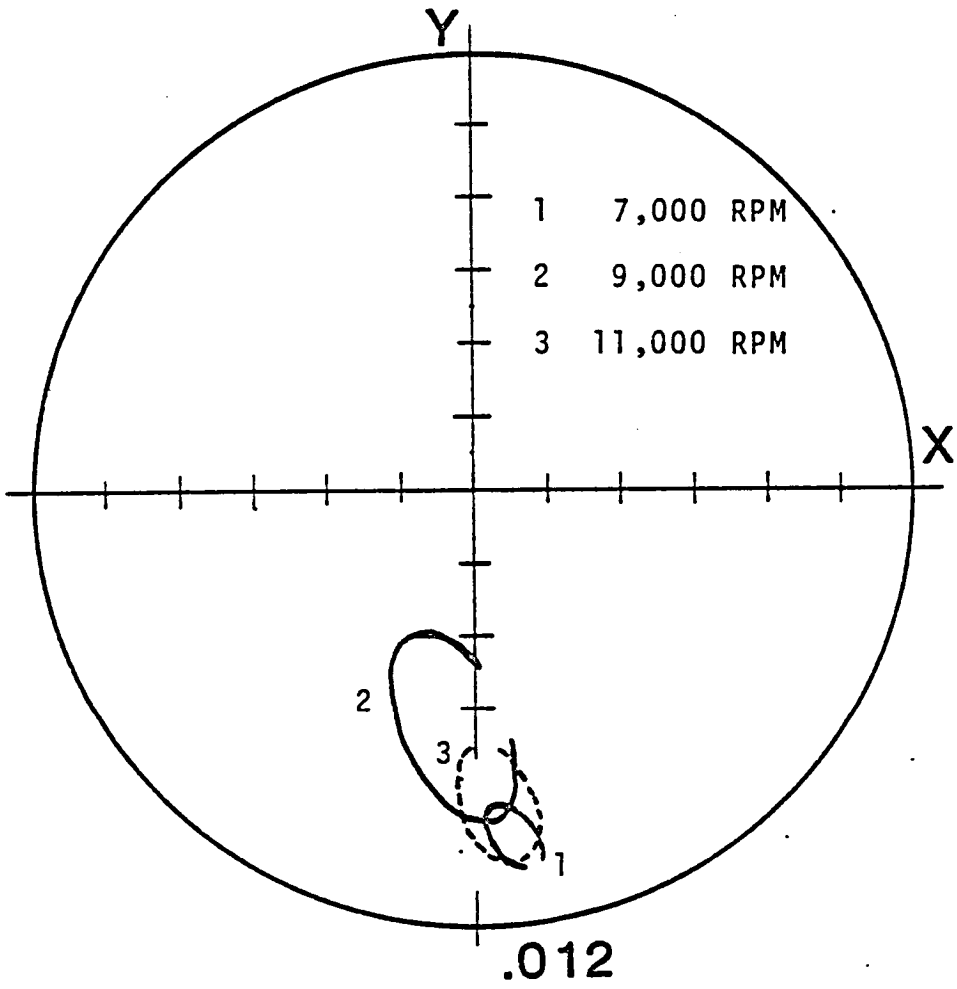

Figure 5.27

critical speed, the amplitude grew and the orbit "lifted off" of the clearance circle with the higher vibration. This figure also portrays the phase shift depicted by the reference gap in the orbit tracings. The rotor operated clockwise while the gap moved counterclockwise with increasing speed.

SFD With End Seals

Figure 5.28 and 5.29 show the effects on rotor response of varying the unbalance with low inlet port pressure. The Bode plots are similar to those for SFD without end seals operating at low inlet pressure. Cavitation noise was again noted beginning at the speed where the peaks became eroded. As before, increasing unbalance created greater excitation and thus more energy dissipation.

With the inlet port at the bottoms of the damper "lift off" was aided by the inlet pressure. Figure 5.30 depicts lift off due to increasing port pressure.

Increasing the inlet pressure again decreased cavitation and lessened energy dissipation (Figures 5.31 through 5.35) despite creating larger orbits and offsets (Figure 5.30). As with SFD without end seals, larger clearances or higher temperatures yielded softer damping and better performance for this system.

With low inlet pressure the dampers lifted off with speed as with grooved inlets. With higher pressures

Midshaft Displacement vs. Rotor Speed

Port Feed, C = 020°, 80°F, P_{in} = 18 psi

1 U = .0166 (.5 gm)

2 U = .0331 (1 gm)

3 U = .0662 (2 gm)

4 U = .0993 (3 gm)

5 U = .1225 (3.7 gm)

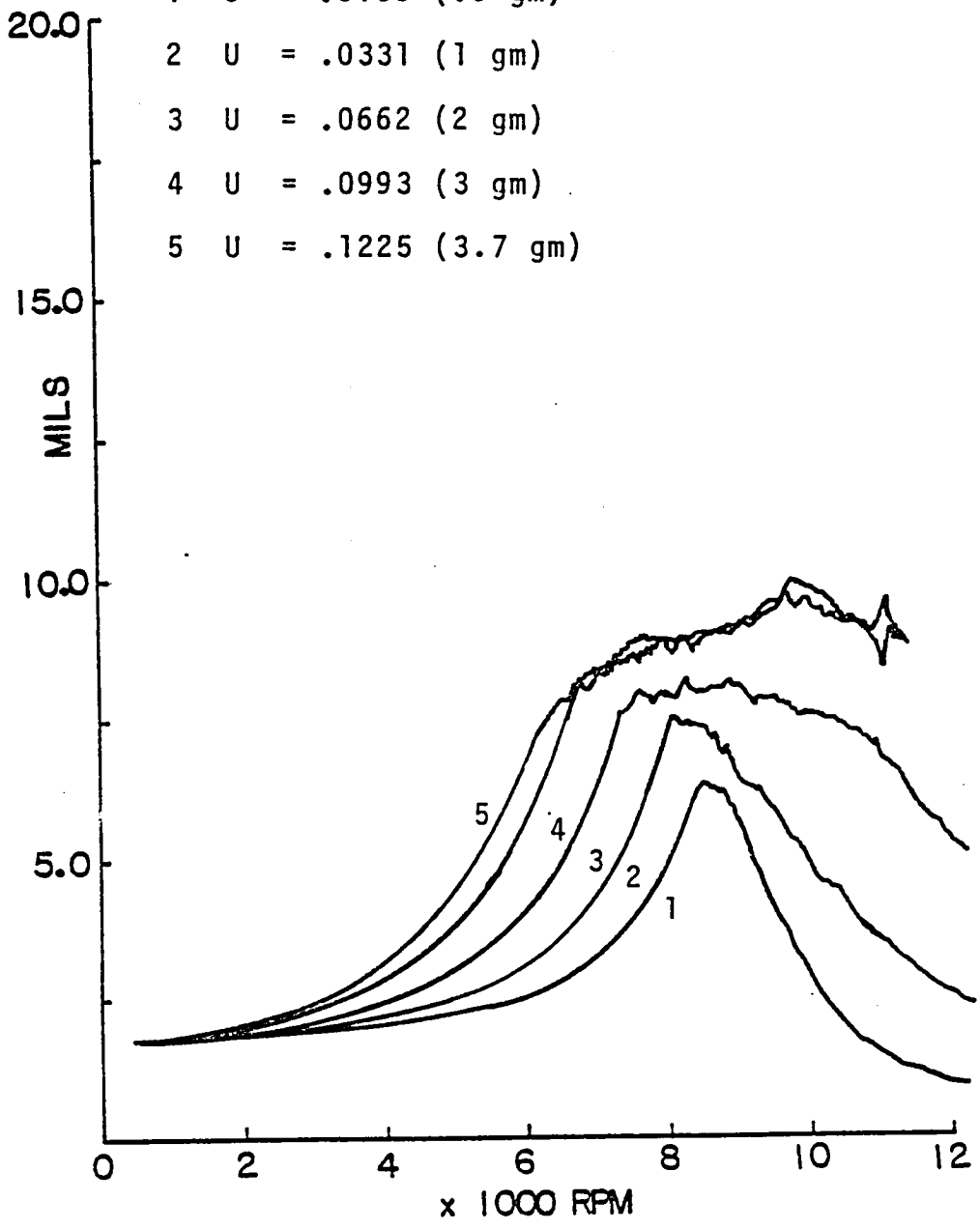

Figure 5.28

Midshaft Phase vs. Rotor Speed

Port Feed, 80°F, P_{in} = 18 psi, C = .020"

1 U = .0166 (.5 gm)

2 U = .0331 (1 gm)

3 U = .0993 (3 gm)

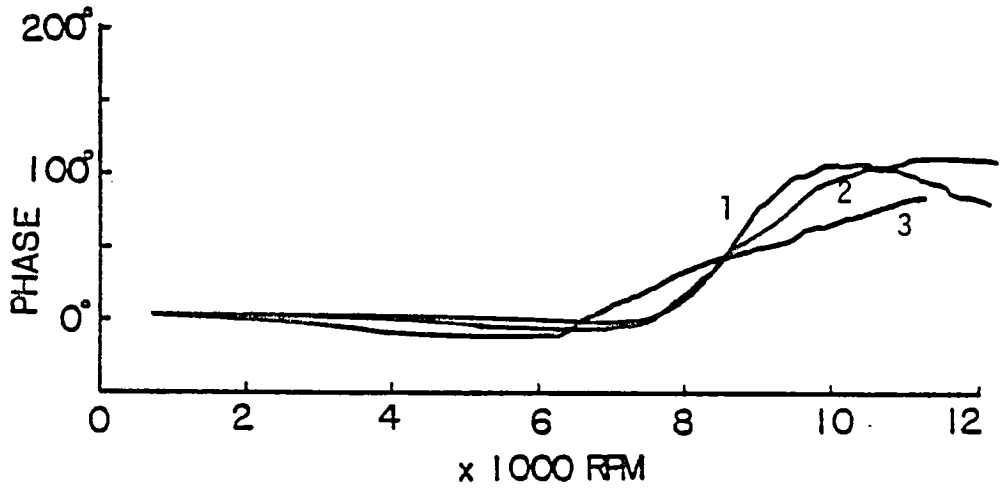

Figure 5.29

Damper Orbits Relative to Clearance Circle

Port Feed, 80°F, u = 3 gm, 9000 RPM

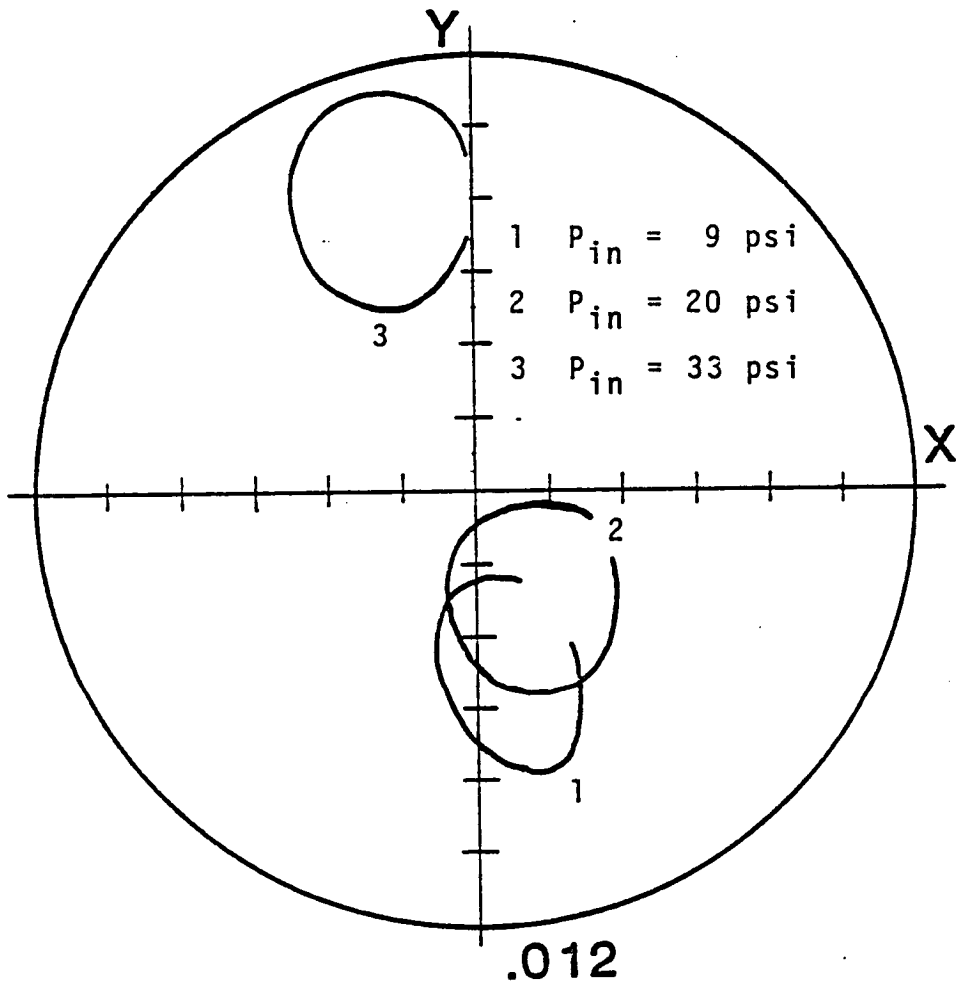

Figure 5.30

Midshaft Phase vs. Rotor Speed

Port Feed, C = .020", 80°F, u = 1.0 gm

1 P_{in} = 25 psi

2 P_{in} = 40 psi

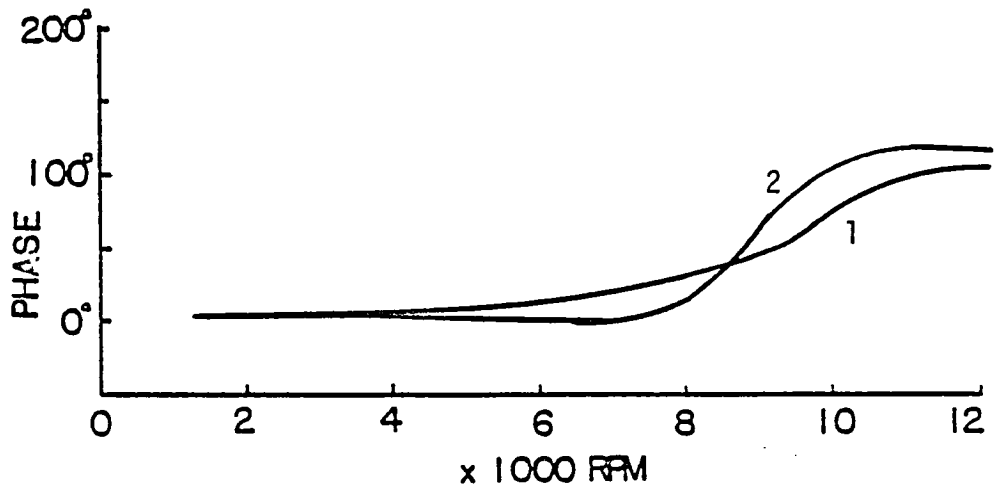

Figure 5.31

Midshaft Displacement vs. Rotor Speed

Port Feed, C = .020°, 80°F, u = 1.0 gm

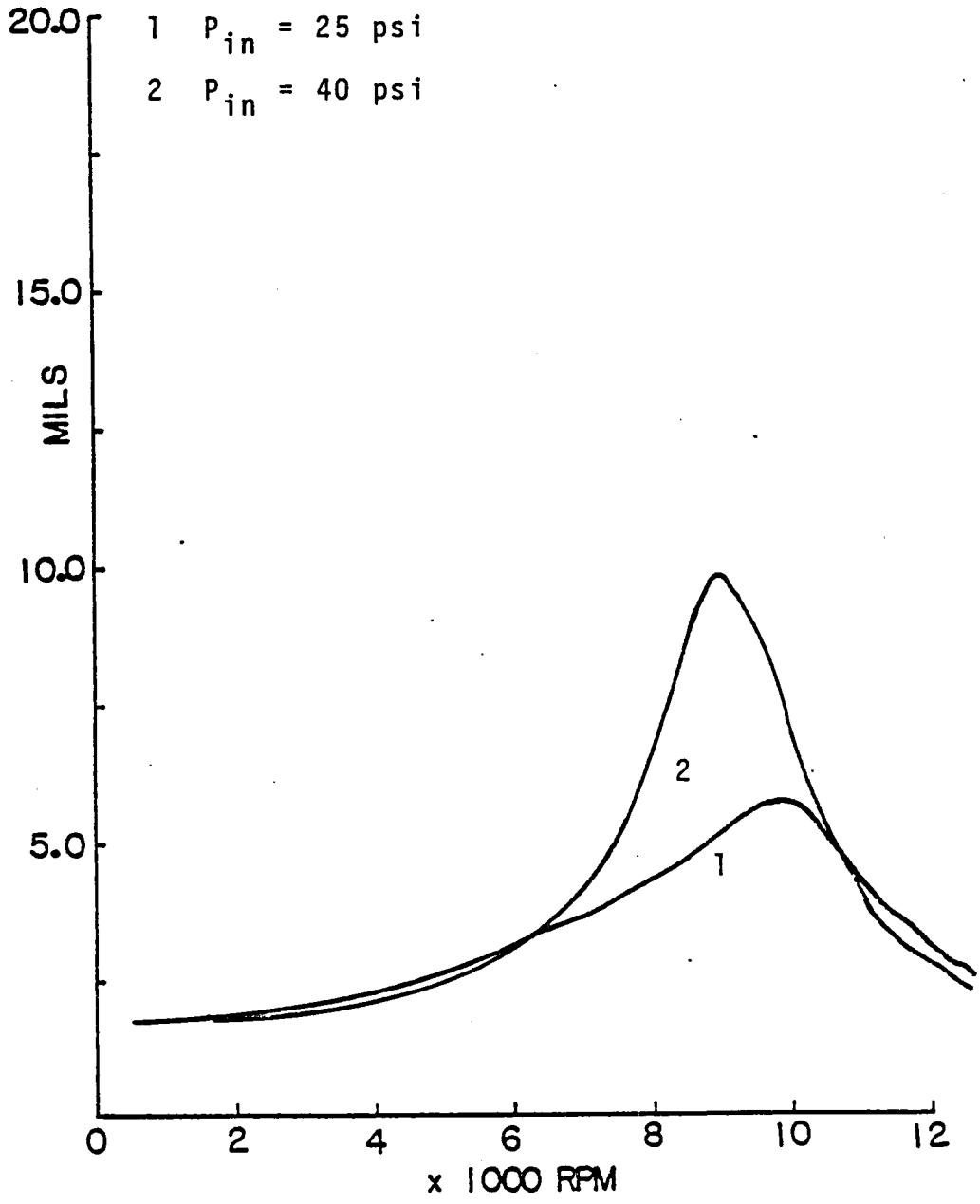

Figure 5.32

Midshaft Phase vs. Rotor Speed

Port Feed, C = .010", 80°F, u = 3 gm

1 P_{in} = 15 psi

2 P_{in} = 23 psi

3 P_{in} = 40 psi

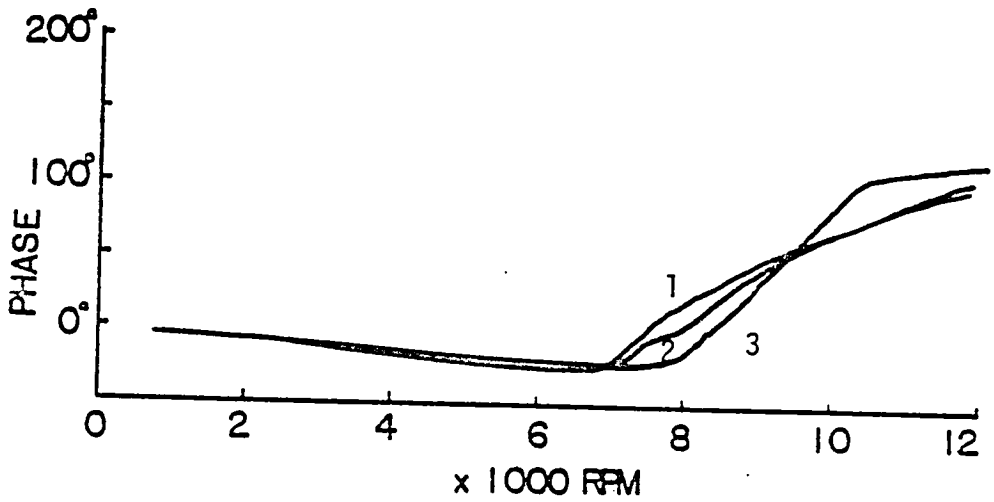

Figure 5.33

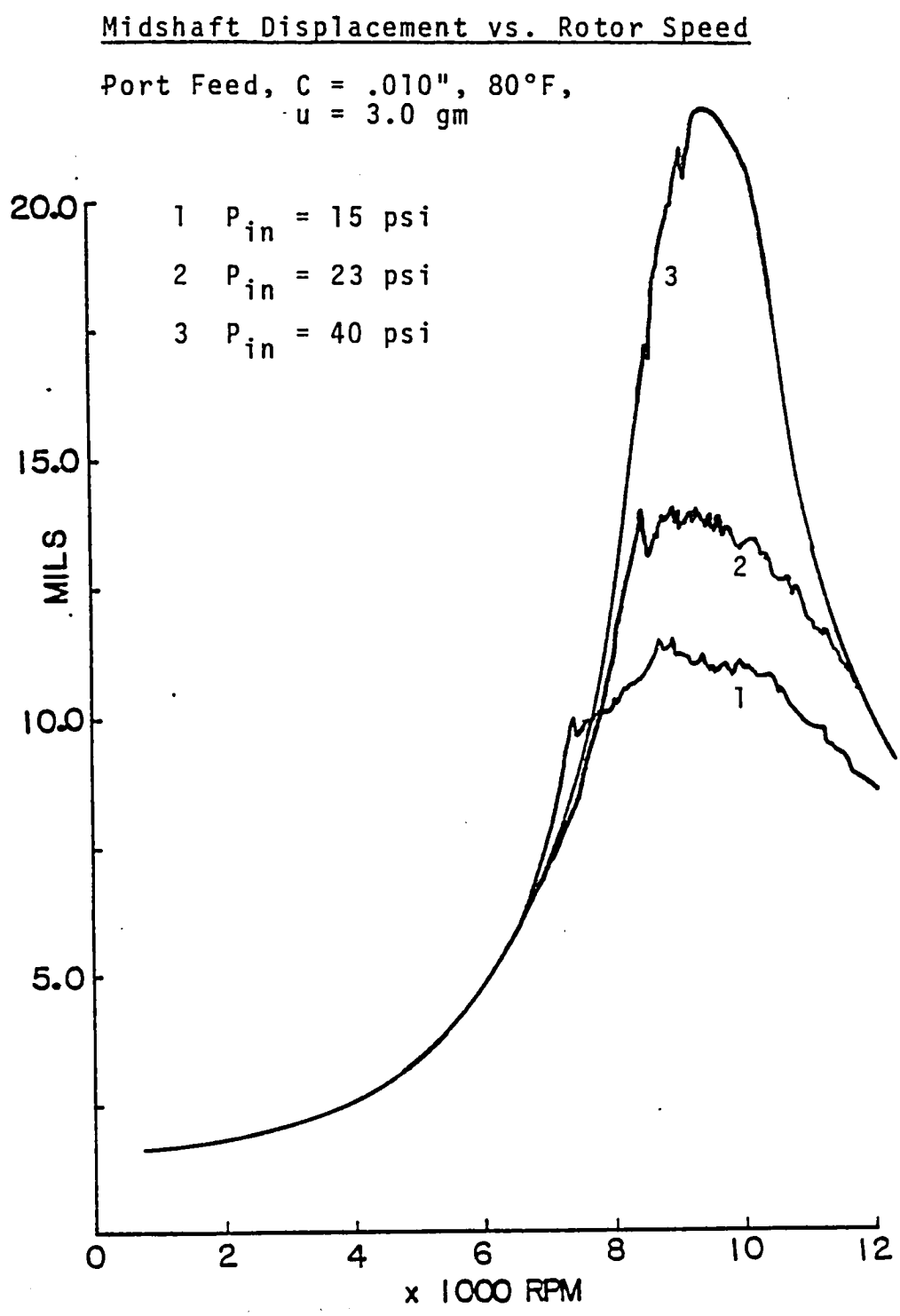
Midshaft Displacement vs. Rotor Speed
Port Feed, C = .010", 80°F,
u = 3.0 gm
1 P_{in} = 15 psi
2 P_{in} = 23 psi
3 P_{in} = 40 psi
20.0
15.0
10.0
5.0
MILS
0
2
4
6
8
10
12
x 1000 RPM
1
2
3

Figure 5.34

Midshaft Displacement vs. Rotor Speed

Port Feed, C = .006", 80°F, u = 2.0 gm

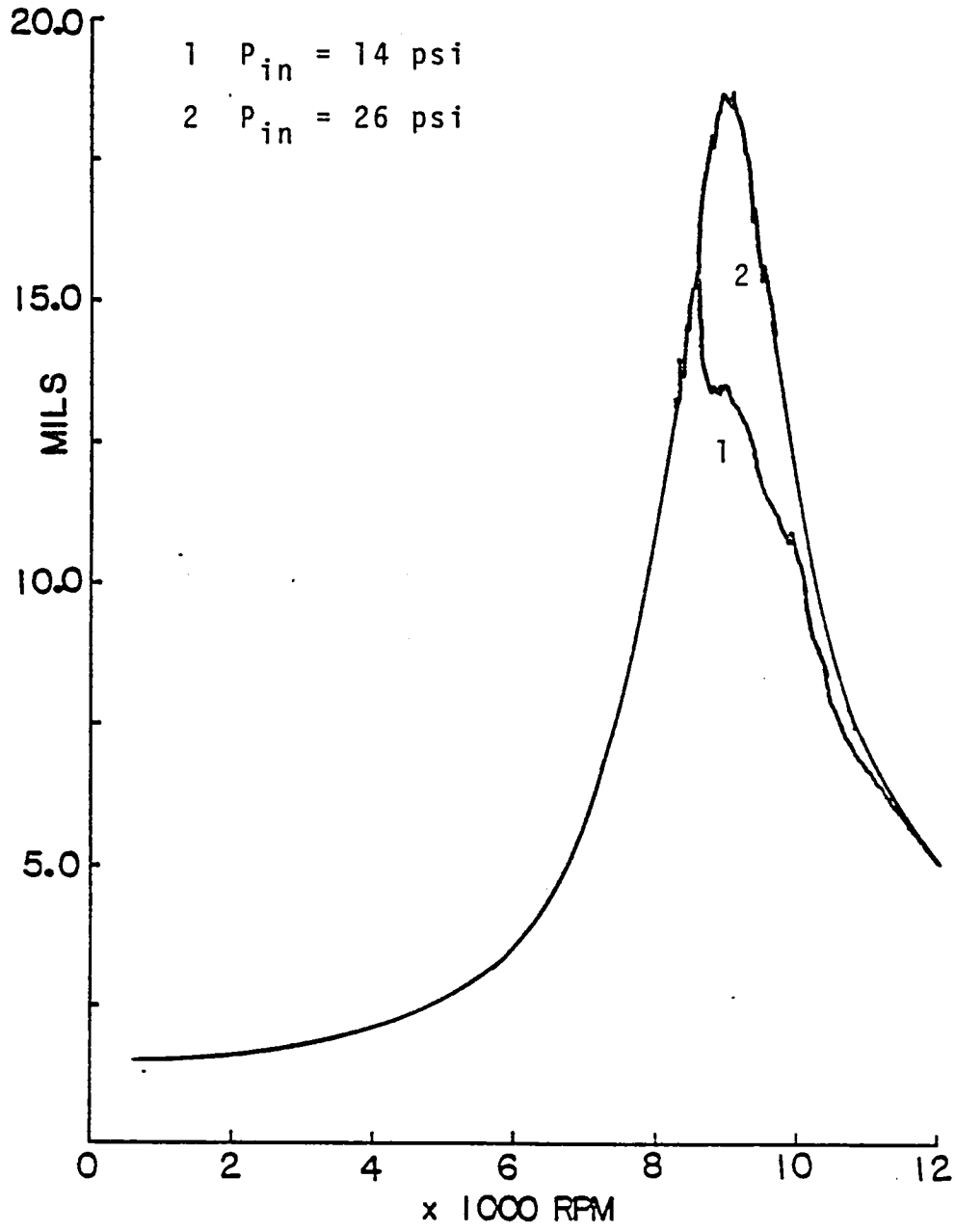

Figure 5.35

the damper journals lifted off to the top of the clearance circle at low speed then the critical speed excitation forced a "lift off" downward as shown in Figure 5.36. A medium pressure could cause a lift off with speed that centered the orbit at the critical speed as in Figure 5.37. This is noteworthy since some analysts in the past have assumed circular centered orbits near the critical speed for ease of analytic solution.

Damper Orbits Relative to Clearance Circle

Port Feed, 80°F, u = 3 gm, P_{in} = 43 psi

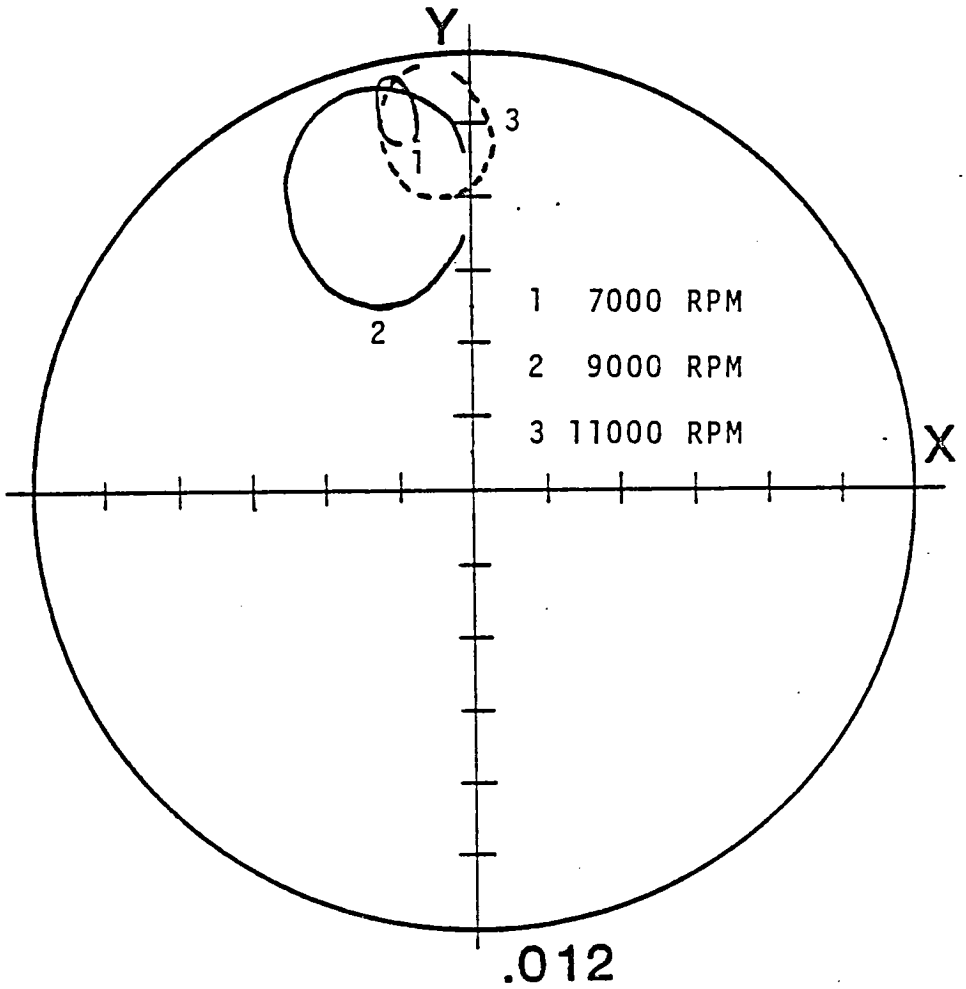

Figure 5.36

Damper Orbits Relative to Clearance Circle

Port Feed, 80°F, u = 2 gm, P_{in} = 22 psi

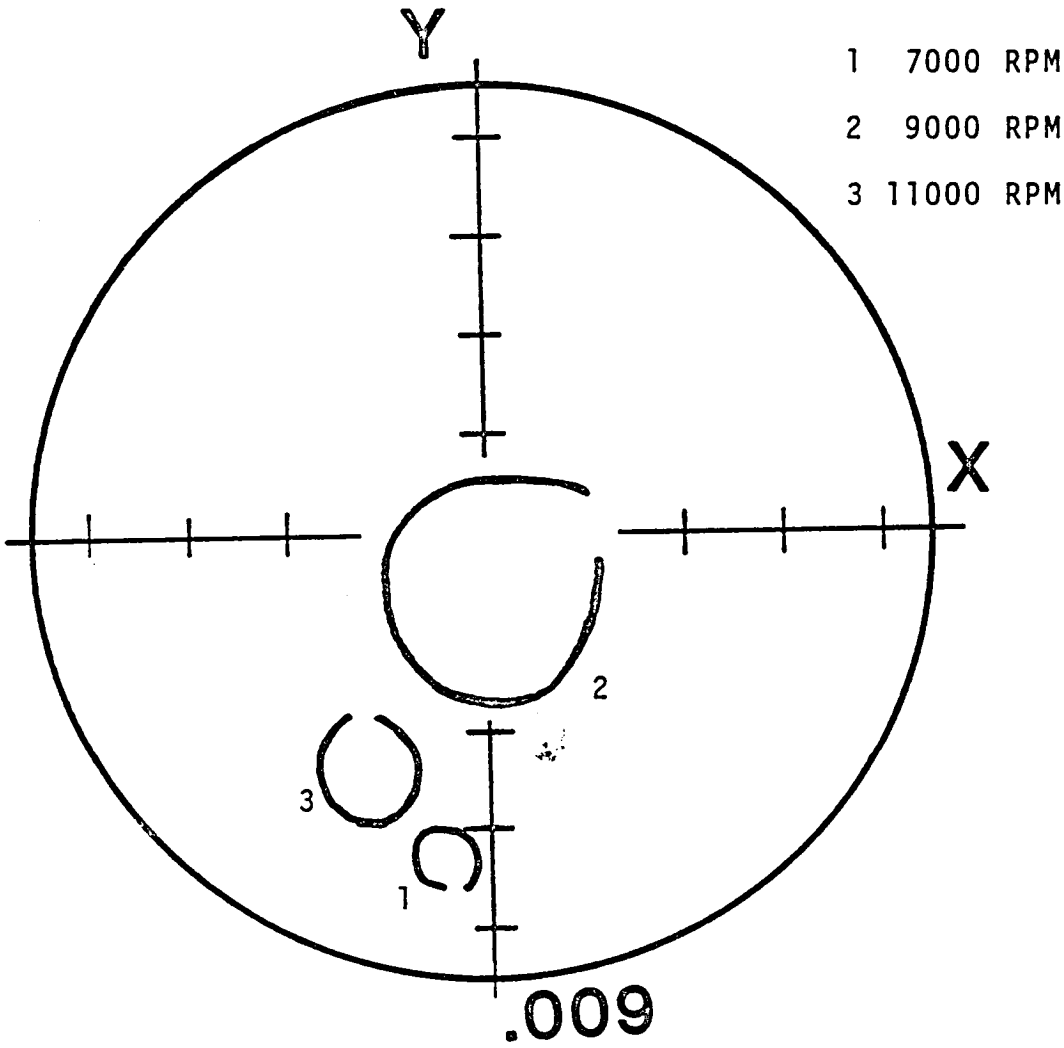

Figure 5.37

CHAPTER 6

COMPARISONS WITH A SIMPLIFIED COMPUTER MODEL

The rotor was modeled using an available code, assuming the rotor to be rigid (14). Of course, the rotor was not rigid at the speeds which the experimental results were obtained. Thus, the damper excitation was not necessarily the same and direct comparisons could not be made. However, qualitative comparisons concerning the general character of the orbits were found to be useful. All computed cases presented were run at 10,000 RPM, with 3 gm unbalance and low inlet pressure using a short bearing approximation of the Reynolds equation.

Considering Figures 6.1, 6.2, 6.3, with increasing viscosity, the orbits' amplitudes and offsets decreased, showing the damper to be growing stiffer. This agrees with the experimental results (see Figure 5.25, 5.26). Also, as the offset decreased, the orbits became more circular, which also agress with experimental evidence. All of the computer produced orbits (clockwise rotations) are left of center (e.g. see Figure 6.2) and approach the center line (y axis) with decreasing offset. Comparing with Figures 5.9, 5.10, 5.11, this is also the

Damper Orbits Relative to Clearance Circle

Groove Feed, Low P_{in}, u = 3.2 gm, 10,000 RPM

1 $\mu = 10^{-6}$ Reyns. (160°F)

2 $\mu = 5x10^{-6}$ Reyns. (100°F)

3 $\mu = 10x10^{-6}$ Reyns. (80°F)

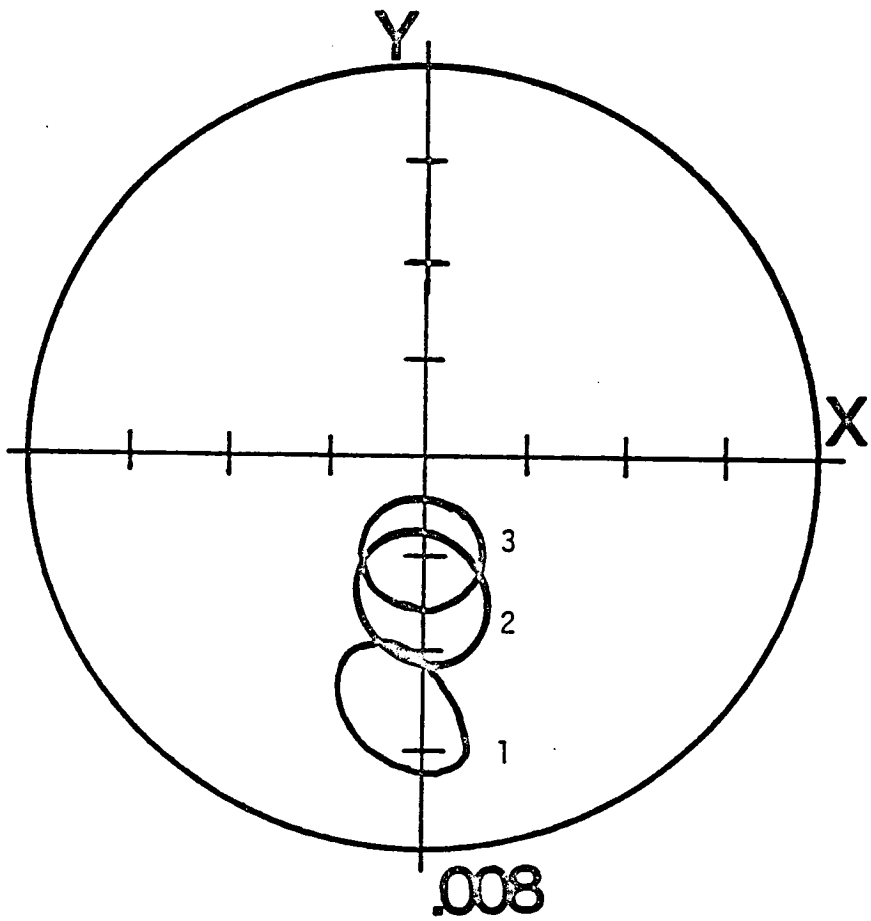

Figure 6.1

Damper Orbits Relative to Clearance Circle

Groove Feed, Low P_{in}, u = 3.2 gm, 10,000 RPM

1 10^{-6} Reyns. (160°F)

2 $5x10^{-6}$ Reyns. (100°F)

3 $10x10^{-6}$ Reyns. (80°F)

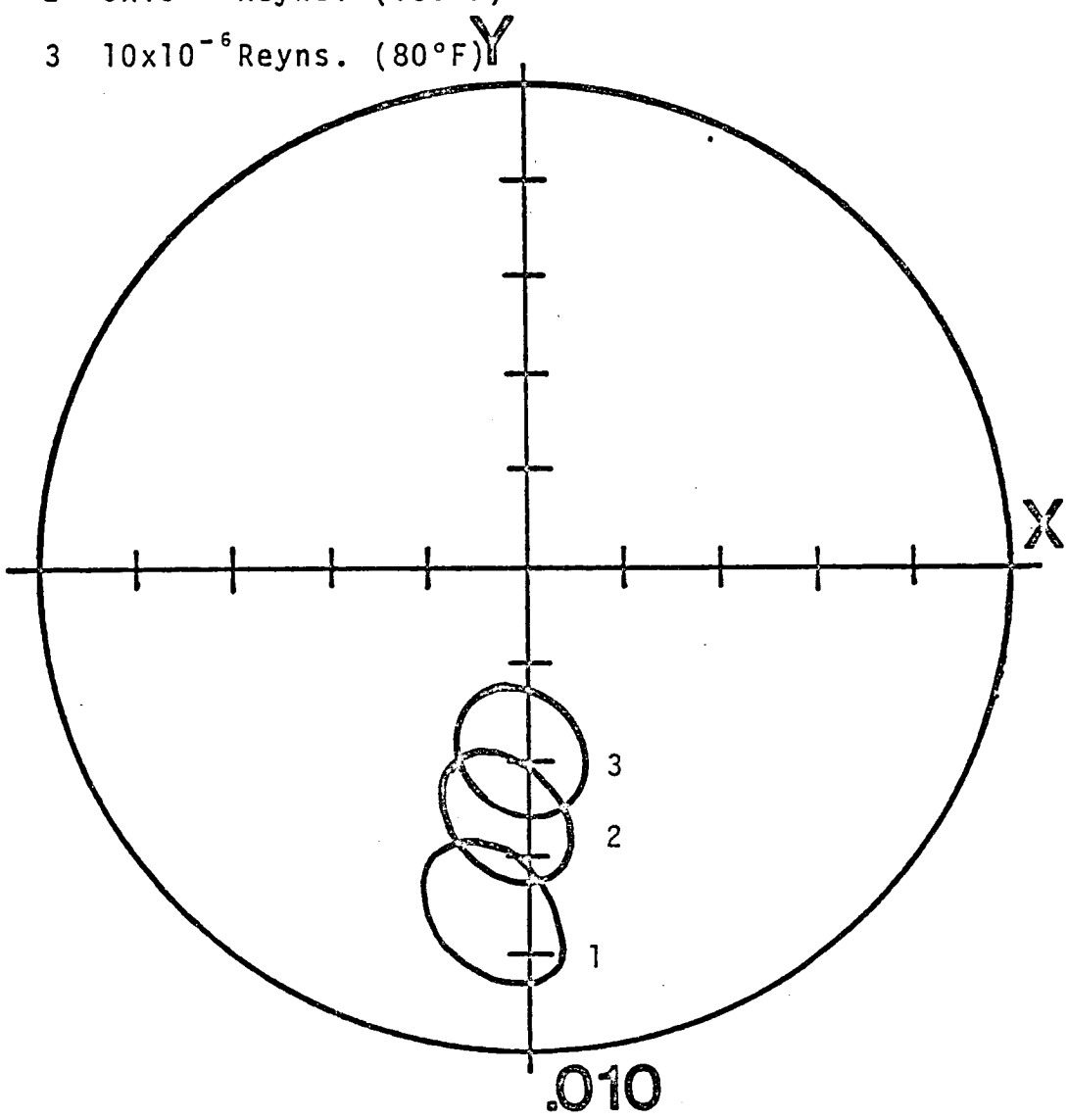

Figure 6.2

Damper Orbit Relative to Clearance Circle

Groove Feed, Low P_{in}, u = 3.2 gm, 10,000 RPM

1 10^{-6} Reyns. (160°F)

2 10×10^{-6} Reyns. (80°F)

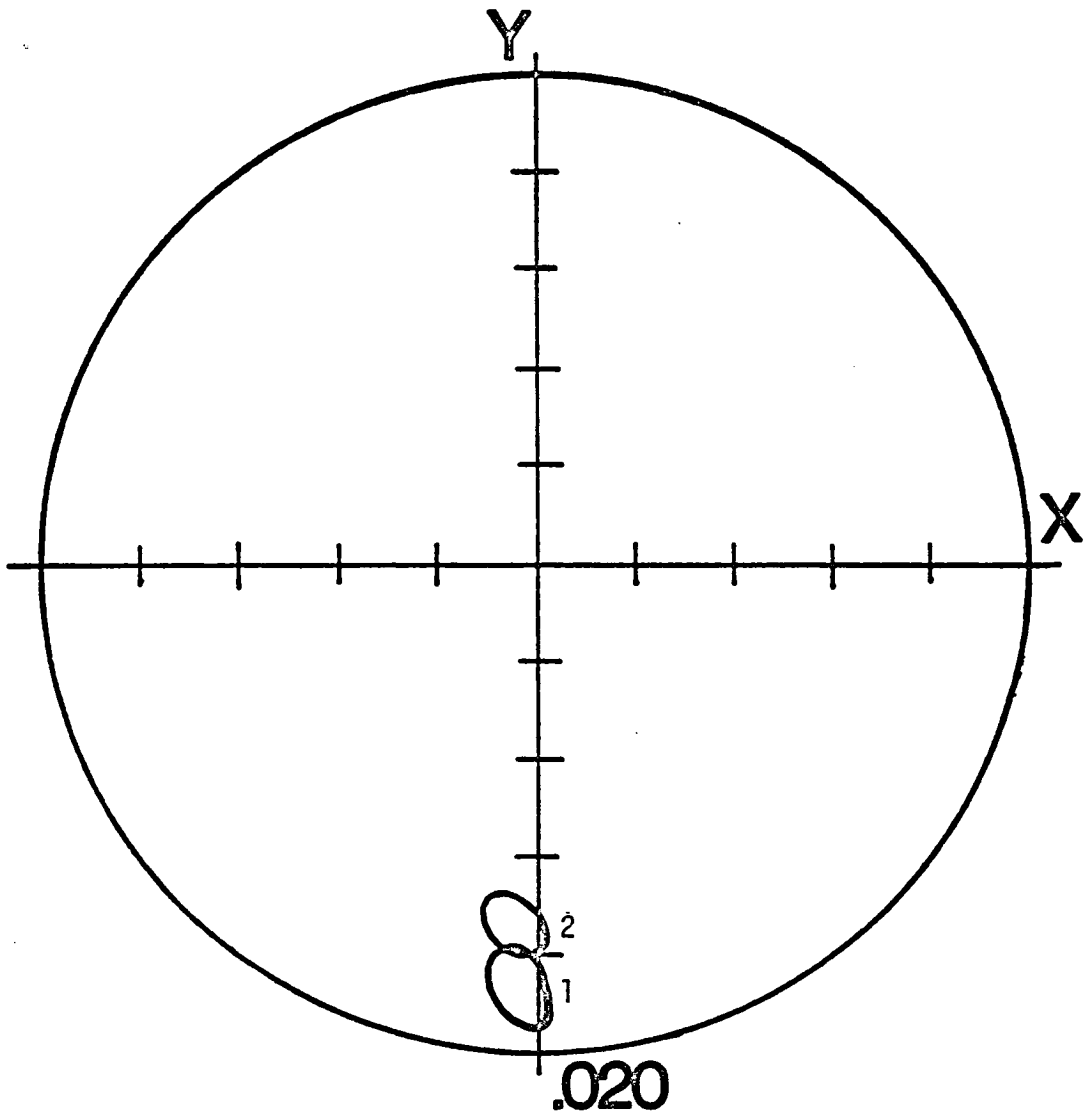

Figure 6.3

the general rule for the experimentally obtained orbits. From this last comparison it can be seen that increasing the clearance in both cases produced larger orbits and offsets and thus a softer damper.

CHAPTER 7

SUMMARY

In previous analysis a nondimensional damping parameter was typically used, originating from the Reynolds equation, that was proportional to μ/C^3 (see page 39). This parameter was used to express the stiffness of the damper. As has been shown, experimental evidence tends to support this.

Cookson and Kossa used two nondimensional parameters, a bearing parameter ($\overline{B}$) and a gravity parameter ($\overline{W}$), for SFD design and suggested values of these to smooth critical speed transition. Their suggestions of $\overline{W} \leq .1$, implies that $C \geq .004$ inches for this system. With C = .01 inches, the suggested value of $\overline{B} = .1$, requires the viscosity to be decreased by a factor of five from the room temperature value or the temperature to be raised to 150°F. This tends to agree with experimental evidence. However, for C = .02 inches, an increase in viscosity is recommended which is not in agreement.

In order to eliminate some difficulties that were encountered a recommended improvement is the use of tapered damper inserts. The present damper inserts were

machined to be easily removed from the bearing and interchanged, not requiring a pressed fit. This required a radial clearance of one to two mils. This annular clearance was filled with oil during damper operation and acted as a second SFD in series with the desired damper. The idea was that if this secondary SFD had a clearance much smaller than the desired damper, it would be much stiffer and would not significantly offset the performance of the damper. However, with low inlet pressure this secondary damper might have been starved of oil thus affecting the damper as a whole. Also, this smaller clearance added to the measured damper clearance, so that for instance the measured 12 mil clearance was probably actually closer to 10 mils. This also provided difficulty in locating the orbit locations within the clearance circle, possibly explaining the lateral difference in orbit positions on Figures 5.25 and 5.26. These difficulties could be overcome easily with the use of tapered inserts that would be lightly pressed into the damper bearings, requiring only slight modifications.

If increased energy dissipation is desired for this rotor system, it has been shown that the dampers need to be softened. A lighter lubricant is recommended to avoid heating the oil or using larger clearances. Large clearances are both unusual in practice and

difficult to model due to the necessity of involving inertial effects (16).

The parametric study conducted here, hopefully provided some insights into the workings of an SFD, especially concerning the effects of cavitation. More importantly, the test rig has been shown to be capable of providing useful data so that with the above mentioned improvement, data can be taken with a more specific purpose to be compared with computer analysis.

REFERENCES

REFERENCES

1. E. J. Gunter, "Influences of Flexibly Mounted Rolling Element Bearings on Rotor Response, Part I - Linear Analysis", Journal of Lubrication Technology, Vol. 92, Series E, No. 1, January 1970, pp. 59-69.

2. Melbourne F. Giberson, "Taming Rotor Whirl With Film-Damper Bearings", Machine Design, Vol. 45, No. 7, March 22, 1973, pp. 176-181.

3. S. Mohan and E. J. Hahn, "Design of Squeeze Film Damper Supports for Rigid Rotors", Journal of Engng. for Industry, Trans. ASME, Series B, Vol. 96, 1974, pp. 976-982.

4. R. E. Cunningham, D. P. Fleming, and E. J. Gunter, "Design of a Squeeze Film Damper for a Multimass Flexible Rotor", J. Engng. Ind., Trans. ASME, B97 (4), pp. 1383-1389 (1975).

5. Jorgen Tonnesen, "Experimental Squeeze Bearing Orbit Studies", J. Engng. Ind., Trans. ASME, B97 (4), pp. 83-95.

6. P. N. Bansal and D. H. Hibner, "Experimental and Analytical Investigation of Squeeze Film Bearing Damper Forces Induced by Offset Circular Whirl Orbits", Journal of Mech. Design, Vol. 100, No. 3, July 1978, pp. 549-557.

7. D. H. Hibner, P. N. Bansal and D. F. Berano, "Analysis and Experimental Investigation of the Stability of Intershaft Squeeze Film Dampers - Part 2: Control of Instability", Journal of Mechanical Design, Vol. 100, No. 3, July 1978, pp. 558-562.

8. E. J. Hahn, "Unbalance Behavior of Squeeze Film Supported Rigid Rotors", Journal of Mechanical Design, Vol. 100, No. 3, July 1978, pp. 176-188.

9. John M. Vance, "A Current Review of Rotordynamics Problems in High Speed Lightweight Turbomachinery and Power Shafting", Proceedings of the "Conference on the Stability and Dynamic Response of Rotors with Squeeze Film Bearings", University of Virginia, Charlottesville, May, 1979, pp. 7-19.

10. D. H. Hibner and P. N. Bansal, "Effects of Fluid Compressibility on Viscous Damper Characteristics", Proceedings of the "Conference on the Stability and Dynamic Response of Rotors with Squeeze Film Bearings", University of Virginia, Charlottesville, May, 1979, pp. 116-132.

11. R. Holmes, "The Control of Rotor Vibration Using Squeeze Film Dampers", Proceedings of the "Conference on the Stability and Dynamic Response of Rotors with Squeeze Film Bearings", University of Virginia, Charlottesville, May, 1979, pp. 53-72.

12. R. A. Cookson and S. S. Kossa, "The Effectiveness of Squeeze-Film Damper Bearings Supporting Flexible Rotors Without a Centralizing Spring", Int. J. Mech. Sci., Vol. 22, May, 1980, pp. 313-324.

13. R. A. Cookson and S. S. Kossa, "The Vibration Isolating Properties of Uncentralized Squeeze-Film Damper Bearings Supporting a Flexible Rotor", International Gas Turbine Conference, Houston, Texas, March 1981.

14. M. L. Adams, J. Padovan and D. G. Fertis, "Finite Element for Rotor/Stator Interactive Forces in General Engine Dynamic Simulation", NASA CR-165214, October, 1980.

15. M. L. Adams, E. Makay and J. P. Dimmer, "Feed Pump Vibration Research-Interstage Fluid Annuli", Joint Power Generation Conference, Phoenix, Arizona, September 28-October 2, 1980.

APPENDICES

APPENDIX A

DESIGN CALCULATIONS

A rotor shaft was to be designed to operated on the existing Bently-Nevada test rig platform. This constrained the bearing to bearing shaft length to 18" or less. The use of proximity probes to measure displacement required the material to be carbon steel. Bearing and damper considerations suggested a diameter of 13/16". With the rotor disks positioned in the center of the shaft, it was desired that the rotor would have its first bending critical speed near the end of the operating speed range (0 to 12,000 RPM). The critical speed was chosen to be about 9000 RPM. Given the above considerations, the bearing to bearing length of the shaft was to be determined.

The stiffness (κ) at the center of a simply supported beam is

$$\kappa = \frac{48EI}{L^3}$$

where E is the modulus of elasticity and I is the section modulus. An estimate of the first natural frequency of

the shaft is then $\omega_c = \sqrt{k/m}^{1/2}$ where m is a lumped mass at the center of a massless shaft. Combining the above equations and solving for L,

$$L = \left(\frac{48EI}{m\omega^2}\right)^{1/3}$$

Using the mass of the two rotor disks (2.5 lb) as the lumped mass and the above mentioned critical speed and dimensions, this equation yields 17.5". Calculating the mass of a shaft of this length (3 lb) and lumping half of this mass in the center in addition to the disks, the above equation then yields 15.0". This was taken as the final estimate since the design allowed for some adjustment room. This estimate proved to be satisfactory, yielding a critical speed of about 9200 RPM.

Using the above equations along with the experimentally measured critical speed, the above method was reversed yielding the bearing and disk masses necessary to simulate the shaft as massless for operation through the first critical speed. These values were helpful for data analysis. Solving for the disk mass,

$$m_D = \frac{48EI}{L^3\omega^2}$$

This equation yields m_D = 3.992 lb using the appropriate

design parameters. The total rotor mass was measured as 6.591 lb. Half the difference of the disk and total rotor masses equaled the mass to be lumped at each bearing station, m_B = 1.300 lb. So that the mass ratio (M) was 1/3.

A quill shaft was to be designed to be used as a flexible coupling between the rotor and rotor shaft. The quill had to be strong enough to transmit the maximum torque of the motor, yet flexible in bending so as to constrain minimally the translation of the rotor. Also, the first critical speed of the quill was required to be well above the operating speed of the rotor, so that the dynamic behavior of the quill would not offset that of the rotor.

Considering the dimensions of the rotor, a diameter of 1/8" seemed reasonable for the quill. The motor was rated at 1/10 hp. at 10,000 RPM or a maximum torque (T) of .1728 in.-lb. From the equation

$$\tau = \frac{Tr}{J}$$

the maximum shear stress was calculated to be 450 psi. This was deemed suitable for a steel shaft.

Given the length of the rotor and the length constraint of the test rig base, a maximum quill length of 6" was determined. The first bending natural frequency

of a clamped beam is given by

$$f = \frac{(4.73)^2}{2\pi L^{3/2}} \left(\frac{EI}{m}\right)^{1/2}$$

For a 6" steel shaft with a 1/8" diameter, this equation yields f = 37,600 RPM which is over three times the operating speed of the rotor. This design was then considered satisfactory.

APPENDIX B

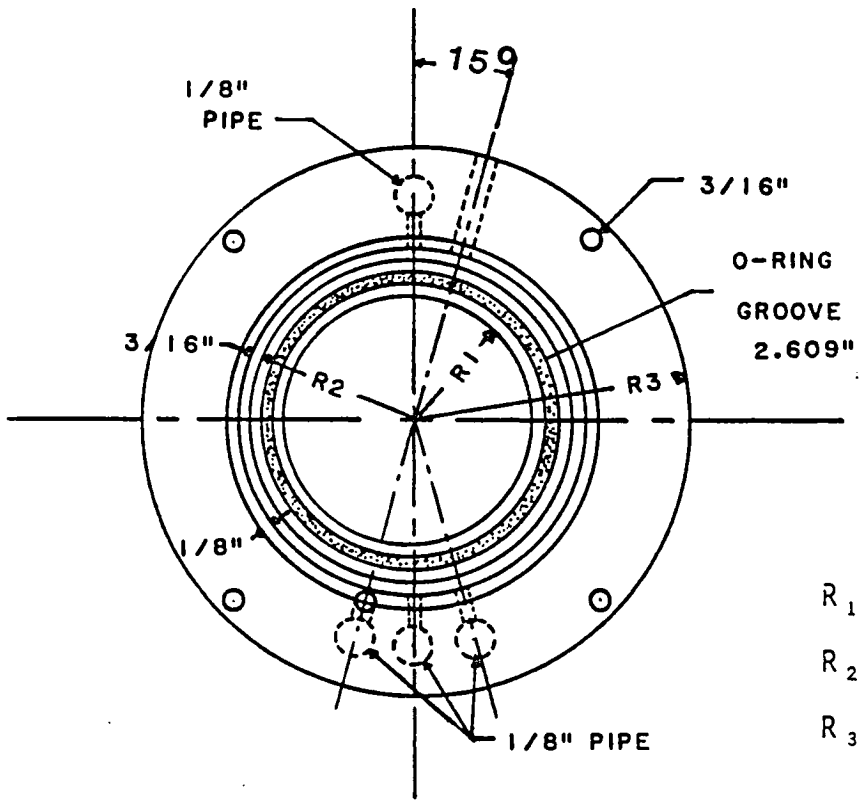

R_1 = 1-5/32"

R_2 = 1-19/32"

R_3 = 2-5/8"

1/2 Scale

Aluminum

2 Reqd.

Figure B-1. Damper Bearing

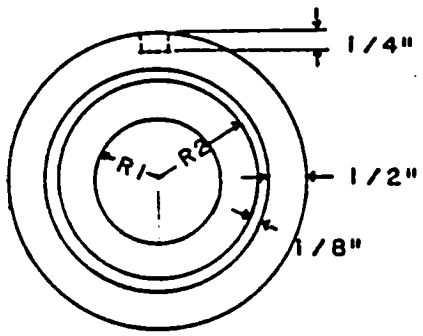

R_1 = .650"

R_2 = .9262"

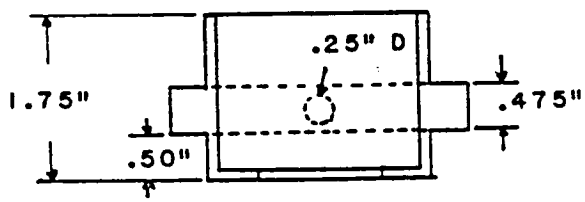

1/2 Scale

Aluminum

2 Reqd.

Figure B-2. Damper Journal/Bearing Holder

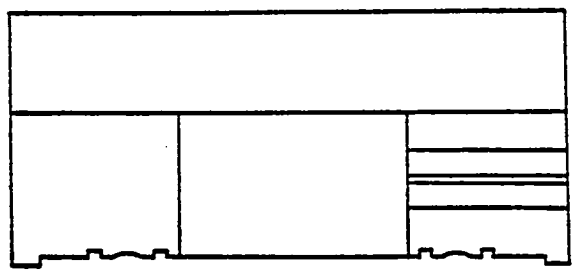

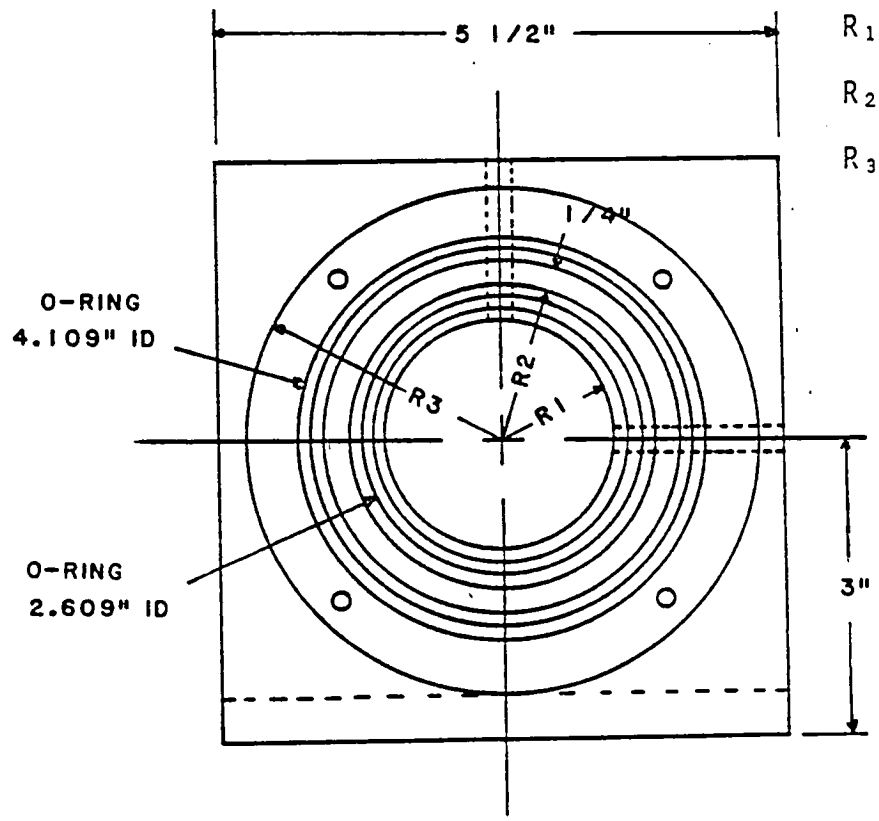

1/2 Scale

Aluminum

2 Reqd.

Figure B-3. Bearing Housing

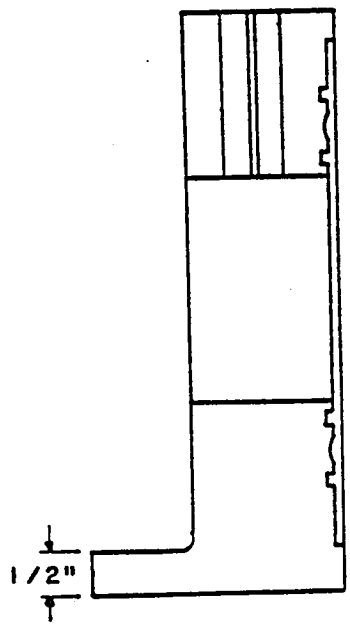

R_1 = 1-5/32"

R_2 = 1-19/32"

R_2 = 2-5/8"

1/2 Scale

Aluminum

2 Reqd.

Figure B-4. Bearing Housing Side View

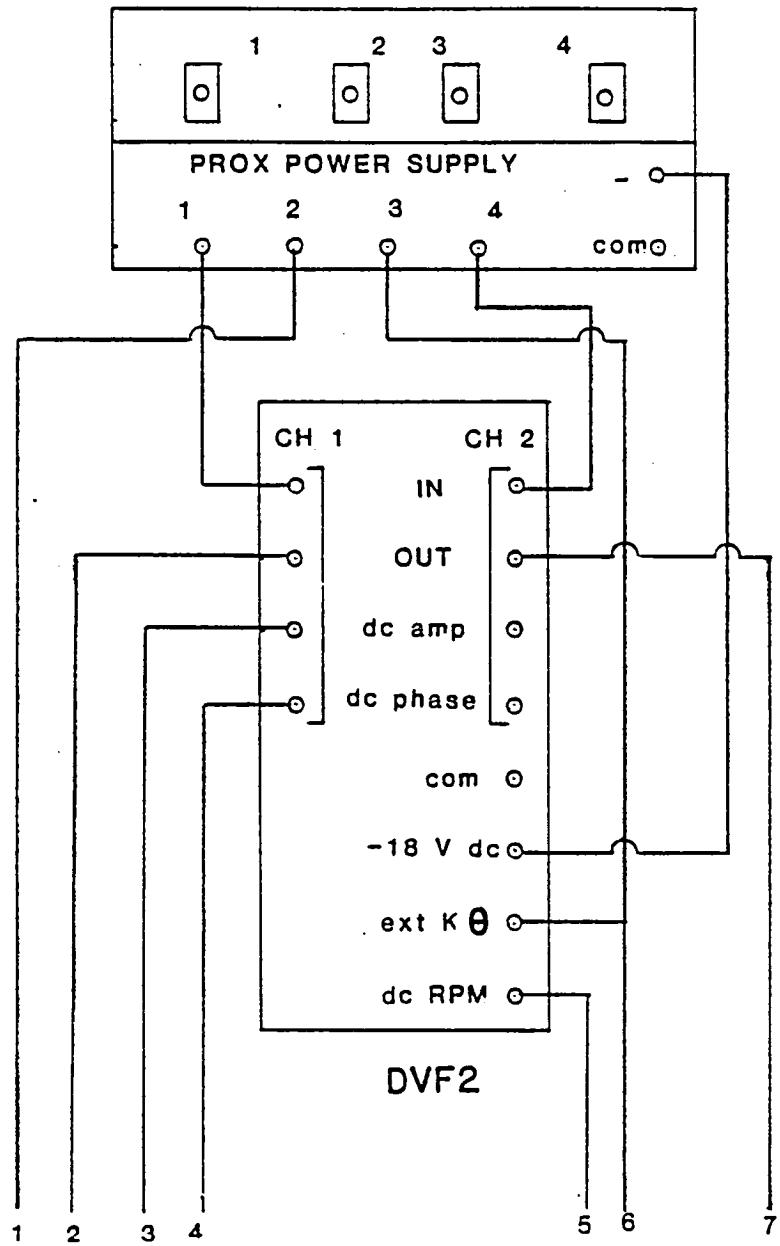

Figure B-5. Wiring Schematic

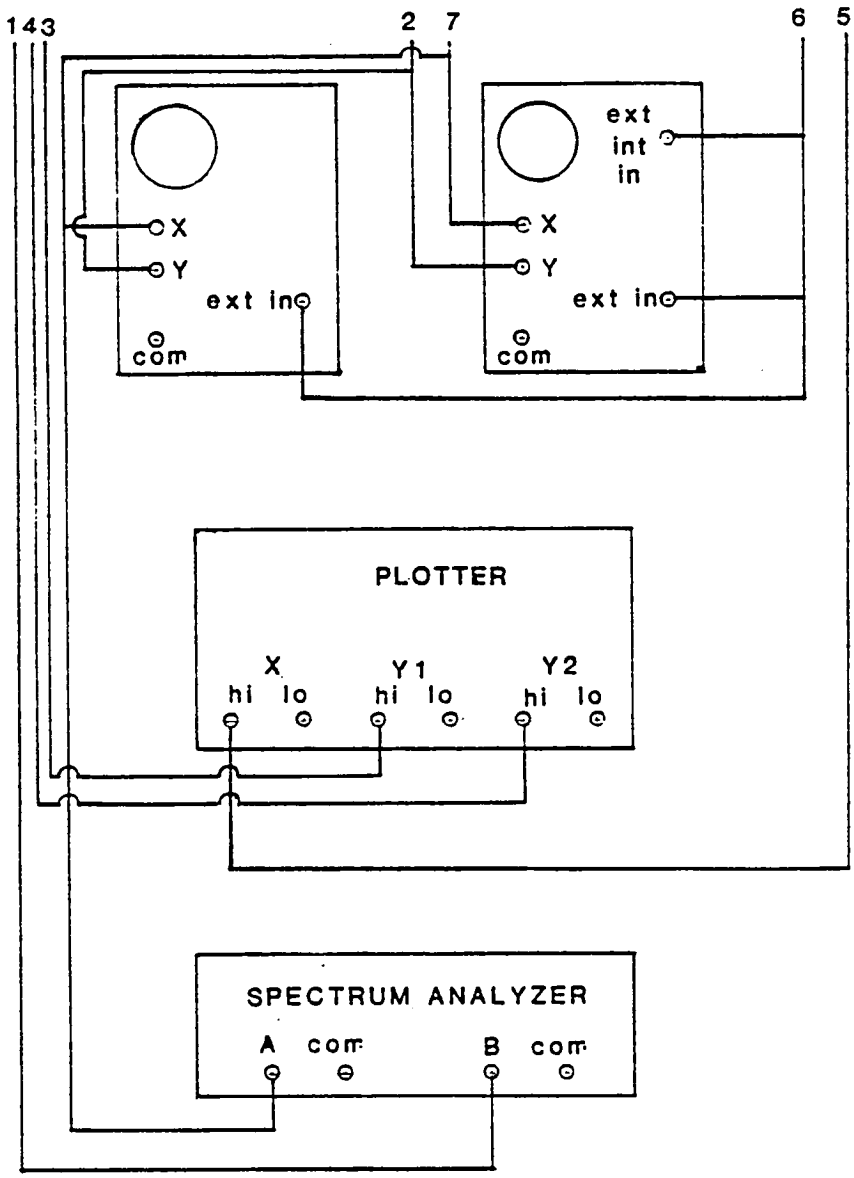

Figure B-5. Wiring Schematic (Continued)

DISTRIBUTION LIST FOR TOPICAL REPORT
NASA CR-168317
EXPERIMENTAL STUDY OF UNCENTRALIZED SQUEEZE FILM DAMPERS
GRANT NSG-3283

	Mail Stop	Copies
NASA Lewis Research Center 21000 Brookpark Road Cleveland, OH 44135		
Attn: Contracting Officer	500-312	1
Technical Report Control Officer	5-5	1
Technology Utilization Office	3-16	1
AFSC Liaison Office	501-3	1
S&MT Division Contract File	49-6	2
Library	60-3	1
L. Berke	49-6	1
R. H. Johns	49-6	1
L. J. Kiraly	23-2	1
C. C. Chamis	49-6	7
M. S. Hirschbein	49-6	1
J. A. Ziemianski	49-6	1
W. J. Anderson	23-2	1
D. J. Gauntner	23-2	1
D. P. Fleming	23-2	1
A. F. Kascak	23-2	1
G. V. Brown	49-6	1
M. H. Tang	49-6	1
R. E. Kielb	49-6	1
National Aeronautics & Space Administration Washington, DC 20546		
Attn: NHS-22/Library		1
RTM-6/C. F. Bersch		1
RTM-6/M. A. Greenfield		1
NASA-Ames Research Center Moffett Field, CA 94035		
Attn: Library	202-3	1
NASA-Goddard Space Flight Center Greenbelt, MD 20771		
Attn: 252/Library		1
NASA-John F. Kennedy Space Center Kennedy Space Center, FL 32931		
Attn: Library	AD-CSO-1	1
NASA-Langley Research Center Hampton, VA 23665		
Attn: Library	185	1
M. F. Card	244	1

	Mail Stop	Copies
NASA-Lyndon B. Johnson Space Center Houston, TX 77001 Attn: JM6/Library		1
NASA-George C. Marshall Space Flight Center Marshall Space Flight Center, AL 35812 Attn: AS61/Library		1
Jet Propulsion Laboratory 4800 Oak Grove Drive Pasadena, CA 91103 Attn: Library B. Wada R. Levi		1 1 1
NASA S&T Information Facility P.O. Box 8757 Baltimore-Washington Int. Airport, MD 21240 Attn: Acquisition Department		10
Air Force Aeronautical Propulsion Laboratory Wright Patterson AFB, OH 45433 Attn: Z. Gershon E. Bailey		1 1
Air Force Systems Command Aeronautical Systems Division Wright-Patterson AFB, OH 45433 Attn: Library C. W. Cowie J. McBane		1 1 1
Aerospace Corportion 2400 E. El Segundo Blvd. Los Angeles, CA 90045 Attn: Library-Documents		1
Air Force Office of Scientific Research Washington, DC 20333 Attn: A. K. Amos		1
Department of the Army U.S. Army Material Command Washington, DC 20315 Attn: AMCRD-RC		1
U.S. Army Ballistics Research Laboratory Aberdeen Proving Ground, MD 21005 Attn: Dr. Donald F. Haskell	DRXBR-BM	1
Mechanics Research Laboratory Army Materials & Mechanics Research Center Watertown, MA 02172 Attn: Dr. Donald W. Oplinger		1

	Mail Stop	Copies
U.S. Army Missile Command Redstone Scientific Information Center Redstone Arsenal, AL 35808 Attn: Document Section		1
AFFDL/FBE Wright-Patterson AFB, OH 45433 Attn: D. W. Smith		1
Commanding Officer U.S. Army Research Office (Durham) Box, CM, Duke Station Durham, NC 27706 Attn: Library		1
Bureau of Naval Weapons Department of the Navy Washington, DC 20360 Attn: RRRE-6		1
Commander U.S. Naval Ordnance Laboratory White Oak Silver Springs, MD 20910 Attn: Library		1
Director, Code 6180 U.S. Naval Research Laboratory Washington, DC 20390 Attn: Library		1
Denver Federal Center U.S. Bureau of Reclamation P.O. Box 25007 Denver, CO 80225 Attn: P. M. Lorenz		1
Naval Air Propulsion Test Center Aeronautical Engine Department Trenton, NJ 08628 Attn: Mr. James Salvino		1
Naval Air Propulsion Test Center Aeronautical Engine Department Trenton, NJ 08628 Attn: Mr. Robert DeLucia		1
Federal Aviation Administration Code ANE-214, Propulsion Section 12 New England Executive Park Burlington, MA 01803 Attn: Mr. Robert Berman		1

	Mail Stop	Copies
Federal Aviation Administration DOT Office of Aviation Safety, FOB 10A 800 Independence Ave., S.W. Washington, DC 20591 Attn: Mr. John H. Enders		1
FAA, ARD-520 2100 2nd Street, S.W. Washington, DC 20591 Attn: Commander John J. Shea		1
National Transportation Safety Board 800 Independence Ave., S.W. Washington, DC 20594 Attn: Mr. Edward P. Wizniak	TE-20	1
Arizona State University Department of Aerospace Engineering and Engineering Science Tempe, AZ 85281 Attn: H. D. Nelson		1
Rockwell International Corporation Los Angeles International Airport Los Angeles, CA 90009 Attn: Mr. Joseph Gausselin	D 422/402 AB71	1
Rensselaer Polytechnic Institute Troy, NY 12181 Attn: R. Loewy		1
Cleveland State University Department of Civil Engineering Cleveland, OH 44115 Attn: Dr. P. Bellini		1
M.I.T. Cambridge, MA 02139 Attn: K. Bathe J. Mar E. A. Witmer J. Dugundji		1 1 1 1
University of Illinois at Chicago Circle Department of Materials Engineering Box 4348 Chicago, IL 60680 Attn: Dr. Robert L. Spilker		1

	Mail Stop	Copies
Detroit Diesel Allison General Motors Corporation Speed Code T3, Box 894 Indianapolis, IN 46206 Attn: Mr. William Springer Mr. J. Byrd		1 1
General Motors Corporation Warren, MI 48090 Attn: R. J. Trippet		1
AVCO Lycoming Division 550 South Main Street Stratford, CT 06497 Attn: Mr. Herbert Kaehler		1
Beech Aircraft Corporation, Plant 1 Wichita, KA 67201 Attn: Mr. M. K. O'Connor		1
Bell Aerospace P.O. Box 1 Buffalo, NY 14240 Attn: G. C. C. Smith		1
Boeing Aerospace Company Impact Mechanics Lab P.O. Box 3999 Seattle, WA 98124 Attn: Dr. R. J. Bristow		1
Boeing Commercial Airplane Company P.O. Box 3707 Seattle, WA 98124 Attn: Dr. Ralph B. McCormick		1
Boeing Commercial Airplane Company P.O. Box 3707 Seattle, WA 98124 Attn: Mr. David T. Powell	73-01	1
Boeing Commercial Airplane Company P.O. Box 3707 Seattle, WA 98124 Attn: Dr. John H. Gerstle		1
Boeing Company Wichita, KA Attn: Mr. C. F. Tiffany		1

	Mail Stop	Copies
McDonnell Douglas Aircraft Corporation P.O. Box 516 Lambert Field, MO 63166 Attn: Library		1
Douglas Aircraft Company 3855 Lakewood Blvd. Long Beach, CA 90846 Attn: Mr. M. A. O'Connor, Jr.	36-41	1
Garrett AiResearch Manufacturing Co. 111 S. 34th Street P.O. Box 5217 Phoenix, AZ 85010 Attn: L. A. Matsch		1
General Dynamics P.O. Box 748 Fort Worth, TX 76101 Attn: Library		1
General Dynamics/Convair Aerospace P.O. Box 1128 San Diego, CA 92112 Attn: Library		1
General Electric Company Interstate 75, Bldg. 500 Cincinnati, OH 45215 Attn: Dr. L. Beitch Dr. M. Roberts Dr. V. Gallardo	K221 K221 K221	1 1
General Electric Company Aircraft Engine Group Lynn, MA 01902 Attn: Mr. Herbert Garten		1
Grumman Aircraft Engineering Corp. Bethpage, Long Island, NY 11714 Attn: Library H. A. Armen		1 1
IIT Research Institute Technology Center Chicago, IL 60616 Attn: Library		1
Lockheed California Company P.O. Box 551 Dept. 73-31, Bldg. 90, PL. A-1 Burbank, CA 91520 Attn: Mr. D. T. Pland		1

	Mail Stop	Copies
Lockheed California Company P.O. Box 551 Dept. 75-71, Bldg. 63, PL. A-1 Burbank, CA 91520 Attn: Mr. Jack E. Wignot		1
Northrop Space Laboratories 3401 West Broadway Hawthorne, CA 90250 Attn: Library		1
North American Rockwell, Inc. Rocketdyne Division 6633 Canoga Avenue Canoga Park, CA 91304 Attn: Library, Dept. 596-306		1
North American Rockwell, Inc. Space & Information Systems Division 12214 Lakewood Blvd. Downey, CA 90241 Attn: Library		1
Norton Company Industrial Ceramics Division Armore & Spectramic Products Worcester, MA 01606 Attn: Mr. George E. Buron		1
Norton Company 1 New Bond Street Industrial Ceramics Division Worcester, MA 01606 Attn: Mr. Paul B. Gardner		1
United Aircraft Corporation Pratt & Whitney Group Government Products Division P.O. Box B2691 West Palm Beach, FL 33402 Attn: Library R. A. Marmol		1 1
United Aircraft Corporation Pratt & Whitney Aircraft Group 400 Main Street East Hartford, CT 06108 Attn: Library R. Liss D. H. Hibner C. Platt		1 1 1 1

	Mail Stop	Copies
United Aircraft Corporation Hamilton Standard Division Windsor Locks, CT 06096 Attn: Dr. G. P. Towsend Dr. R. A. Cornell		1 1
Aeronautical Research Association of Princeton, Inc. P.O. Box 2229 Princeton, NJ 08540 Attn: Dr. Thomas McDonough		1
Republic Aviation Fairchild Hiller Corporation Farmington, Long Island, NY Attn: Library		1
Rohr Industries Foot of H Street Chula Vista, CA 92010 Attn: Mr. John Meaney		1
TWA.Inc. Kansas City International Airport P.O. Box 20126 Kansas City, MO 64195 Attn: Mr. John J. Morelli		1
Stevens Institute of Technology Castle Point Station Hoboken, NJ 07030 Attn: F. Sisto A. T. Chang		1 1
Mechanical Technologies Inc. Latham, NY Attn: M. S. Darlow		1
Shaker Research Corporation Northway 10, Executive Park Ballston Lake, NY 12019 Attn: L. Lagace		1
Lockheed Palo Alto Research Labs Palo Alto, CA 94304 Attn: D. Bushnell		1
Lockheed Missiles and Space Company Huntsville Research & Engineering Center P.O. Box 1103 Huntsville, AL 18908 Attn: H. B. Shirley		1

	Mail Stop	Copies
MacNeal-Schwendler Corporation 7442 North Figueroa Street Los Angeles, CA 90041 Attn: R. H. MacNeal		1
MARC Analysis Research Corporation 260 Sheridan Avenue, Suite 314 Palo Alto, CA 94306 Attn: P. V. Marcel		1
United Technologies Research Center East Hartford, CT 06108 Attn: Dr. A. Dennis		1
Georgia Institute of Technology School of Civil Engineering Atlanta, GA 30332 Attn: S. N. Atluri		1
Georgia Institute of Technology 225 North Avenue Atlanta, GA 30332 Attn: G. J. Simitsis		1
Lawrence Livermore Laboratory P.O. Box 808, L-421 Livermore, CA 94550 Attn: M. L. Wilkins		1
Lehigh University Institute of Fracture and Solid Mechanics Bethlehem, PA 18015 Attn: G. T. McAllister		1
Materials Science Corporation 1777 Walton Road Blue Bell, PA 19422 Attn: W. B. Rosen		1
National Bureau of Standards Engineering Mechanics Section Washington, DC 20234 Attn: R. Mitchell		1
Purdue University School of Aeronautics & Astronautics West Lafayetee, IN 47907 Attn: C. T. Sun		1
University of Dayton Research Institute Dayton, OH 45409 Attn: F. K. Bogner		1

	Mail Stop	Copies
Texas A&M University Aerospace Engineering Department College Station, TX 77843		
Attn: W. E. Haisler		1
J. M. Vance		1
V. P. I. and State University Department of Engineering Mechanics Blacksburg, VA 24061		
Attn: R. H. Heller		1
University of Arizona College of Engineering Tucson, AZ 87521		
Attn: R. H. Gallagher		1
H. Kamel		1
University of California Department of Civil Engineering Berkeley, CA 94720		
Attn: E. Wilson		1
University of Kansas School of Engineering Lawrence, KS 66045		
Attn: R. H. Dodds		1
University of Virginia School of Engineering & Applied Science Charlottesville, VA 22901		
Attn: E. J. Gunter		1